Dissertation zur Erlangung des Doktorgrades

der Fakultät für Chemie und Pharmazie

der Ludwig-Maximilians-Universität München

Subcutaneous delivery of high concentrated mAb-formulations using novel application systems

Andreas Stelzl

aus München

2021

Erklärung

Diese Dissertation wurde im Sinne von § 7 der Promotionsordnung vom 28. November 2011 von Herrn Prof. Dr. Gerhard Winter von der Fakultät für Chemie und Pharmazie betreut.

Eidesstattliche Versicherung

Diese Dissertation wurde eigenständig und ohne unerlaubte Hilfe erarbeitet.

München, am 25.04.2021

……

Andreas Stelzl

(Unterschrift des Autors)

Dissertation eingereicht am 26.04.2021

1. Gutachter: Prof. Dr. Gerhard Winter

2. Gutachter: Prof. Dr. Wolfgang Frieß

Mündliche Prüfung am 15.06.2021

Acknowledgements

This thesis was prepared between 2016 and 2020 at the Chair of Pharmaceutical Technology and Biopharmaceutics of the Department of Pharmacy of the Ludwig-Maximilians-Universität München under the supervision of Prof. Dr. Gerhard Winter.

First of all, I want to express my deepest gratitude to Prof. Dr. Gerhard Winter. Thank you for providing me the opportunity to further strengthen my research education in your working group. I sincerely thank you for your enthusiastic, inspiring and exceptional scientific guidance throughout the whole project. The high level of freedom you trusted me with, allowed me to develop my scientific toolbox and knowledge further in this interesting and multi-faceted research project. Through all phases I always had the feeling to be in good hands with your scientific advice and guidance.

Prof. Dr. Wolfgang Frieß, I not only want to say thank you for taking over the co-referee, but I particularly enjoyed the scientific and personal discussions with you very much. Additionally, the fun we had during cooking sessions in multiple group events and the effort we put together to organize an outstanding meeting on the occasion of Prof. Dr. Winter's birthday with all his former PhD students and colleagues was very much enjoyed from my side. Thanks for the great time at the University.

The present thesis was in collaboration with Bayer Pharma AG, and was also supervised in person of Dr. Stefan Schneid and partly by Dr. Britta Siekmann, who made this project possible by funding and material support in the first place. I would also like to thank Stefan for his enthusiastic and dedicated contribution to the success of this project and his regular and valuable scientific input during the last years. Additionally, I express my gratitude to Dr. Florian Unger, Dr. Heiner Apeler, Dr. Juliet Padden, Stefan Hege, Stephanie Schiefer, Sandro Lamoratta, and Christoph Bruhn for supporting this thesis either from management side or scientifically by contributing their labor and expertise to the project.

Especially the analysis of samples by LC-MS through the analytical department needs to be honored and is highly valued.

In order to perform parts of my scientific investigations I would like to thank Weibel CDS AG for their collaboration and technical support of the project. In particular the input of Samuel Wyler, Hans Peter Manser and Christoph Egloff was highly appreciated and the collaboration in the development and evaluation of Weibel's large volume injection devices was highly enjoyed by me.

The unrestricted access to submicron particle counting techniques, supported by Adam Grabarek and Tim Menzen in persona and Coriolis Pharma Research GmbH as organization is highly appreciated. This enabled me to carry out additional experiments and to collect data I was not able to gather otherwise.

Also I want to appreciate the friendship over the last years to my former lab-colleagues Teresa Kraus, Ute Rockinger, Bernard Manuel Haryadi and Sebastian Groel. Many thanks go to all other (former-) colleagues and friends from the research groups of Prof. Winter, Prof. Frieß, and Prof. Merkel. Especially, to Alice, Michaela, Simon, Ben, Katharina, Dennis, Carolin, Julian, Hristo, Andreas and Jaqueline. I am grateful for the scientific and personal support of each of you in the last years and it was a pleasure working with you in such an excellent atmosphere with a lot of fun and laughter. Keep up the great team spirit!

I would like to thank all my friends at home for their friendship and encouragement during the last years. Finally, and most important I want to appreciate my family and especially my parents for their dedicative encouragement over the last 9 years of studying, thank you for being a part of me. Ivi, you and your love are the best things that happened in my life! Thank you for your trust, support and love.

GENERAL TABLE OF CONTENT

Chapter 1

Introduction – large volume subcutaneous injection of biopharmaceutical drugs

The treatment of patients with biopharmaceuticals is often conducted via the intravenous (IV), intramuscular (IM) or subcutaneous (SC) route. The less invasive character of the SC injection compared to IM or IV injection usually causes with less pain during and post injection and therefore enhances patient tolerability and compliance, especially when frequent and chronic administration of drugs is necessary [1-3]. The use of prefilled syringes (PFS), autoinjectors, or pens can reduce handling errors and allows the patient to self-administer the drug in a home-care setting which further enhances patient compliance [1-4]. However, SC injections are typically limited to a low injection volume of ≤ 1.5 ml, since adverse effects such as injection site leakage, injection pain, itching and erythema can be caused by larger injection volumes [1, 3-7]. Besides the development of high concentrated protein formulations, large volume injections, multiple injections of smaller volumes or the use of functional excipients like hyaluronidase can be considered as potential ways to achieve therapeutic doses via the SC route [1, 2, 4, 5, 8].

Wearable injection devices

Large volume subcutaneous injections of up to 20 ml via infusion pumps or rapid push injections are currently used in immunoglobulin replacement therapy with good tolerability by the patients as an alternative to treatment via the IV route [9, 10]. The slow infusion of drugs in the SC tissue compared to a regular injection with 1 ml per 10 sec was found to result in increased tolerability of larger injection volumes in pigs through lower tissue backpressure [2] and first publications testing large volume injection devices with human patients conclude good tolerability of wearable injectors as well [11].

These facts, and a growing demand for injection devices with an estimated global market opportunity of US$8.1 billion by 2025, led to a broad variety of injection devices being available [12]. An exemplary overview, showcasing some large volume injection devices and some key features, is given in Table 1 and Figure 21. The majority of injection devices utilizes an electromechanical pump, which is pushing the liquid out of a standard pharmaceutical packaging system such as a syringes or cartridges [13-16]. These pump concepts utilize telescopic or bending plunger rods to push the plunger forward and thereby deliver the solution filled in the container [17]. Other pushing concepts use mechanical pumping mechanisms to push the liquid out of standard and non-standard drug containers. Enable Injections, for example, uses an elastomeric balloon made from e.g. silicone, which is filled with the drug by the patient immediately prior to use [18, 19]. The device then uses the force created by the contraction of the expanded balloon to inject the solution. Other companies such as United Therapeutics Corporation or Subcuject ApS use expanding batteries or osmosis in order to push the liquid out of the drug container and inject it into the patient [20, 21]. Besides pushing concepts, there are also devices available using a pulling concept to draw the liquid out of the container. Sensile Medical AG and Weibel CDS AG, for example, utilize this approach to inject drug solution by using either a micro volumetric rotary piston pump (Sensile Medical AG) or a valve free rotary piston pump (Weibel CDS AG) [22, 23]. In comparison to pushing concepts, the pulling concepts have several advantages including the possibility to physically separate the pump from the container, using several different container types with the same pump or using the pump to fill the drug container within the pump from a standard pharmaceutical vial [17]. On the downside of pulling concepts, the drug gets into contact with pump materials and therefore has a higher risk to be damaged. Additionally, vacuum can be created by the pulling action, which can create air bubbles and air-liquid interfaces and can be detrimental to protein drugs [17, 24-26]. Despite this diversity of injection devices, differing in design features such as primary packaging material, assembly state, needle insertion mechanism, drive

mechanisms, or re-usability, only a limited number of approved drug-device combinations are available utilizing a large volume injection device [27]. For example, Amgen's Repatha® Pushtronex® system utilizes a Smartdose injection device (West Pharmaceuticals) to deliver a dose of 420 mg evolocumab in 3.5 ml during a 9 min injection. Compared to the conventional autoinjector (SureClick®, Amgen), the dosing scheme could be prolonged with the large volume injection device from bi-weekly to monthly which additionally contributes to patient compliance [28].

Table 1: Exemplary overview of wearable injection devices available to the market with key features [13-16, 18, 20-23, 29-31].

Manufacturer	Product or Platform	Primary Packaging		Pump mechanism	Volume
		Type	Material		
Beckton, Dickinson and Company	Libertas™	Cartridge	Glass	n.s.	5 ml
Sonceboz	Large Volume Injector LVI™	Cartridge	n.s.	electro-mechanical	3-20 ml
West Pharmaceutical Services, Inc.	Smartdose	Cartridge	Polymer (COP)	electro-mechanical	3.5 and 10 ml
Ypsomed AG	YpsoDose	Cartridge	Glass	electro-mechanical	2-10 ml
Sensile Medical AG	Patch pump – Large volume injector	Cartridge, Vial	n.s.	Micro volumetric rotary piston pump	3 and 20 ml
Weibel CDS AG	Drug Delivery System	Cartridge, Syringe, Vial, MiniBag	Glass or Polymer (COC)	Valve free dual piston pump	3 and 30 ml
Insulet Corporation	Omnipod	Internal reservoir	n.s.	n.s.	2 ml
Enable Injections	enFuse® On-Body Infusor	Syringe, Vial	n.s.	Elastomeric balloon	10, 25 and 50 ml
Subcuject ApS	Subcuject	Cartridge	glass	Osmosis	1-10 ml
United Therapeutics Corporation	Trevyent Patch Pump	proprietary	proprietary	Expanding battery	n.s.

n.s. = not specified

Figure 1: Exemplary overview of wearable injection devices available to the market [13-16, 18, 20-23, 29-31].

Packaging materials

Besides the development of large volume injection devices for the self-administration of drugs, the development of new large volume primary packaging solutions is fostered as well, since syringes, which are common primary packaging materials for self-administration of small injection volumes, are becoming larger and bulkier when larger filling volumes are tackled [4, 32]. This is expected to compromise the carrying comfort for the patient and could result in reduced patient compliance. As a potential solution to this, the use of a flexible COC-film allowed the development of a flexible pouch, called MiniBag, to store drug product [33]. Due to the flexible COC-film, the MiniBag can be produced with various filling volumes while remaining in a flat and bendable shape even if filling volumes exceeding 30 ml are considered, which potentially leads to increased patient convenience [33-35]. The variability in form, size, and shape, which can be achieved with polymer packaging materials may overcome some of the main drawbacks of the traditionally used glass primary packaging materials.

Historically, the use of glass as primary packaging material is widespread and the majority of PFS or cartridges available on the market are made from glass [32, 36]. Nevertheless, glass as packaging material has distinct disadvantages like breakage potential, surface reactivity, glass delamination at higher pH and the need for siliconization [32, 36-38]. Siliconization of the glass barrel of syringes or cartridges is required to maintain functionality of the packaging material, but migration of silicone oil into the drug product during filling or storage can occur, causing not only increased particle levels, but also protein aggregation [39-47]. Lower levels of silicone oil in solution can be achieved through modern manufacturing techniques such as bake-on or cross-linked siliconization, but are still not a standard configuration today [48, 49]. In comparison to glass, polymer packaging materials made of cyclic olefin polymers (COP) or cyclic olefin copolymers (COC) can offer increased resistance to breakage, and decreased surface reactivity as advantages [36, 38, 50]. Silicone-oil free variants of polymer syringes are available on the market, giving them an advantage for the storage of silicone-oil sensitive products [50]. Despite the reported good protein stability of a mAb and a cytokine in polymer syringes, a main drawback of polymer packaging materials can be found in their permeability to gasses such as oxygen or water vapor, leading to loss in product quality of oxidation sensitive products [36, 37, 50-54]. The combination of polymer packaging materials with secondary packaging materials offering a low-oxygen environment can lead to decreased oxygen levels in solution and consequently reduced protein oxidation [50, 54].

Protein aggregation and submicron particle analysis

Besides the need for large volume injection devices and associated new primary packaging solutions, the development of high concentrated protein formulations brings new challenges with it. A high protein concentration was found to not only affect manufacturing and delivery due to high solution viscosities, but also leads to reduced protein stability due to increased protein aggregation upon storage [7, 8, 55-58]. The assessment of protein aggregation can be done by a multitude of analytical

methods ranging from soluble aggregate levels up to the visible particle range [59]. However, the submicron particle (SMP) characterization and quantification in biopharmaceuticals between 0.1 and 1 µm remains challenging, due to limitations in the availability of analytical methods and their reliability [60-63]. Nevertheless, the immunogenic potential of protein aggregates is recognized and especially the formation of nanoparticles led to a more pronounced immunogenic reaction in mice, fostering the need for better submicron particle counting methods [25, 64, 65]. Due to improvements in micro- and nano-fabrication, resistive pulse sensing (RPS) was introduced as new technique for submicron particle characterization [66, 67]. RPS detects particles based on changes in the electric field between two electrodes upon particle passage through a sensing orifice, which is commonly known as Coulter counter principle [68]. Compared to other available techniques to characterize and quantify submicron particles, studies have shown great accuracy of RPS in characterizing concentration and size of polystyrene bead mixtures or exosomal vesicles [60, 69, 70]. RPS is applied by two manufacturers using either tunable resistive pulse sensing (TRPS, IZON Ltd., Christchurch, New Zealand) or microfluidic resistive pulse sensing (MRPS, Spectradyne LLC., Torrance, CA, USA) to analyze submicron particles. Despite their characteristic differences, both devices use a nano-constriction, separating two electrodes, as sensing zone. Due to the detection of particles via change in electric current or voltage upon particle passage through the orifice, both techniques require sufficient conductivity of the sample in order to detect the particles [68, 71]. If the conductivity of the samples is not suitable for direct measurement, the addition of electrolytes via dilution in phosphate buffered saline was reported as suitable sample preparation protocol [71-73].

References

1. Mathaes, R., et al., *Subcutaneous Injection Volume of Biopharmaceuticals-Pushing the Boundaries.* J Pharm Sci, 2016. **105**(8): p. 2255-9.
2. Doughty, D.V., et al., *Understanding Subcutaneous Tissue Pressure for Engineering Injection Devices for Large-Volume Protein Delivery.* J Pharm Sci, 2016. **105**(7): p. 2105-13.
3. Narasimhan, C., H. Mach, and M. Shameem, *High-dose monoclonal antibodies via the subcutaneous route: challenges and technical solutions, an industry perspective.* Therapeutic Delivery, 2012. **3**(7): p. 889-900.
4. Bittner, B., W. Richter, and J. Schmidt, *Subcutaneous Administration of Biotherapeutics: An Overview of Current Challenges and Opportunities.* BioDrugs, 2018. **32**(5): p. 425-440.
5. Frost, G.I., *Recombinant human hyaluronidase (rHuPH20): an enabling platform for subcutaneous drug and fluid administration.* Expert Opin Drug Deliv, 2007. **4**(4): p. 427-40.
6. Usach, I., et al., *Subcutaneous Injection of Drugs: Literature Review of Factors Influencing Pain Sensation at the Injection Site.* Adv Ther, 2019. **36**(11): p. 2986-2996.
7. Shire, S.J., Z. Shahrokh, and J. Liu, *Challenges in the Development of High Protein Concentration Formulations.* Journal of Pharmaceutical Sciences, 2004. **93**(6).
8. Bookbinder, L.H., et al., *A recombinant human enzyme for enhanced interstitial transport of therapeutics.* J Control Release, 2006. **114**(2): p. 230-41.
9. Shapiro, R., *Subcutaneous Immunoglobulin Therapy by Rapid Push is Preferred to Infusion by Pump: A Retrospective Analysis.* Journal of Clinical Immunology, 2010. **30**(2): p. 301-307.
10. Berger, M., *Principles of and advances in immunoglobulin replacement therapy for primary immunodeficiency.* Immunol Allergy Clin North Am, 2008. **28**(2).
11. Torjman, M.C., et al., *Evaluation of an investigational wearable injector in healthy human volunteers.* Expert Opin Drug Deliv, 2017. **14**(1): p. 7-13.
12. Beddoes, C., *Understanding the market for wearable large volume injectors.* ONdrugDelivery, 2016. **70**.
13. Beckton Dickinson and Company. [31.12.2020 9:00 am]; Available from: https://drugdeliverysystems.bd.com/products-and-services/products/self-injection-systems/libertas-wearable-autoinjector.
14. Sonceboz. [31.12.2020 11:00 am]; Available from: https://www.sonceboz.com/wearable-injectors.
15. West Pharmaceutical Services Inc. [31.12.2020 13:00 pm]; Available from: https://www.westpharma.com/products/self-injection-platforms/smartdose.
16. Ypsomed AG. [31.12.2020 13:30 pm]; Available from: https://yds.ypsomed.com/en/products/wearable-injectors/ypsodose.html.
17. Oakley, T., *Wearable injectors: latest devices & recent trends.* ONdrugDelivery, 2020. **111**.
18. Enable Injections. [31.12.2020 9:30 am]; Available from: https://enableinjections.com/technology/enfuse-on-body-platform/.
19. Hooven, M.D., et al., *Vial transfer and insertion apparatus and method*. 2016, Enable Injections, LLC., US Patent US 2016/0144105 A1.
20. United Therapeutics Corporation. [31.12.2020 12:00 pm]; Available from: https://pipeline.unither.com/product/trevyent-treprostinil-sodium/description/.
21. Subcuject ApS. [31.12.2020 11:30 am]; Available from: https://subcuject.com/.
22. Sensile Medical AG. [31.12.2020 10:30 am]; Available from: https://www.sensile-medical.com/solutions.html.

23. Weibel CDS AG. [31.12.2020 12:30 pm]; Available from: https://weibelcds.com/products/drug-delivery-systems/.
24. Maa, Y.F.H., C.C., *Protein Denaturation by Combined Effect of Shear and Air-Liquid Interface.* Biotechnology and Bioengineering, 1997. **54**(6).
25. Carpenter, J.F., et al., *Overlooking subvisible particles in therapeutic protein products: gaps that may compromise product quality.* J Pharm Sci, 2009. **98**(4): p. 1201-5.
26. Koepf, E., et al., *Notorious but not understood: How liquid-air interfacial stress triggers protein aggregation.* Int J Pharm, 2018. **537**(1-2): p. 202-212.
27. Bauert, D. and A.K. Busimi, *Primary packaging for wearable injection devices*, in *ONdrugDelivery*. 2019.
28. Amgen Inc. *Prescribing information: Repatha®*. 2019; Available from: https://www.repatha.com/.
29. Furness, G., *Wearable Injectors*. ONdrugDelivery. Vol. 100. 2019.
30. Furness, G., *Wearable Injectors*. ONdrugDelivery. Vol. 111. 2020.
31. Insulet Corporation. [31.12.2020 10:00 am]; Available from: http://www.omnipoddelivery.com/.
32. Sacha, G., J.A. Rogers, and R.L. Miller, *Pre-filled syringes: a review of the history, manufacturing and challenges.* Pharm Dev Technol, 2015. **20**(1): p. 1-11.
33. Manser, H.P., C. Egloff, and M.C. King, *Large-volume wearable drug delivery: a vision becomes reality.* ONdrugDelivery, 2019. **100**.
34. Manser, H.P. *MiniBag System*. [14.06.2020 10:30am]; Available from: https://weibelcds.com/products/minibag-system/.
35. Weibel, L.D. and H.P. Manser, *Drugdeliverysystems: Ready to use dor highest patient comfort.* ONdrugDelivery, 2015. **58**.
36. Krayukhina, E., et al., *Effects of syringe material and silicone oil lubrication on the stability of pharmaceutical proteins.* J Pharm Sci, 2015. **104**(2): p. 527-35.
37. Vilivalam, V.D. and F.L. DeGrazio, *Plastic packaging for parenteral drug delivery*, in *Pharmaceutical Dosage Forms: Parenteral Medications, Third Edition, Volume 1: Formulation and Packaging*, S. Nema and J.D. Ludwig, Editors. 2010.
38. Jezek, J., et al., *Biopharmaceutical formulations for pre-filled delivery devices.* Expert Opinion on Drug Delivery, 2013. **10**(6).
39. Yoshino, K., et al., *Functional evaluation and characterization of a newly developed silicone oil-free prefillable syringe system.* J Pharm Sci, 2014. **103**(5): p. 1520-8.
40. Demeule, B., et al., *Characterization of particles in protein solutions: reaching the limits of current technologies.* AAPS J, 2010. **12**(4): p. 708-15.
41. Badkar, A., et al., *Development of biotechnology products in pre-filled syringes: technical considerations and approaches.* AAPS PharmSciTech, 2011. **12**(2): p. 564-72.
42. Thirumangalathu, R., et al., *Silicone oil- and agitation-induced aggregation of a monoclonal antibody in aqueous solution.* J Pharm Sci, 2009. **98**(9): p. 3167-81.
43. Basu, P., et al., *IgG1 aggregation and particle formation induced by silicone-water interfaces on siliconized borosilicate glass beads: a model for siliconized primary containers.* J Pharm Sci, 2013. **102**(3): p. 852-65.
44. Gerhardt, A., et al., *Effect of the siliconization method on particle generation in a monoclonal antibody formulation in pre-filled syringes.* J Pharm Sci, 2015. **104**(5): p. 1601-9.
45. Uchino, T., et al., *Reconstitution of L-Asparaginase in Siliconized Syringes with Shaking and Headspace Air Induces Protein Aggregation.* Chemical and Pharmaceutical Bulletin, 2015. **63**(10): p. 770-779.

46. Majumdar, S., et al., *Evaluation of the effect of syringe surfaces on protein formulations.* J Pharm Sci, 2011. **100**(7): p. 2563-73.
47. Jones, L.S., A. Kaufmann, and C.R. Middaugh, *Silicone oil induced aggregation of proteins.* J Pharm Sci, 2005. **94**(4): p. 918-27.
48. Funke, S., et al., *Silicone Migration From Baked-on Silicone Layers. Particle Characterization in Placebo and Protein Solutions.* J Pharm Sci, 2016. **105**(12): p. 3520-3531.
49. Depaz, R.A., et al., *Cross-linked silicone coating: a novel prefilled syringe technology that reduces subvisible particles and maintains compatibility with biologics.* J Pharm Sci, 2014. **103**(5): p. 1384-93.
50. Werner, B.P., C. Schoneich, and G. Winter, *Silicone Oil-Free Polymer Syringes for the Storage of Therapeutic Proteins.* J Pharm Sci, 2019. **108**(3): p. 1148-1160.
51. Mathaes, R. and A. Streubel, *Parenteral Container Closure Systems*, in *Challenges in protein product development*, N.W. Warne and H.C. Mahler, Editors. 2018, Springer International Publishing.
52. Qadry, S.S., et al., *Model development for O2 and N2 permeation rates through CZ-resin vials.* International Journal of Pharmaceutics, 1999. **2**(188): p. 173-179.
53. Nakamura, K., et al., *A strategy for the prevention of protein oxidation by drug product in polymer-based syringes.* PDA J Pharm Sci Technol, 2015. **69**(1): p. 88-95.
54. Masato, A., F. Kiichi, and S. Uchiyama, *Suppression of Methionine Oxidation of a Pharmaceutical Antibody Stored in a Polymer-Based Syringe.* J Pharm Sci, 2016. **105**(2): p. 623-629.
55. Mahler, H.C., et al., *Protein aggregation: pathways, induction factors and analysis.* J Pharm Sci, 2009. **98**(9): p. 2909-34.
56. Liu, J., et al., *Reversible self-association increases the viscosity of a concentrated monoclonal antibody in aqueous solution.* J Pharm Sci, 2005. **94**(9): p. 1928-40.
57. Wang, W., *Instability, stabilization, and formulation of liquid protein pharmaceuticals.* International Journal of Pharmaceutics, 1999. **185**: p. 129–188.
58. Roberts, C.J., *Protein aggregation and its impact on product quality.* Curr Opin Biotechnol, 2014. **30**: p. 211-7.
59. Zolls, S., et al., *Particles in therapeutic protein formulations, Part 1: overview of analytical methods.* J Pharm Sci, 2012. **101**(3): p. 914-35.
60. Hubert, M., et al., *A Multicompany Assessment of Submicron Particle Levels by NTA and RMM in a Wide Range of Late-phase Clinical and Commercial Biotechnology-Derived Protein Products.* J Pharm Sci, 2019.
61. Singh, S.K., et al., *An industry perspective on the monitoring of subvisible particles as a quality attribute for protein therapeutics.* J Pharm Sci, 2010. **99**(8): p. 3302-21.
62. Scherer, T.M., et al., *Issues and challenges of subvisible and submicron particulate analysis in protein solutions.* AAPS J, 2012. **14**(2): p. 236-43.
63. Hawe, A., et al., *Subvisible and Visible Particle Analysis in Biopharmaceutical Research and Development*, in *Biophysical Characterization of Proteins in Developing Biopharmaceuticals*. 2015. p. 261-286.
64. Kijanka, G., et al., *Submicron Size Particles of a Murine Monoclonal Antibody Are More Immunogenic Than Soluble Oligomers or Micron Size Particles Upon Subcutaneous Administration in Mice.* J Pharm Sci, 2018. **107**(11): p. 2847-2859.
65. Moussa, E.M., et al., *Immunogenicity of Therapeutic Protein Aggregates.* Journal of Pharmaceutical Sciences, 2016. **105**(2): p. 417-430.

66. Song, Y., J. Zhang, and D. Li, *Microfluidic and Nanofluidic Resistive Pulse Sensing: A Review.* Micromachines (Basel), 2017. **8**(7).
67. Kozak, D., et al., *Advances in Resistive Pulse Sensors: Devices bridging the void between molecular and microscopic detection.* Nano Today, 2011. **6**(5): p. 531-545.
68. Rhyner, M.N., *The Coulter principle for analysis of subvisible particles in protein formulations.* AAPS J, 2011. **13**(1): p. 54-8.
69. Anderson, W., et al., *A comparative study of submicron particle sizing platforms: accuracy, precision and resolution analysis of polydisperse particle size distributions.* J Colloid Interface Sci, 2013. **405**: p. 322-30.
70. van der Pol, E., et al., *Particle size distribution of exosomes and microvesicles determined by transmission electron microscopy, flow cytometry, nanoparticle tracking analysis, and resistive pulse sensing.* J Thromb Haemost, 2014. **12**(7): p. 1182-92.
71. Anderson, W., et al., *Observations of Tunable Resistive Pulse Sensing for Exosome Analysis: Improving System Sensitivity and Stability.* Langmuir, 2015. **31**(23): p. 6577-87.
72. Vogel, R., et al., *A standardized method to determine the concentration of extracellular vesicles using tunable resistive pulse sensing.* J Extracell Vesicles, 2016. **5**: p. 31242.
73. Maas, S.L., et al., *Possibilities and limitations of current technologies for quantification of biological extracellular vesicles and synthetic mimics.* J Control Release, 2015. **200**: p. 87-96.

Chapter 2

Objectives of the thesis

The overall aim of this thesis was to evaluate, compare and potentially improve the performance of several large volume injection devices for subcutaneous delivery of high concentrated protein formulations. After thorough market research, sourcing of injection devices proved to be difficult, limiting the number of available injection devices. Besides performance evaluations of different injection devices under varying conditions, protein stability was of high importance [1-6]. First, a focus was set to the influence of different primary packaging materials, which are available for injection devices, on the stability of high concentrated monoclonal antibody formulations. Then, the influence of injection devices on protein stability during pumping was investigated, and measures to improve the quality of injected protein drug solutions were investigated by e.g. implementing an in-line sterile filtration step in the injection process.

Two large volume injection devices, one tailored for the needs of basal delivery of long acting drugs, such as insulin, as well as for the bolus delivery of drugs and a second one especially designed to suit the needs for the bolus delivery of large volumes of high concentrated biopharmaceuticals at high flow rates were evaluated in **Chapter 3**. Both investigated injection devices were developed by Weibel CDS AG and utilize a valve-free dual piston suction pump mechanism, which draws the liquid out of the drug container and delivers it to the patient. Therefore the pump itself can be combined with a variety of different primary packaging materials (e.g., glass cartridge, glass syringe, collapsible cyclic-olefin-copolymer (COC) MiniBag). Factors such as flow rate, solution viscosities, temperatures, fluid path design, and shear behavior were evaluated with regard to the dose accuracy of a high concentrated liquid monoclonal antibody (mAb) formulation by using both injection devices. Besides injection device

performance, the impact on protein stability when delivering a high concentrated mAb solution with both injection devices was investigated. The incorporation of an in-line filtration step to decrease the particle burden of the delivered solution was critically assessed with regards to the size limitation of wearable injectors, potential benefits for biopharmaceuticals, and the impact on the delivered dose.

A flexible pouch, called MiniBag, laminated from a cyclic olefin copolymer-polychlorotrifluoroethylene (COC/PCTFE) flexible film, CETA160, has been developed by Weibel CDS AG (Waldstatt, Switzerland) to store drug product. In **Chapter 4**, the chemical and physical stability of a mAb formulation at 140 mg/ml protein concentration after storage in the novel MiniBag system for up to 24 weeks at three storage temperatures was critically assessed and compared to the protein stability after filling of commonly used siliconized glass syringes and silicone-oil free cyclic olefin polymer (COP) syringes. In addition to storage at atmosphere, a N_2-filled aluminum pouch was used as secondary packaging for polymer primary packaging materials in order to overcome the drawback of weaker barrier properties of polymer packaging materials and to potentially reduce protein oxidation.

Due to improvements in micro- and nano-fabrication, resistive pulse sensing (RPS) was introduced as new technique for submicron particle analysis between 0.1 and 1 µm [10, 11]. In **Chapter 5 and 6**, tunable resistive pulse sensing (TRPS) was evaluated as analytical technique to characterize and quantify submicron particles in proteinaceous samples. Therefore a suitable sample preparation as well as data evaluation method was developed, investigating approaches to avoid large sample dilution **(Chapter 5)**. Additionally, the comparability of TRPS to other submicron particle analysis techniques such as resonant mass measurement (RMM), nanoparticle tracking analysis (NTA) and microfluidic resistive pulse sensing (MRPS) was investigated **(Chapter 6)**. As both RPS techniques rely on sufficient ionic strength present in the sample solution, the effect of adding electrolytes to a sample solution and the implications thereof for analytical strategies was critically assessed.

References

1. Shire, S.J., Z. Shahrokh, and J. Liu, *Challenges in the Development of High Protein Concentration Formulations.* Journal of Pharmaceutical Sciences, 2004. **93**(6).
2. Mahler, H.C., et al., *Protein aggregation: pathways, induction factors and analysis.* J Pharm Sci, 2009. **98**(9): p. 2909-34.
3. Liu, J., et al., *Reversible self-association increases the viscosity of a concentrated monoclonal antibody in aqueous solution.* J Pharm Sci, 2005. **94**(9): p. 1928-40.
4. Wang, W., *Instability, stabilization, and formulation of liquid protein pharmaceuticals.* International Journal of Pharmaceutics, 1999. **185**: p. 129–188.
5. Roberts, C.J., *Protein aggregation and its impact on product quality.* Curr Opin Biotechnol, 2014. **30**: p. 211-7.
6. Carpenter, J.F., et al., *Overlooking subvisible particles in therapeutic protein products: gaps that may compromise product quality.* J Pharm Sci, 2009. **98**(4): p. 1201-5.
7. Bookbinder, L.H., et al., *A recombinant human enzyme for enhanced interstitial transport of therapeutics.* J Control Release, 2006. **114**(2): p. 230-41.
8. Kijanka, G., et al., *Submicron Size Particles of a Murine Monoclonal Antibody Are More Immunogenic Than Soluble Oligomers or Micron Size Particles Upon Subcutaneous Administration in Mice.* J Pharm Sci, 2018. **107**(11): p. 2847-2859.
9. Moussa, E.M., et al., *Immunogenicity of Therapeutic Protein Aggregates.* Journal of Pharmaceutical Sciences, 2016. **105**(2): p. 417-430.
10. Song, Y., J. Zhang, and D. Li, *Microfluidic and Nanofluidic Resistive Pulse Sensing: A Review.* Micromachines (Basel), 2017. **8**(7).
11. Kozak, D., et al., *Advances in Resistive Pulse Sensors: Devices bridging the void between molecular and microscopic detection.* Nano Today, 2011. **6**(5): p. 531-545.

Chapter 3

Technical considerations and approaches for large volume subcutaneous injection of biopharmaceuticals with wearable injection devices

This chapter is intended for publication.

Authors: Andreas Stelzl[1], Stefan Schneid[2], Gerhard Winter[1]

[1] Ludwig-Maximilians Universität München, Department of Pharmacy, Pharmaceutical Technology and Biopharmaceutics, Butenandtstraße 5-13, 81377 Munich, Germany

[2] Bayer AG, Pharmaceuticals, Formulation Development Parenterals, Friedrich-Ebert-Str. 475, 42096 Wuppertal, Germany

The presented experiments were conducted by Andreas Stelzl. Scientific guidance was provided by Dr. Stefan Schneid and Prof. Dr. Gerhard Winter.

Abstract

Wearable injection devices can be used to increase the subcutaneous injection volume of biopharmaceuticals, resulting in a higher therapeutic dose and potentially less frequent dosing schemes. This, in combination with self-administration by the patient without mandatory assistance of health-care professionals, comes with the expectation of an increased patient compliance.

In this study, the performance of two large volume injection devices at variable flow rates (0.05 – 3.0 ml/min) was investigated, and the accuracy in dosing was assessed in dependence of protein concentration, injection temperature, shear behavior, and fluid path design. The influence of the pumping operation on antibody stability was evaluated in an in-use stability study based on size exclusion and ion exchange chromatography as well as subvisible particle analysis as stability indicating methods. The incorporation of an in-line filtration step during injection was evaluated for the impact on injection device performance as well as the ability to reduce particle burden.

Viscosity, fluid path design, and flow rate were identified as main factors influencing the performance of large volume injection devices, and an optimal adjustment of these parameters is required to ensure reliable and predictable dosing. Protein aggregation and the formation of subvisible particles during the pumping of high concentrated protein solutions were observed, but part of the particle level increase was due to the selected primary packaging material.

Keywords:

Subcutaneous injection, large volume injection devices, wearable injection device, dose accuracy, in-use stability, monoclonal antibody, high concentration liquid formulation, biopharmaceuticals, rheology, in-line filtration

1. Introduction

From a patient perspective, subcutaneous (SC) injection offers several advantages over intravenous (IV) or intramuscular (IM) delivery of biopharmaceuticals, such as less pain during injection and post-injection pain and the less invasive character of a SC injection [1-3]. Prefilled syringes, autoinjectors, or pens can often be used in self-administration by the patient without the need for a health-care professional, which safes costs and possibly supports patient compliance [1-4]. The limited injection volume of ≤ 1.5 ml is commonly recognized as a drawback of SC injections [3, 5, 6]. The limitation in injection volume often requires the development of high concentrated protein formulations for subcutaneous delivery in order to achieve administration of the therapeutic dose. This need can affect manufacturing and delivery due to high solution viscosities and can reduce protein stability upon storage [7-11].

Other approaches such as large volume injections, multiple injections of smaller volumes or the use of functional excipients like hyaluronidase need to be considered, if the desired dosing scheme cannot be met by highly concentrated formulation combined with an injection volume of ≤ 1.5 ml [1, 2, 4, 5, 7]. To increase SC injection volumes, first large volume injection devices have been presented and are currently still being further developed in the pharmaceutical industry. Publications are available presenting good tolerability of wearable injectors for the patients [12]. Another application for large volume s.c. injections is the immunoglobulin replacement therapy, which was done mainly via the intravenous route in the past [13, 14].

Studies have shown that subcutaneous injections of up to 20 ml using infusion pumps or by rapid push injections are also well tolerated by patients [13, 14]. A decrease from the commonly used 1 ml/10 sec flow rate led to a good tolerability of up to 10 ml injection volumes in pigs due to lower tissue-backpressure [2]. The distribution of phosphate-buffered saline and povidone solutions in the s.c.

tissue, simulating low and high viscosity solutions, was hereby comparable at all investigated flow rates [2].

Only a very limited number of drug-device combinations for large volume s.c. application of biopharmaceuticals are approved to date, although a number of manufacturers are offering a multitude of large volume injection devices and the growing market has an estimated global market opportunity of US$8.1 billion by 2025 [15]. As a result of the diverse market, a broad variety of injection devices is available (Table 2), differing in design features such as primary packaging material, assembly state, needle insertion mechanism, drive mechanisms, or re-usability [16]. For example, the approved drug-device combination Repatha® Pushtronex® system utilizes a Smartdose (West Pharmaceuticals) injection device to deliver 420 mg evolocumab in 3.5 ml over 9 min of injection time. A monthly dosing scheme was achieved compared to a bi-weekly dosing scheme with an autoinjector (SureClick®) containing 140 mg/ml evolocumab [17].

Table 2: Design features and exemplary solutions offered by device manufacturers [16].

Design feature	Exemplary solutions offered by device manufacturers
Primary packaging material	Glass or polymer cartridge, collapsible bladders or bags
Assembly state	Pre-assembled or assembled by patient
Needle insertion mechanism	Integrated or separate, manual or automated, soft or rigid cannula
Drive mechanism	Spring-based, motor-driven, rotary pump, pressurized gas, expanding polymer
Re-usability	Re-use of electronics possible for some devices

Previous studies have described that the injection forces in syringe-needle combinations depend on needle diameters, rheological data, friction forces, and injection speed [18-21]. Therefore, the performance of large volume injection devices is expected to be governed by the maximum pumping pressure the device can achieve and subsequently the volume flow of the to be injected solution

through a tube as described by the Hagen-Poiseuille-law [22]. Developing a large volume injection device requires the optimization of the fluid path design for optimal volume flow in parallel to good patient compliance [6]. Additionally, the pressure difference can be altered by changing the flow rate applied by the injection device.

Apart from promotional studies by device manufacturers presenting their own devices [23-27], no publicly available studies evaluating the performance of large volume injection devices and factors governing the accuracy and reliability of such devices are available to date. Therefore, this study aims to investigate and present influence factors such as flow rate, solution viscosities, temperature effects, fluid path design and shear behavior, and their effect on the accuracy in dosing of a high concentrated liquid monoclonal antibody (mAb) formulation by using two injection devices. Intermediate results and lessons learned are provided for further improvement and optimization of the performance of injection devices, and the presented results are intended to provide an approach on how to assess the performance of injection devices thoroughly and critically. Both investigated injection devices used within the study were developed by Weibel CDS AG as an on-body wearable injector offering an automated needle insertion system, comprising a 27G cannula and re-usable electronics. The drive mechanism is based on a valve-free rotary suction pump design with adaptable fit to variable primary packaging materials (e.g., glass cartridge, glass syringe, collapsable cyclic-olefin-copolymer (COC) Minibag).

This study additionally presents “in-use” protein stability data for a mAb solution that has passed the injection device. Subvisible particle formation quantified by fluid imaging as well as the formation of soluble aggregates (SEC) and chemically modified variants (IEX) were used as descriptive parameters to assess protein quality prior to and after delivery by the injection device. The incorporation of an in-

line filtration step to decrease the particle burden of the delivered solution was critically assessed with regards to the function and impact on the delivered dose.

2. Materials and Methods

2.1 Materials

Glycerol, glycine, L-methionine, polyethylene glycol PEG300, polysorbate 80, and sucrose were obtained from Merck KGaA (Darmstadt, Germany), and L-histidine and L-histidine monohydrochloride monohydrate from Alfa Aesar (Kandel, Germany). Miglyol® 812 was purchased from Caesar & Lorentz GmbH (Hilden, Germany). Highly purified water (HPW) (conductivity 0.055 µs/cm) was dispensed from an Arium®Pro purification system (Sartorius, Göttingen, Germany). An IgG 1 monoclonal antibody (mAb) was provided by Bayer AG (Wuppertal, Germany). The mAb was formulated at a protein concentration between 5 – 200 mg/mL protein in 10 mM histidine buffer at pH 5.5, further containing 130 mM glycine, 5% sucrose, 20 mM Methionine, and 0.05% polysorbate 80.

Two different injection devices were purchased from Weibel CDS AG (Waldstatt, Switzerland), both using a valve-free dual piston suction pump. A small device (3 mm pump diameter, approx. 10.5 µl/cycle) and a large device (9 mm pump diameter, approx. 190 µl/cycle) were compared in this study. The small device was developed for basal delivery of long acting drugs, such as e.g. insulin, as well as for the bolus delivery of drugs. The large device was especially developed to suit the needs of bolus delivery of large volumes of high concentrated biopharmaceuticals at high flow rates. The fluid path of the small device comprises a 27G cannula, which connects the drug-containing 3 ml glass cartridge with the pump unit. A second 27G needle is used as outlet towards the injection site. The large pump contained a male luer-connector as inlet to the pump mechanism. Connection of either a tubing by which the liquid is drawn from any suitable container, or of a syringe (e.g. 10 ml Normject (Henke-Sass Wolf GmbH, Tuttlingen, Germany)) to the luer-connector e.g. using a female-female

Combifix® adapter (B.Braun, Melsungen, Germany). A tubing is connected to the outlet of the pump mechanism, and towards the injection site a short 27G thin wall (TW) needle is attached to the tubing.

2.2 Injection device performance

The relative dose of a bolus injection was determined as delivered volume relative to the nominally delivered volume for each investigated device setting/experimental setup. A testbench (Weibel CDS AG, Waldstatt, Switzerland) was used as an external drive for the injection device, and the control software of the testbench offered different injection modes, delivering either a defined volume (e.g. 100 µl per dose) or a specified number of cycles (e.g. 5 delivery cycles). An analytical balance (Mettler Toledo AB304S, Gießen, Germany) was used to record the exact weight of each dose after collecting the liquid in a 2R glass vial. All experiments, if not stated otherwise, were conducted at room temperature (23°C ± 2°C).

First, each injection device was calibrated by weighing the amount of HPW delivered in 10 delivery cycles at a flow rate of 50 µl/min or 1 ml/min for the small and large pump, respectively. Thereby, the volume per cycle was determined and used as calibration setting in the control software of the testbench. The calibration allowed to account for fluctuations in the delivered volume per cycle between different injection devices and thereby ensured similar flow rates across different devices.

After calibration of each injection device, a volume of 100 µl or 5 delivery cycles of HPW for small and large pump, respectively, was set as target dose at varying flow rates (60 – 300 µl (small pump) or 1 – 3 ml/min (large pump)). Three replicates at each flow rate were conducted. The delivered volume was derived directly from the weight difference (ΔW) recorded by the balance between discrete doses and the density δ of the delivered liquid using Equation 1. The relative dose was calculated according to Equation 2. After ensuring accurate dosing of HPW across the range of flow rates, further

experiments with different protein drug formulations as described below were conducted with the injection devices.

Equation 1

$$delivered\ volume\ [l] = \frac{\Delta W\ [g]}{\delta\ [\frac{g}{l}]}$$

Equation 2

$$relative\ dose = \frac{delivered\ volume}{target\ volume} * 100\%$$

2.2.1 High protein concentration

The relative doses after delivering high concentrated monoclonal antibody (mAb) formulations ranging from 50 – 200 mg/ml mAb were determined for flow rates ranging from 60 – 300 µl/min or 1 – 3 ml/min for the small and large pump, respectively. For this purpose, three doses of 100 µl or 5 delivery cycles for the small and large pump, respectively, were set for each protein concentration, and relative doses were calculated according to Equation 1 and Equation 2. Each protein concentration was investigated for three injection device units per size, and data are presented as mean ± standard deviation.

2.2.2 Temperature

The effect of temperature on the relative doses was determined using a 100 mg/ml or 200 mg/ml mAb formulation for the small and large pump, respectively. Testbench, injection devices, and mAb formulations in the respective primary packaging materials were equilibrated either at 6°C in a cold chamber, at 23°C on the lab bench, or at 32°C in an incubator overnight. Injection device performance testing was performed within the cold chamber or incubator to keep the temperature constant during the tests. The solutions were delivered at flow rates ranging from 60 – 300 µl/min or 1 – 3 ml/min for the small and large pump, respectively. Three doses of 100 µl or 5 delivery cycles for the small and

large pump, respectively, were set as target, and relative doses were calculated according to Equation 1 and Equation 2. The influence of each injection temperature was investigated for three injection devices and data are depicted as mean ± standard deviation.

2.2.3 Inlet geometries

The inlet of the small pump is constructed in a way that the product container is connected via a 33 mm long 27G cannula to the pumping mechanism. To evaluate the influence of varying inlet diameters and lengths on injection device performance, the device housing of the injection device was opened and the original inlet cannula was detached from the pump mechanism. A 20G 1 ½", 27G 1 ½", 26G ½", 27G ½", or 30G ½" cannula (Sterican®, B.Braun) was attached, respectively, as new inlet to the pump mechanism using epoxy resin (UHU®plus endfest, UHU GmbH & Co. KG, Bühl/Baden, Germany). The Injection device performance was evaluated at a protein concentration of 100 mg/ml mAb with a flow rate ranging from 60 – 300 µl/min (compare section 2.2.1), after calibration and verification of the device performance with HPW.

2.2.4 In-line filtration

The prototype of the large pump used in this study contained a male luer-connector at the inlet to which the container with the drug product solution could be directly attached (i.e. syringe with luer-luer adapter) or via a tubing to another container (i.e. 2R vial). A 10 ml syringe was connected to the injection device using a female-female Combifix® adapter (B.Braun). Either no filter or a 13 mm Pall Acrodisc filter with a 0.22 µm polyethersulfone (PES) membrane (Pall Corporation, Ann Arbor, MI, USA) was placed between syringe and injection device. Alternatively, a Neodyne Neo filter with 0.22 µm nylon membrane (Pall Corporation) was connected directly to the injection device and the liquid was drawn through the filter from a 10R glass vial. The connections were sealed using silicone paste (Kurt

Obermeier GmbH & Co. KG, Bad-Berleburg, Germany) to prevent air leakage through the connectors since in-line filtration was conducted at the inlet and therefore at negative pressure.

2.2.5 Shear behavior

The effect of varying viscosity and rheological behavior on injection device performance was evaluated by pumping different solutes. The relative doses for different concentrations of mAb, glycerol, PEG 300 or Miglyol 812 were compared at a flow rate of 200 µl/min or 3 ml/min for the small and large pump, respectively. Three doses of 100 µl or 5 delivery cycles for small and large pump, respectively, were set for each solution, and relative doses were calculated according to Equation 1 and Equation 2. Each solution was investigated for three injection devices, and data are depicted as mean ± standard deviation.

2.2.6 In-use stability

Protein stability prior to and after pumping with the small and large pump was assessed by subvisible particle counting (section 2.5) as well as size exclusion chromatography (section 2.7) and ion exchange chromatography (section 2.8) to detect aggregation or chemical changes of the protein.

The small pump was fitted to the Testbench and a flow rate of 200 µl/min was used for the in-use stability testing. 2 ml of a 100 mg/ml mAb formulation were filled into a 3 ml glass cartridge and the in-use stability testing was conducted using a stoppered cartridge as well as an open cartridge configuration in order to investigate particle formation through the pumping action (schematic drawing Figure 2A). Aliquots were drawn for analysis from the cartridge prior to and after pumping, and the pumped material (1 ml at 200 µl/min) was collected in a 2R vial. In order to draw the aliquot from the stoppered cartridge, the septum was pierced with a 21 G needle and the stopper was removed by blowing in 0.22 µm filtered air into the air pocket of the cartridge, thereby avoiding

foaming. The cartridge was stoppered a second time after drawing the aliquot prior to pumping and the cartridge was subsequently used for the experiments.

The large pump was fitted to the testbench and protein stability was investigated after pumping the solutions with a flow rate of 1 ml/min from a 10R glass type I vial used as a reservoir. The solution was aspirated by the pump through a tubing connected to the luer-inlet (schematic drawing Figure 2B). A 100 mg/ml mAb formulation was drawn from the vial using a short tubing, and the pumped material (1 ml at 1 ml/min) was collected in a 2R vial. Protein stability was assessed prior to and after pumping.

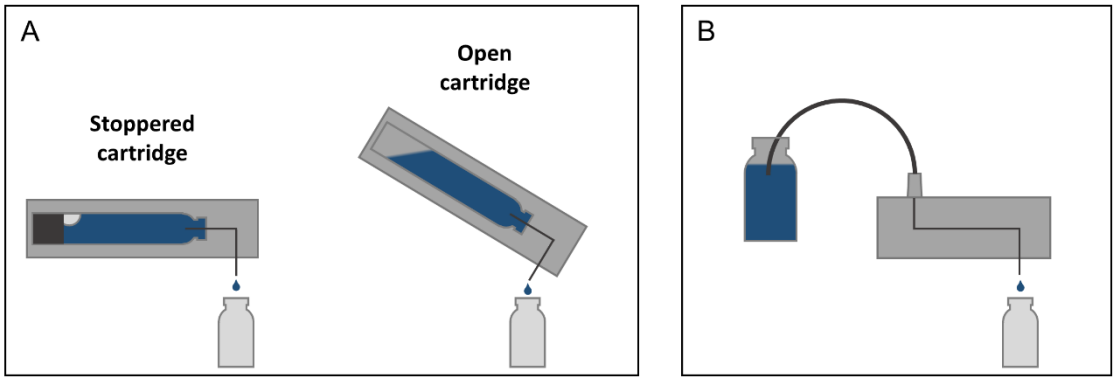

Figure 2: Schematic drawing of A. the small pump with stoppered and open cartridge and B. the large pump during in-use stability testing. Dimensions are schematic and not representative of real dimensions.

2.3 Density measurement

The density of glycerol-HPW mixtures, PEG 300-HPW mixtures, Miglyol 812 and HPW was determined with a pycnometer at 20°C. The pycnometer was filled without air bubbles and weight difference as well as the volume of the pycnometer were used to calculate the density of the sample according to Equation 3.

Equation 3

$$density\ \delta\ \left[\frac{g}{l}\right] = \frac{weight_{pycnometer,\ filled}\ [g] - weight_{pycometer,\ empty}\ [g]}{volume\ [l]}$$

The density of high concentrated protein samples was determined by using a 100 µl direct dispensing pipet. Three dispenses were performed for each concentration and the density (mean ± standard deviation (SD)) was calculated by dividing the recorded weight by the nominal dispensing volume of the pipet (100 µl).

2.4 Determination of viscosity and rheological behavior

2.4.1 mVROC

The viscosity of the samples was measured using a mVROC viscometer (Rheosense Inc., San Ramon, CA, USA) equipped with a RA05-100-087 flow cell. Viscosity was determined at 20°C and at a flow rate of 50 µl/min resulting in a corresponding shear rate of 632 1/s. Samples were filled in a 250 µl-Hamilton syringe without introducing air bubbles.

2.4.2 Plate-cone rheometer

Approximately 0.55 ml sample were loaded between a plate and cone (50 mm diameter, 1° angle) with a gap of 0.5 mm in a MCR100 rheometer (Anton Paar, Graz, Austria). Viscosity was measured while increasing the shear rate from 300 1/s to 5000 1/s at 23°C.

2.5 Subvisible particle counting

Subvisible particles in the range of 1 – 80 µm were analyzed using a FlowCam 8100 (Fluid Imaging Technologies, Inc., Scarborough, ME, USA), equipped with a 10x magnification and a FOV80 flow-cell (80 µm × 700 µm). 150 µl sample were analyzed at a flow rate of 0.15 ml/min and an auto image frame rate of 9 frames/second. Particles were identified by thresholds set to 10 and 13 for light and dark pixels, respectively, and a distance to the nearest neighbor of 3 µm. Particle size was reported as

equivalent spherical diameter (ESD) using VisualSpreadsheet® 4.7.6 software for data collection and evaluation.

2.6 Submicron particle counting

Submicron particles were analyzed by tunable resistive pulse sensing (TRPS) on a qNano Gold system (IZON Ltd., Christchurch, New Zealand) using a NP300 nanopore with an analysis range of 150 - 900 nm. Submicron particle levels were determined and evaluated as described in chapter 5.

In brief, a radial stretch of 47 mm was applied to the nanopore and the nanopore was coated using coating solution and protocol provided by IZON Ltd. The coating solution was removed and upper and lower fluid cell were rinsed with HPW and dried with filtered (0.22 µm) pressurized air without removing the nanopore. 70 µl electrolyte (placebo + 50 mM NaCl) were added to the lower fluid cell. 35 µl sample (mAb solution or placebo + 50 mM NaCl) were added to the upper fluid cell and measurement of submicron particles was conducted at a pressure setting of +10 mbar at a current of approximately 100 nA.

Detection of less than 10 particles in electrolyte within 10 min measurement duration were used as requirement to ensure cleanliness of the system. Sample measurements were stopped and data were analyzed once at least 500 particles or a maximum recording time of 10 minutes were reached for protein samples or calibration beads. Upon blockages, the recording was paused and the blockage was removed according to the manufacturer's advice [28] before continuing the recording.

2.7 Size exclusion chromatography (SEC)

SEC was performed on a Dionex Ultimate 3000 system (ThermoFisher Scientific, Dreieich, Germany) after dilution of the samples to a concentration of 5 mg/ml using filtered (0.22 µm) placebo. 2 µl sample were injected on a Waters Acquity UPLC® Protein BEH SEC column (200Å, 1.7 µm, 4.6 × 150

mm, Waters Corporation, Milford, MA, USA) and the elution of the mAb was detected at 280 nm with a VWD-3400RS UV detector (Thermo Fisher). The mobile phase was 50 mM sodium phosphate (pH 6.5) with 300 mM sodium chloride at a flowrate of 0.3 ml/min. Peaks were integrated using Chromeleon V7.2 (ThermoFisher Scientific) and the relative areas of the monomer, high molecular weight aggregates (HMWA) and lower molecular weight species (LMWS) were calculated in percentage.

2.8 Ion exchange chromatography (IEX)

mAb samples were diluted to 5 mg/ml using filtered (0.22 µm) placebo, and 10 µl were injected on a ProPac WCX-10 Analytical Column (4x250 mm) with a ProPac WCX-10G Guard Column (4x50 mm) (Thermo Fisher) attached to a Dionex Ultimate 3000 system (ThermoFisher Scientific) with a VWD-3400RS UV detector (ThermoFisher Scientific). Detection was performed at a wavelength of 280 nm. Mobile phase A was 20 mM sodium phosphate (pH 6.5) and mobile phase B was 20 mM sodium phosphate (pH 6.5) with 300 mM NaCl at a flow rate of 1 ml/min in a linear gradient mode (time in min vs. % B = 0:0, 5:0, 35:30, 36:100, 46:100, 47:0, 57:0). Chromatograms were integrated with Chromeleon V7.2 (ThermoFisher Scientific) and the relative areas of the acidic variants, main peak, and basic variants were calculated in percentage.

2.9 Filter hold-up volume

The hold-up volume of 4 mm, 13 mm, and 25 mm PES filter with 0.22 µm pore size was assessed by filtration of 1 ml HPW. The weight of each filter was recorded prior to filtration, after filtration and after 1 ml air purge. The hold-up volume was calculated as difference between the weight prior to and after filtration.

3. Results

3.1 Reducing sample consumption for device studies and maintaining high data quality

Measuring injection device performance and assessing precision and recovery of injection devices for highly concentrated biopharmaceuticals, which are intended to be given as a bolus, is prone to become time and material consuming for large bolus injections. The investigation of these factors while using as little sample as possible could be beneficial, e.g. by evaluating different injection settings by delivering multiple small doses from a single container.

However, caution has to be taken when using a non-continuous pump such as rotary lobe pumps or valve-free dual piston pumps, for example. The non-continuous delivery of fluid required a careful consideration of the delivered dose relative to the volume delivered per cycle. The presented study investigated two types of pump bodies delivering approx. 10.5 µl/cycle for the small and 190 µl/cycle for the large pump. At 10.5 µl/cycle and a dose of 100 µl, resulting in 9.5 delivery cycles, the systematic error of the small pump was calculated to be 6.4% for a triplicate measurement since the filling and ejection of the fluid may not end up in the same weighing. This error is low compared to other wearable insulin infusion pumps [29] and can be accepted for later experiments. With 5 delivery cycles for the large pump per weighing, the systematic error was excluded entirely, and 950 µl were delivered per dose.

Sample consumption during injection device performance testing could be reduced as low as 100 µl per data point, while only introducing a minor systematic error of 6.4% for the small pump due to non-integral number of delivery cycles.

3.2 Influence of protein concentration and associated high viscosity on injection device performance

Antibody formulations for subcutaneous delivery are often formulated at a high protein concentration. High protein concentrations lead to an exponential increase in viscosities as known from literature and as shown in Figure 3 for the mAb used in the presented study [30, 31].

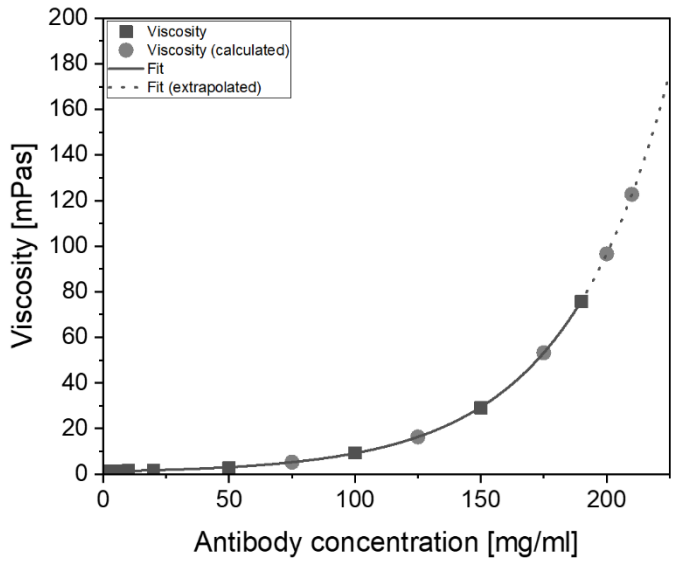

Figure 3: Viscosity of the mAb at different protein concentrations.

The observed relative doses for the small device highly varied with changes in viscosities and flow rates (Figure 4 A). The data achieved were evaluated based on an exemplary minimal relative dose of 80 %. A concentration of 50 and 75 mg/ml did not impact relative doses across the whole range of flow rates up to 300 µl/min. Increasing the concentrations to 100 and 125 mg/ml resulted in 100% relative doses at the lowest flow rate of 60 µl/min, but strongly decreased relative doses of 60% and 40% at the highest flow rate, respectively. At 150 mg/ml, a relative doses of only 80% was achieved at the lowest flow rate, and dramatically decreasing injection device performance was found at higher protein

concentrations and flow rates. A relative dose of more than 80% was achieved either for up to 150 mg/ml (30 mPa·s) at a flow rate of 60 µl/min or up to 125 mg/ml (15 mPa·s) at 100 µl/min. Higher flow rates or mAb concentrations were not suitable due to the high viscosities of the mAb formulations.

Injection device performance of the large device were concentration and therefore viscosity dependent as well (Figure 4 B), but to a much lower extent due to optimized fluid paths. Hereby, all tested concentrations reached a relative dose of 88% and higher at any flow rate up to 3 ml/min.

In general, an indirectly proportional relationship between relative dose and protein concentration/viscosity was observed. The following aspects were limiting for the filling of the pump chamber of the valve-free dual piston pump during the filling cycle: high solution viscosities or high flow rates. To improve the injection device performance for a drug-device combination, either the reduction in flow rate or the reduction of protein concentration and corresponding viscosity is suitable. Formulation approaches to reduce solution viscosity, while remaining at a constant protein concentration are considered feasible, as well as increasing the device performance [32]. Besides accurate dosing, the duration for a bolus injection of a biopharmaceutical product is considered to be an important factor in evaluating injection device performance.

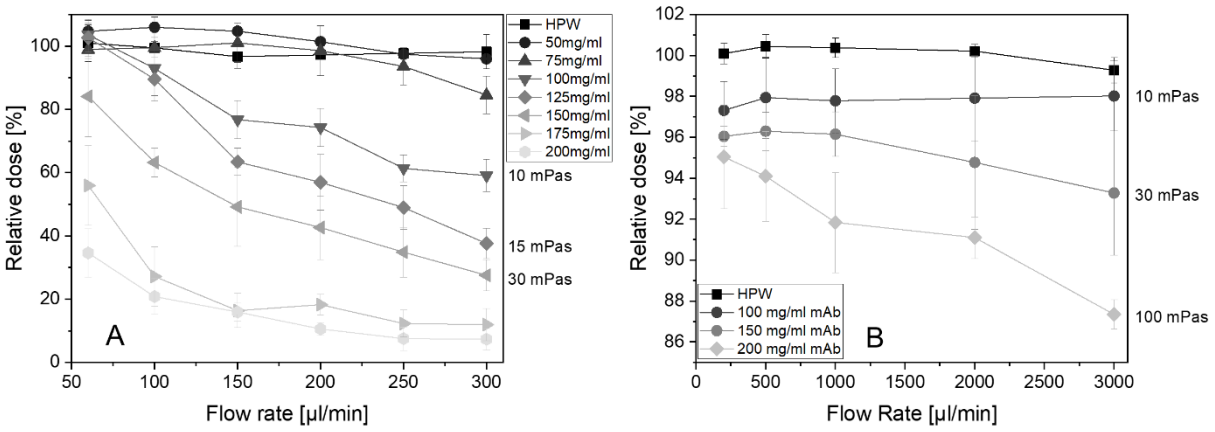

Figure 4: Influence of protein concentration on relative dose. A.) small injection device, B.) large injection device. Mean ± standard deviation of three doses from three separate injection devices per data point are depicted.

The total duration for the application of a 3 ml dose of the investigated antibody was calculated based on the measured relative doses for the small injection device at different protein concentrations and different flow rates (Figure 5). At concentrations of 100 – 150 mg/ml, a faster application of a 3 ml dose was only visible up to 200 µl/min. Above 200 µl/min, the decrease in relative dose led to an almost constant application time regardless of the injection speed setting.

Now, the duration for the application of a 450 mg dose of the antibody was calculated for concentrations ranging from 50 – 150 mg/ml (Table 3). Lower concentrations required higher injection volumes, whereas less volume is needed at high protein concentrations. Taking the relative doses observed at a flow rate of 200 µl into account, the shortest duration was found between 75 – 125 mg/ml. Increasing the concentration to 150 mg/ml led to longer injection durations despite lower injection volume, due to drastically reduced relative doses (Figure 4A). However, decreasing the protein concentration even further (e.g. 50 mg/ml) would result in 100% relative dose, but with a very high injection volume and thereby longer delivery time.

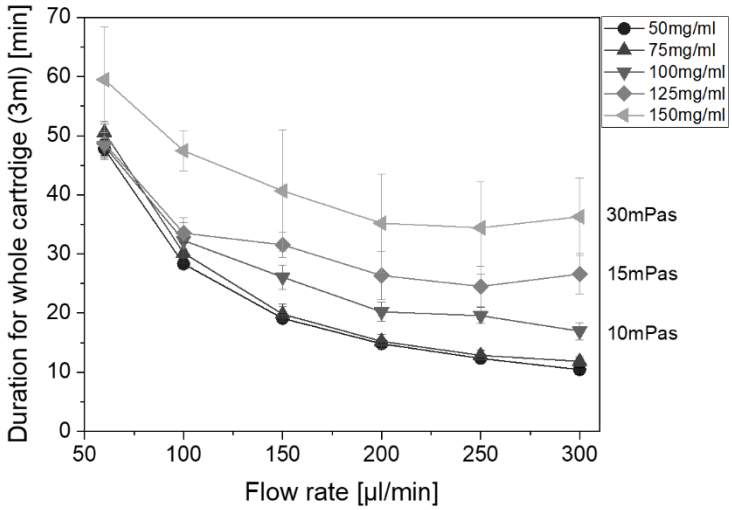

Figure 5: Duration for the application of a 3 ml dose using the small injection device. Mean ± standard deviation of three doses from three separate injection devices per data point depicted.

Table 3: Application options for a 450 mg mAb dose and subsequent injection durations at 200 µl/min.

Dose [mg]	c_{mAb} [mg/ml]	Volume [ml]	Duration at 200 µl/min [min]
450	50	9.00	44.4
450	75	6.00	30.4
450	100	4.50	30.3
450	125	3.75	31.6
450	150	3.00	35.2

For large bolus injections, the concept that a reduced relative dose can be compensated by increasing the run time of the injection device could be applied. This may not always be feasible, depending on inter-unit-variability of the injection devices as well as inter-batch variability of the drug product. Precise basal rate adjustment cannot be assured, if the relative dose is affected by the solution viscosity to a large extent.

3.3 Influence of shear behavior on injection device performance

The effect of different solutes (e.g., protein, glycerol-water mixtures, and PEG300-water mixtures) on injection device performance in a similar range of viscosities was investigated using both a small and large injection device at constant flow rates of 200 µl/min and 3 ml/min, respectively. Besides the impact of solution viscosity described in section 3.2 , the impact of Newtonian vs non-Newtonian fluids on injection device performance was evaluated.

A drastic influence of solution viscosity was found for the small pump, and a reduction to ≤ 50% relative dose was reached at around 15 - 20 mPas, independent of the liquid tested (Figure 6 A). On the contrary, even at high viscosities of up to 100 mPas, relative doses of more than 50% were achieved for all solutes by using the large pump at a flow rate of 3 ml/min (Figure 6 B). For a mAb formulation at 200 mg/ml (100 mPas), a relative dose of > 85% was observed. However, despite comparable "starting" viscosities of the tested solutes, differences in relative doses of up to 30% were observed for the large pump (Figure 6B) and therefore shear behavior was evaluated additionally (Figure 7). The antibody turned from Newtonian at low concentrations to a shear thinning behavior at higher concentrations, which was also reported for other proteins [19, 20]. Newtonian behavior was observed for PEG300 and Miglyol 812 whereas shear thickening behavior was observed for glycerol-HPW and PEG300-HPW mixtures. Although viscosity differences depending on the shear rate were small, they may play an important role in the actual injection device due to much higher shear rates present during injection. The apparent shear rate of a Newtonian liquid during injection can be calculated, taking the volume flow and the inner diameter of a tubing or needle into account [33]. For a 27G thin wall needle, as used in the large injection device, a shear rate of around 36'000 1/s was calculated for a flow rate of 3 ml/min, respectively. This exceeded by far the limit of the rheometer's capabilities, which could assess the shear behavior only up to 5000 1/s. Nevertheless, the effect of shear thinning or shear

thickening behavior on injection device performance is expected to me more pronounced at higher flow rates.

Shear behavior therefore plays an important role, when considering the relative doses achievable for a particular drug-device combination. Especially for high concentrated mAb solutions, relative doses better than anticipated from surrogates (e.g. PEG300-HPW and glycerol-HPW mixtures) could be expected due to the shear thinning behavior of high concentrated mAb solutions. Limitations of the device could possibly be altered by changes in fluid path design or changes in flow rate.

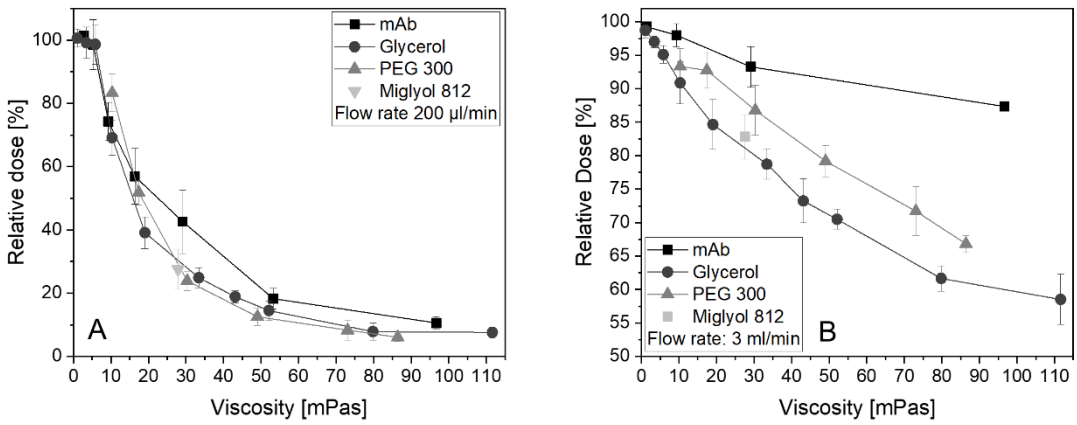

Figure 6: Influence of different solutes on relative dose. A.) small injection device, B.) large injection device. Mean ± standard deviation of three doses from three separate injection devices per data point depicted.

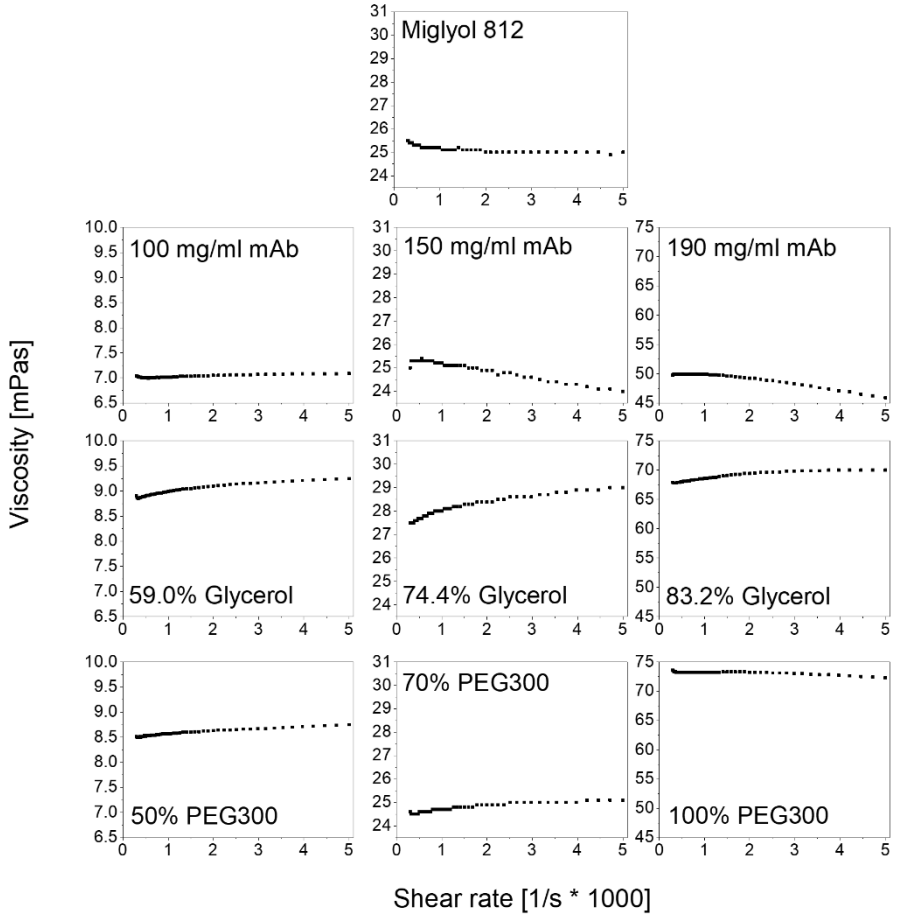

Figure 7: Shear behavior of mAb solutions, Glycerol-HPW mixtures, PEG300-HPW mixtures and Miglyol 812. Rows: different solutes. Columns: comparable viscosity ranges.

3.4 Changing inlet geometries to adapt injection devices for high viscosities

The delivery of liquids by using a suction pump, such as the valve-free dual piston pump used in both injection devices, includes several steps during pumping. The filling step of the pump chamber was found to be a critical step influencing overall performance of the injection device. The drastic decrease in relative doses observed for the small pump upon delivering high concentrated mAb solutions was considered to be caused by a non-ideal filling of the pump chamber during the filling step. Therefore, a reduction in flow rate, subsequently resulting in a prolongation of the filling step, provided better relative doses due to improved filling of the chamber (section 3.2).

We investigated the effect of different inlet geometries on the observed relative doses and exchanged the inlet cannula from the original 27G cannula to other cannulas providing larger inner diameters or shorter lengths. Based on the Hagen-Poiseuille equation [22], a reduction of the length of the cannula leads to a linearly increased volume flow through the cannula, while enlarging the radius of the cannula increases the volume flow through the cannula by the power of 4. The ratio of radius and length "R" according to the Hagen-Poiseuille-equation was used as a parameter to describe the expected volume flow compared to the original cannula. For normalized ratios > 1, an increased volume flow through the cannula compared to the original cannula is expected, which leads to higher relative doses.

The original cannula (33 mm, 27G) was replaced by a 27G 1 ½" or 20G 1 ½" cannula (Figure 8 A) and relative doses were determined. Similar results compared to the original cannula were obtained with the 27G 1 ½" cannula. Increasing the diameter of the cannula with a 20G needle resulted in a relative dose of 100% at up to 300 µl/min. The filling of the pump chamber was sufficient in all settings, ensuring good injection device performance, as expected from theoretical considerations based on the Hagen-Poiseuille-law (Table 4).

Then, the original cannula was replaced by shorter lengths with 27G ½", 26G ½" and 30G ½" cannulas (Table 4). Both the 27G ½" and 26G ½" needle theoretically provide an increased volume flow based on Hagen-Poiseuille-equation due to the shorter length (Table 4). Accordingly, the observed relative doses for the 27G cannula increased and > 90% relative dose were determined at all flow rates, compared to 60% relative dose at 300 µl/min with the original design (Figure 8 B). Increasing the diameter to 26G led to similar results, but better performance can be expected for higher flow rates and especially higher viscosities (Table 4). Decreasing the diameter to 30G expectedly led to drastically reduced relative doses of only 75% and 30% at 100 µl/min and 300 µl/min, respectively.

Careful inlet design can be used to increase the performance of non-continuous pump based injection devices, which require suction-based filling of the pump chamber during pumping. Increasing the diameter of the inlet cannula of the pump is the most powerful way of increasing volume flow during the filling step. Decreasing the length may also be suitable, however, in practice a very short cannula may not always be feasible due to the placement of the compounds within the injection device housing. A minor drawback of a larger inlet diameter is the increased hold-up volume. However, exchanging the original 27G cannula to a 20G 1 ½" cannula, which can provide drastically higher volume flow, added only 8.51 µl of additional hold-up volume in the tested devices. For an intended application of several ml of a mAb solution, the additional hold-up volume could be neglected.

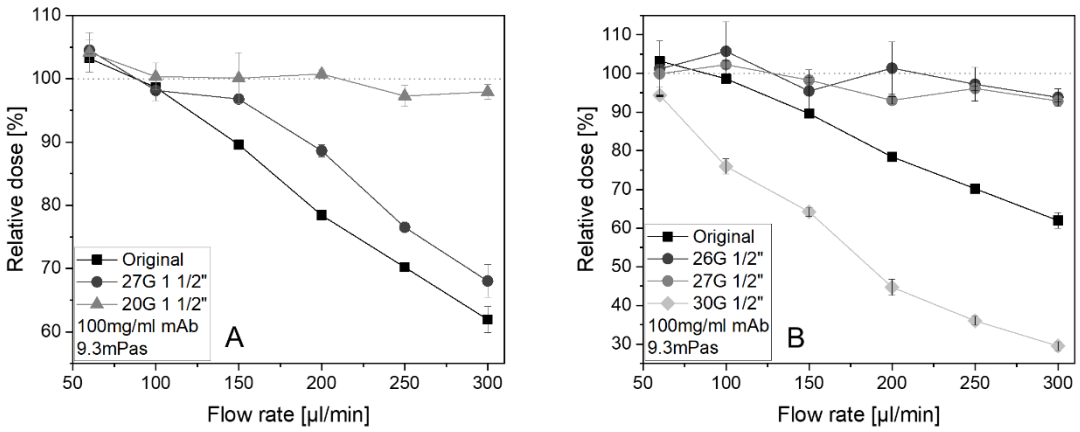

Figure 8: Optimization of inlet design by changing inlet cannulas. A.) Larger diameter at similar length to original. B.) Shorter length than original. Mean ± standard deviation of three doses from three separate injection devices per data point depicted.

Table 4: Inlet cannula dimensions and calculated effect on filling efficiency based on the Hagen-Poiseuille-law based in the ratio between radius and length "R" of a cannula.

Cannula type	Cannula length [mm]	Cannula inner diameter [mm]	Holdup-volume (inlet) [µl]	Additional Holdup-volume [µl]	$R = \frac{cannula\ radius^4}{cannula\ length}$ (normalized to original)
27G original	33.0	0.184	0.88	± 0	1.0
27G 1 1/2"	38.1	0.184	1.01	+ 0.14	0.9
20G 1 1/2"	38.1	0.560	9.38	+ 8.51	74.3
26G 1/2"	12.7	0.232	0.54	- 0.34	6.6
27G 1/2"	12.7	0.184	0.34	- 0.54	2.6
30G 1/2"	12.7	0.133	0.18	- 0.70	0.7

3.5 Influence of temperature on injection device performance

As injection devices can foster self-administration by the patient, handling differences among the patients may occur due to the typical storage of biopharmaceuticals at 2 – 8°C [9]. In one scenario, the patient would take both the injection device and drug out of the refrigerated storage and start the application immediately. Other patients may equilibrate both at room temperature for a certain period of time (e.g. 30 min) and in other cases, the injection device could lie at a warm spot, causing the device and drug container to heat up to higher temperatures. In case it matters, the device could be programmed to start the injection only after allowing the device and drug container to get equilibrated to skin temperature of 32°C.

In this study, the differences in injection device performance based on three different injection temperatures of 6°C, 23°C, and 32°C were investigated for the small and large pump using a 100 mg/ml

or 200 mg/ml mAb formulation, respectively (Figure 9). Injections at 23°C and 32°C were more effective for the small pump. With a flow rate of ≥ 150 µl/min, a difference in relative dose of approximately 40 percentage points was observed between injections at 6°C and 32°C. A higher temperature and therefore a decreased viscosity drastically improved the relative doses delivered via the small pump (section 3.2) due to the flow restrictions of the inlet (section 3.4). At a flow rate of 150 µl/min, a relative dose of 100% was observed after equilibration to 32°C, whereas a relative dose of only 60% was observed at 6°C. The large pump was not affected in its performance by different temperatures due to improved inlet geometries and less viscosity dependence.

This demonstrates the importance of correct training of the patient for self-administration by the health care professionals in order to reduce handling errors during administration. Additionally, improved fluid path designs or the implementation of a temperature equilibration step after initializing the injection are expected to reduce the temperature-dependent injection device performance.

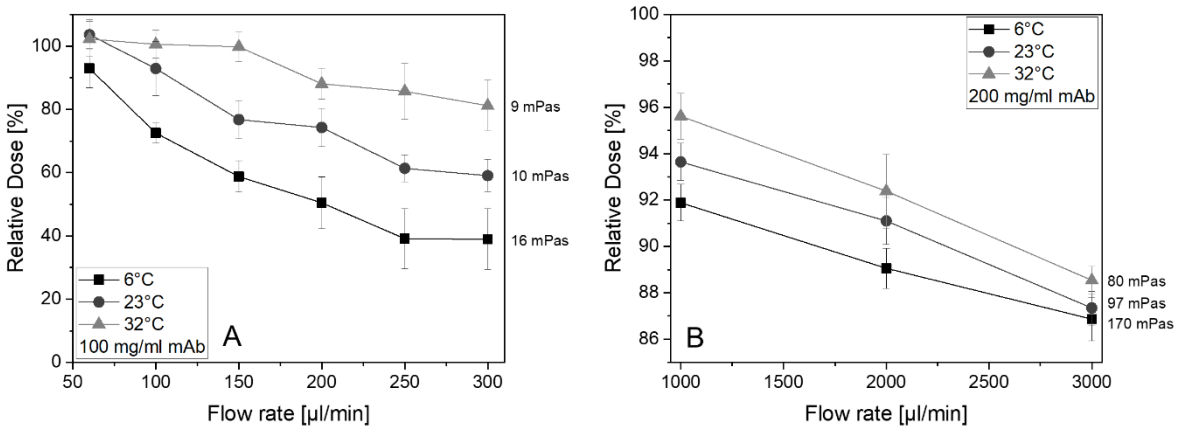

Figure 9: Influence of injection temperature on relative dose. A.) Small injection device, B.) large injection device. Mean ± standard deviation of three doses from three separate injection devices per data point depicted.

3.6 Influence of pumping on protein stability

The influence of the pumping procedure on protein stability (in-use stability) was investigated in order to evaluate the potential stress applied to the protein during pumping with the small and large injection device [9, 34, 35]. For this purpose, subvisible particle levels, aggregation and fragmentation of the protein by SEC as well as chemical denaturation by IEX were assessed in a 100 mg/ml mAb formulation prior to and after pumping at 200 µl/min or 1 ml/min with the small or large injection device, respectively.

Neither an increase of soluble aggregates or fragments, nor the formation of acidic or basic species was found during delivery of a 100 mg/ml mAb solution with the small or large pump, resulting in unchanged monomer and main peak contents (compare Table 5).

Table 5: SEC and IEX prior to and after pumping with injection device.

		Prior pumping	After pumping
Monomer content by SEC [%rel.area]	3mm pump	93.0 ± 0.1	93.0 ± 0.1
	9mm pump	93.0 ± 0.1	92.9 ± 0.1
Main peak content by IEX [%rel.area]	3mm pump	70.0 ± 0.8	69.8 ± 1.6
	9mm pump	70.9 ± 0.3	70.6 ± 0.7

Subvisible particle levels ≥ 1 µm were analyzed after pumping highly purified water, placebo and a 100 mg/ml mAb solution with the small (Figure 10A) or large (Figure 10B) pump. Subvisible particle levels ≥ 10 µm and ≥ 25 µm are provided in Figure 13S and Figure 14S in the supporting information. Comparably low particle levels were found after pumping of HPW or placebo with the small pump, whereas using a 100 mg/ml mAb formulation resulted in drastically increased particle levels in the

collected material after pumping (Figure 10A). The large pump on the other hand showed much less particle formation during the pumping process at 1 ml/min after delivering a 100 mg/ml mAb solution compared to the mAb sample from the small pump, but still a considerable increase relative to HPW or placebo (Figure 10B). Besides differences in the fluid path between both devices, the primary packaging material differed as well. Due to the early development stage of the large pump, a glass vial was used as a reservoir and connected to the luer-inlet of the large pump through a short tubing, whereas a 3 ml glass cartridge was used as primary packaging material for the small pump.

The closed glass cartridge caused the stopper to move along the glass barrel during pumping, and therefore the influence of the stopper movement was investigated in additional experiments (cf. Figure 2 and Figure 11 below as well as Figures 15S and 16S in the supporting information). To determine the cause of subvisible particle formation after pumping of a 100 mg/ml mAb solution with the small pump, the particle concentration was determined in: (i) a re-opened cartridge prior to pumping (“prior”), in the collected solution afterwards (“pumped”), and in the again re-opened cartridge afterwards (“remaining”); (ii) an open cartridge prior to pumping (“prior”), in the collected solution afterwards (“pumped”), and in the open cartridge afterwards (“remaining”).

A low particle level in 100 mg/ml mAb solutions was found prior to pumping in filled and stoppered glass cartridges after re-opening. The pumping of the solution resulted in increased particle levels ≥ 1 µm in both, the collected material and, to a similar extent, in the liquid remaining in the 3ml glass cartridge (Figure 11). Due to the pumping process, the stopper in the siliconized 3 ml glass cartridge moved, possibly causing silicone oil migration into the mAb solution as observed after morphological analysis of the obtained FlowCam images (data not shown)[36]. Further, an open cartridge setup was used, excluding the movement of the stopper as a factor (Figure 2 and Figure 11). Here, particle levels did not increase in the cartridge during the pumping process (Figure 11). Furthermore, particle level in

the pumped and collected solution was decreased compared to the regular stoppered setup. Thus, the pumping process itself was found to cause an increase the particle level to a certain extent, but additionally silicone oil removal from the glass wall and the stopper surface due to stopper movement contributed to the subvisible particle levels in the pumped and remaining solution as well. Of particles larger than 5 µm, more than 50% were classified as silicon-oil like particles according to a method described by Strehl et al.[36].

In summary, particle formation during pumping of a 100 mg/ml mAb solution using both injection devices was observed, and thorough investigations of particle formation were conducted to identify causes of particle formation. Besides the pumping action and the injection device itself, the primary packaging material was also found to have an impact on subvisible particle level of the pumped solution. Improved product quality of the injected solution may be achieved by applying low stress conditions during the delivery of the drug (e.g. large diameter cannula/tubing as in the large pump), but also through suitable primary packaging material (e.g. improved siliconization process, or switch to a collapsible PPM without moving parts).

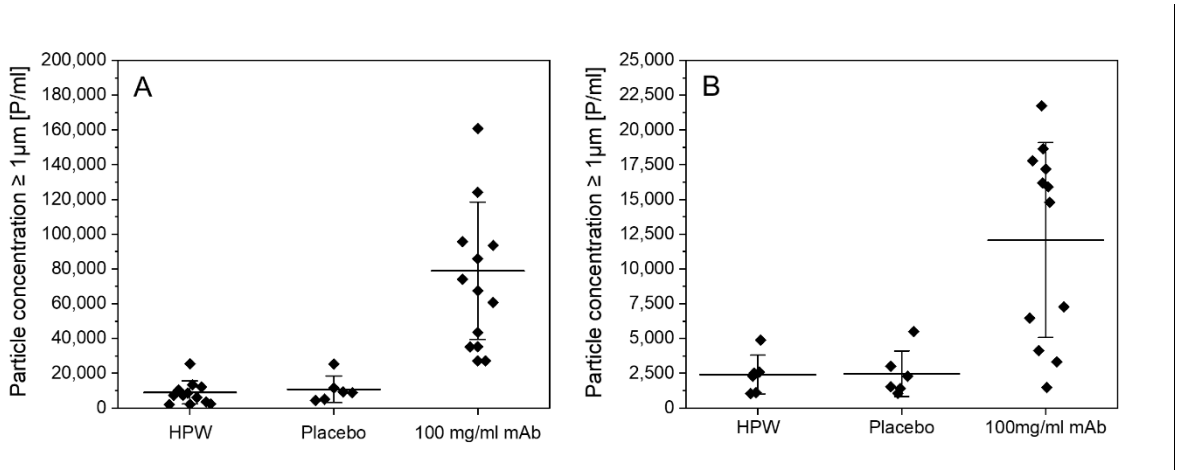

Figure 10: Subvisible particle levels ≥ 1 µm after pumping highly purified water, placebo, or 100 mg/ml mAb using A.) the small pump or B.) the large pump. A new injection device was used for each data point and mean ± standard deviation (n = 6 – 14) are depicted by line and whiskers.

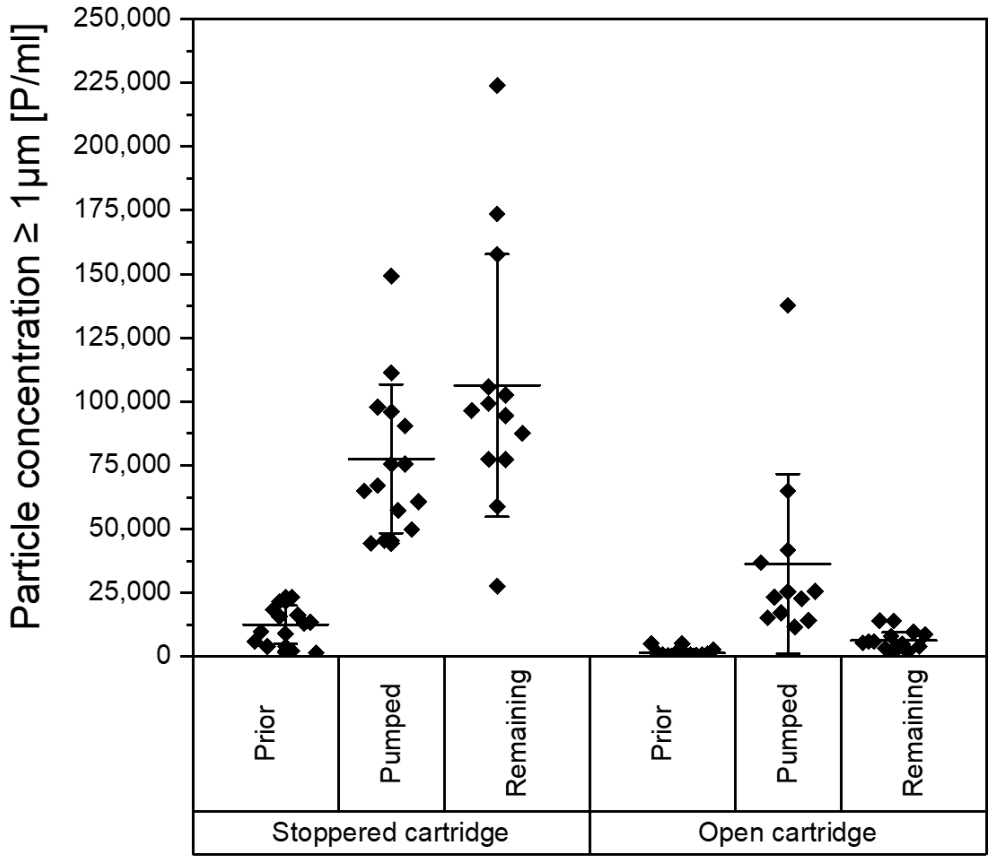

Figure 11: Contribution of pumping action and primary packaging materials of the small pump to subvisible particle levels ≥ 1 µm. A new injection device was used for each data point and mean ± standard deviation (n = 11 – 14) are depicted by line and whiskers.

3.7 Incorporation of an in-line filtration in large-volume s.c. injection devices

The incorporation of an in-line filtration step into the injection devices was investigated in order to reduce particle burden and improve product quality of injectable drugs [37, 38]. Due to size limitations, large filter geometries are not suitable for injection devices, therefore, smaller filter sizes of 4-15 mm diameter were investigated in this study and compared to a 25 mm diameter filter. Pre-tests with syringe filtration determined the effect of filter size, reduced flow rates and high protein concentration on subvisible as well as submicron particle counts (Figure 12 A-C). An efficient reduction of subvisible particles, as described in literature [39], was achieved with all 0.22 µm filter sizes from 4 mm to 25 mm diameter (Figure 12B). Additionally, a large fraction of 300 – 1000 nm submicron particles were

removed from heat stressed mAb solutions by a 0.22 µm filtration (Figure 12C). Flow rates between 10 – 3000 µl/min, tested with syringes, were equally efficient in reducing particle burden of stir stressed mAb solutions (data not shown). Up to 10 ml of a 100 mg/ml mAb solution (η = 10 mPas) could be filtered through a 13 mm PES syringe filter at a flow rate of 120 µl/min without an increase in injection force (data not shown). However, a drawback of in-line filters in general is their hold-up volume of 100 – 150 µl (4 mm and 13 mm syringe filter) up to 600 µl (25 mm syringe filter) as shown in Figure 12A.

A 13 mm syringe filter (Acrodisc, 0.22µm PES membrane) was the most promising option from the pre-tests, combining sufficient filtration performance with low hold-up volume and a small geometry, which could allow the incorporation into an injection device. As a proof of concept, a 13 mm syringe filter (Acrodisc, 0.22µm PES membrane) as well as a 15 mm filter designed for infusion sets (Neodyne Neo, 0.22µm nylon membrane) were fitted between reservoir and the luer-cone at the inlet of the large pump. Relative doses were determined after delivering placebo and 100, 150, and 200 mg/ml mAb solutions at 1 ml/min (Figure 12D). The incorporation of a 13 mm syringe filter (Acrodisc, 0.22µm PES membrane) led to a reduced relative dose of 80% and 40% at 100 mg/ml and 150 mg/ml mAb, respectively, compared to 100% relative dose without filter. At a protein content of 200 mg/ml, a relative dose of about 10% was observed, due to insufficient chamber filling caused by flow restrictions of the sterile filter. Another filter-type, designed for in-line use in infusion sets containing a 0.22 µm nylon membrane (Neodyne Neo) seemed more suitable as relative doses were 75% at 150 mg/ml and around 50% at 200 mg/ml. However, it would require further investigation for use with proteins due to known protein binding properties of nylon membranes [40]. The reduction in relative doses after incorporation of both in-line filters was related to flow restrictions caused by the filters during the filling of the pump chamber.

The feasibility for implementing an in-line filter into the fluid path of an injection device was successfully proven, and the reduction of subvisible as well as submicron particles through a 0.22 µm filtration was demonstrated. However, an in-line filter attached on the inlet of the pump led to a reduction in relative dose for high mAb concentrations at medium to high flow rates of 1 ml/min. Nevertheless, the implementation of an in-line filter into a large volume injection device is encouraged by the benefits it can provide. The attachment to the outlet side of pump, for example, is expected to improve overall relative doses as the solution would be filtered by over-pressure instead of under-pressure as used in this study.

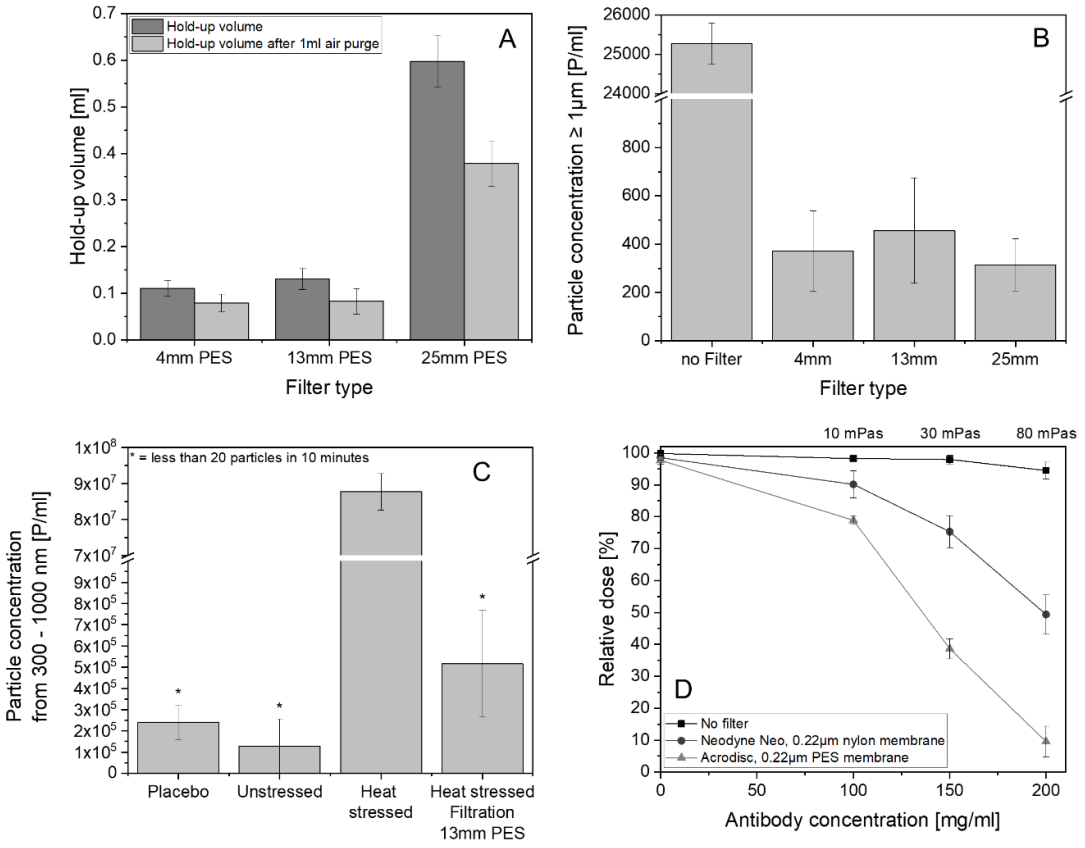

Figure 12: In-line filtration of antibody solutions. A.) Hold-up volume of selected filters, B.) Reduction of subvisible particles by filtration of stir stressed 5 mg/ml mAb, C.) Reduction of submicron particles by filtration of heat stressed 5 mg/ml mAb, D.) Relative doses with in-line filters at the inlet of the large injection device at a flow rate of 1 ml/min. Pretests with syringe filtration (A-C) and implementation in injection devices (D).

4. Conclusion

This study was laid out to investigate technical limitations of drug-device combinations under the aspect of large volume subcutaneous delivery a biopharmaceutical drug product. Main focus was to assess and potentially improve the accuracy of two injection devices to deliver a high concentrated monoclonal antibody solution. By using a valve-free dual piston suction pump design, the investigated injection devices can be adapted to a wide range of primary packaging materials of variable size and shape. Influencing factors such as solution viscosity, flow rate, fluid path design and temperature were critically evaluated, and solutions to improve dosing accuracy are provided.

Along with increasing protein concentration, the increased solution viscosity at high protein concentrations is the main factor impacting the observed relative doses. Especially for high protein concentrations and high flow rates a drastic reduction in relative doses was observed which could be improved by either reducing the protein concentration or the flow rate set-point on the device. Due to the drastic reduction in relative dose observed at high flow rates, a plateau in injection duration for a 3 ml dose became apparent at flow rates exceeding 200 µl/min for the small pump type. A careful balancing of solution viscosity and flow rate of the injection device can therefore be utilized to achieve the shortest duration of injection. For example, the shortest injection time for the delivery of a 450 mg dose of the mAb with the small pump was calculated at a flow rate of 200 µl/min and 100 mg/ml protein concentration.

The observed limitations were mainly related to an insufficient filling of the pump chamber of the investigated valve-free dual piston suction pump during the filling cycle. Drastic improvements of the injection device performance were observed when the inlet-design of the injection device was altered and either shorter cannulas or cannulas/tubes with larger inner diameter were used. Comparing the large and small pump used in the study, the suggested optimizations of the fluid path were already

adapted in the large pump by using only a short 27 G thin wall needle on the injection side and large diameter tubing to connect the different parts of the injection device.

Other factors influencing viscosity such as injection temperature and shear behavior were found to also affect the observed relative dose. The shear thinning behavior of the high concentrated antibody solution at high shear rates resulted in higher relative doses than those observed with shear thickening PEG-HPW or Glycerol-HPW mixtures. Additionally, a decrease in relative dose of up to 40 percentage points was observed for the small device when comparing the effect of different injection temperatures resembling refrigerated and skin surface temperatures [41]. This emphasizes the importance of correct training of the patient for self-administration by the health care professionals in order to reduce handling errors during administration. Additionally, improved fluid path designs or the implementation of a temperature equilibration step after initializing the injection are expected to reduce the temperature-dependence of injection device performance.

In-use stability was investigated for the investigated drug-device combination. Only subvisible particle concentration revealed changes, whereas SEC and IEX chromatography results showed no deterioration of product quality. Particle formation was induced through the pumping action of both pumps, but in this study the small pump exhibited a more pronounced formation of aggregates. However, particle formation was not only limited to the pumping action itself, but also drastically influenced by the primary packaging material. Especially for the siliconized glass cartridge, a high number of subvisible particles was found after pumping in the collected aliquot but also within the cartridge. The gliding action of the stopper along the barrel was found as a main factor when compared to an artificial open setup without stoppering the cartridge. This outlines the importance of in-use stability testing of the system including the appropriate primary packaging material. Based on the presented results, the use of siliconized cartridges may be questionable since superior alternatives

such as silicone-oil free variants or packaging materials without moving parts (e.g. collapsible cyclic olefin copolymer bags (chapter 4)) are available [38].

Studies have shown the capability of in-line filters to reduce particle burden of biopharmaceutical drug products [37, 39]. In a concept study, the effect of implementing a 0.22 µm filter into the fluid path of an injection device on device performance was investigated. Filtration was possible up to a protein concentration of up to 150 mg/ml depending on the filter type. However, the implementation of an inline-filter on the suction side of the large pump resulted in a decrease in relative doses due to flow limitations introduced by the filter. Nevertheless, further design alterations with the implementation of an inline-filter into injection devices are highly encouraged. The drastic reduction of subvisible as well as submicron particles was proven, also for very small filter geometries suitable for the implementation into the housing of injection devices. Influences of filter size, flow rate, protein concentration and volume on the filtration efficiency were investigated and were found to be negligible, whereas filter-hold-up volumes were found as only drawback aside from reduced relative doses in combination with the injection device.

This study was conducted with two injection devices, both of which comprised a suction pump mechanism to draw the liquid out of a container and inject it subcutaneously. Some of the presented results may be specific to the suction pump mechanisms, but other findings can be applied to injection devices in general. The raised questions and presented solutions hopefully support the future development of large volume injection devices and provide valuable considerations for the progression of drug-device combinations for the sake of safe, easy and reliable subcutaneous drug delivery of biopharmaceuticals.

5. Supplementary data

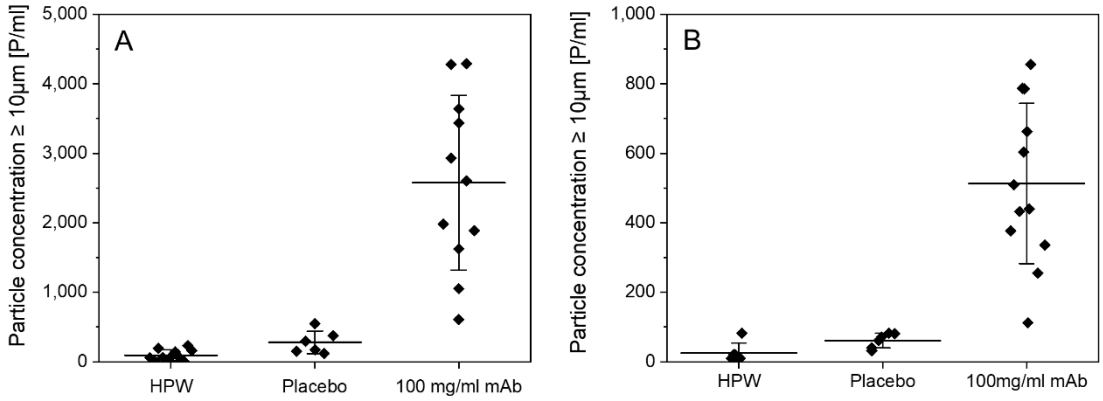

Figure 13S: Subvisible particle levels ≥ 10 µm after pumping highly purified water, placebo, or 100 mg/ml mAb using A.) the small pump or B.) the large pump. A new injection device was used for each data point and mean ± standard deviation (n = 6 – 14) are depicted by line and whiskers.

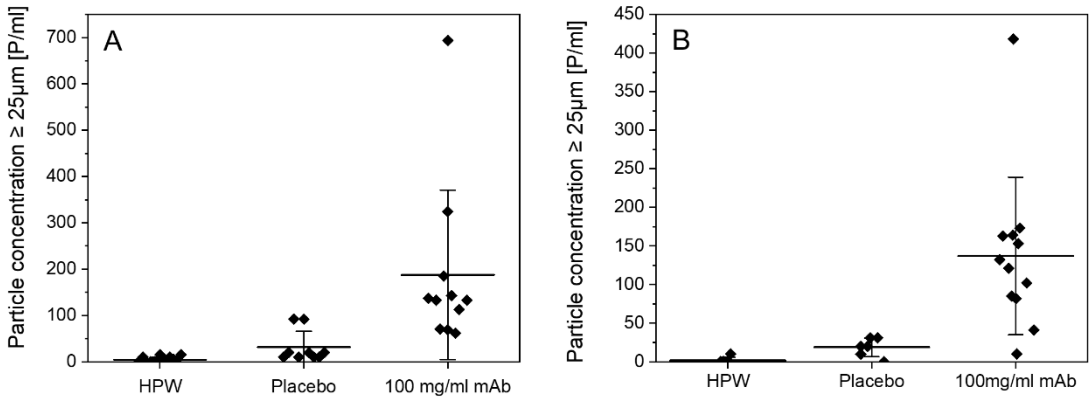

Figure 14S: Subvisible particle levels ≥ 25 µm after pumping highly purified water, placebo, or 100 mg/ml mAb using A.) the small pump or B.) the large pump. A new injection device was used for each data point and mean ± standard deviation (n = 6 – 14) are depicted by line and whiskers.

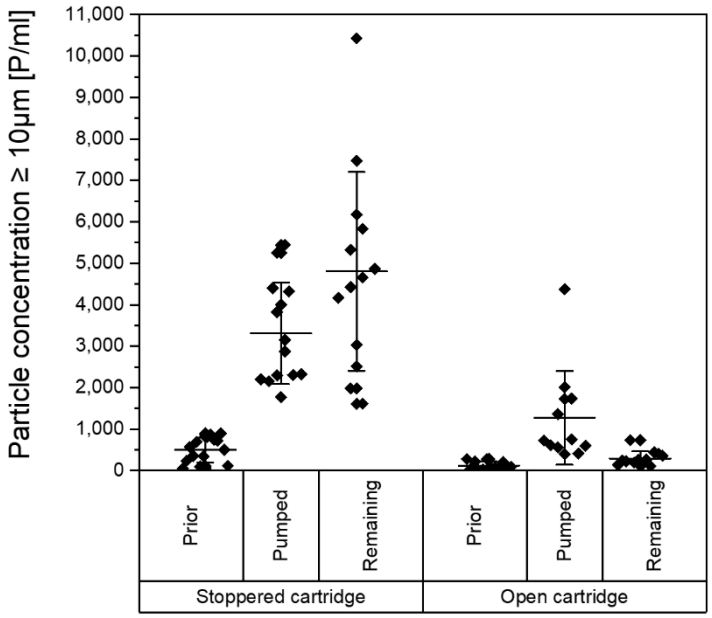

Figure 15S: Contribution of pumping action and primary packaging materials of the small pump to subvisible particle levels ≥ 10 µm. A new injection device was used for each data point and mean ± standard deviation (n = 11 – 14) are depicted by line and whiskers.

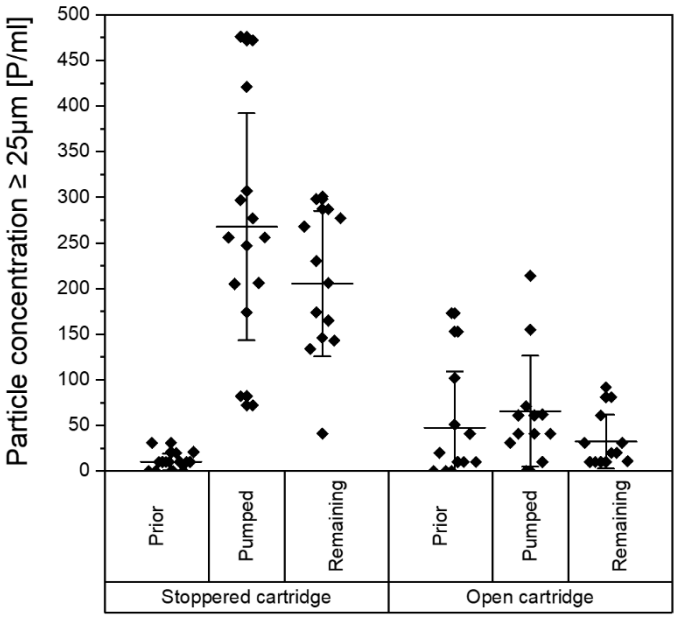

Figure 16S: Contribution of pumping action and primary packaging materials of the small pump to subvisible particle levels ≥ 25 µm. A new injection device was used for each data point and mean ± standard deviation (n = 11 – 14) are depicted by line and whiskers.

Disclaimer

The injection devices were commercially available through Weibel CDS AG (now part of SHL Medical AG) and the study was conducted independent of the device manufacturer.

References

1. Mathaes, R., et al., *Subcutaneous Injection Volume of Biopharmaceuticals-Pushing the Boundaries.* J Pharm Sci, 2016. **105**(8): p. 2255-9.
2. Doughty, D.V., et al., *Understanding Subcutaneous Tissue Pressure for Engineering Injection Devices for Large-Volume Protein Delivery.* J Pharm Sci, 2016. **105**(7): p. 2105-13.
3. Narasimhan, C., H. Mach, and M. Shameem, *High-dose monoclonal antibodies via the subcutaneous route: challenges and technical solutions, an industry perspective.* Therapeutic Delivery, 2012. **3**(7): p. 889-900.
4. Bittner, B., W. Richter, and J. Schmidt, *Subcutaneous Administration of Biotherapeutics: An Overview of Current Challenges and Opportunities.* BioDrugs, 2018. **32**(5): p. 425-440.
5. Frost, G.I., *Recombinant human hyaluronidase (rHuPH20): an enabling platform for subcutaneous drug and fluid administration.* Expert Opin Drug Deliv, 2007. **4**(4): p. 427-40.
6. Usach, I., et al., *Subcutaneous Injection of Drugs: Literature Review of Factors Influencing Pain Sensation at the Injection Site.* Adv Ther, 2019. **36**(11): p. 2986-2996.
7. Bookbinder, L.H., et al., *A recombinant human enzyme for enhanced interstitial transport of therapeutics.* J Control Release, 2006. **114**(2): p. 230-41.
8. Shire, S.J., Z. Shahrokh, and J. Liu, *Challenges in the Development of High Protein Concentration Formulations.* Journal of Pharmaceutical Sciences, 2004. **93**(6).
9. Mahler, H.C., et al., *Protein aggregation: pathways, induction factors and analysis.* J Pharm Sci, 2009. **98**(9): p. 2909-34.
10. Liu, J., et al., *Reversible self-association increases the viscosity of a concentrated monoclonal antibody in aqueous solution.* J Pharm Sci, 2005. **94**(9): p. 1928-40.
11. Wang, W., *Instability, stabilization, and formulation of liquid protein pharmaceuticals.* International Journal of Pharmaceutics, 1999. **185**: p. 129–188.
12. Torjman, M.C., et al., *Evaluation of an investigational wearable injector in healthy human volunteers.* Expert Opin Drug Deliv, 2017. **14**(1): p. 7-13.
13. Shapiro, R., *Subcutaneous Immunoglobulin Therapy by Rapid Push is Preferred to Infusion by Pump: A Retrospective Analysis.* Journal of Clinical Immunology, 2010. **30**(2): p. 301-307.
14. Berger, M., *Principles of and advances in immunoglobulin replacement therapy for primary immunodeficiency.* Immunol Allergy Clin North Am, 2008. **28**(2).
15. Beddoes, C., *Understanding the market for wearable large volume injectors.* ONdrugDelivery, 2016. **70**.
16. Bauert, D. and A.K. Busimi, *Primary packaging for wearable injection devices*, in *ONdrugDelivery*. 2019.
17. Amgen Inc. *Prescribing information: Repatha®*. 2019; Available from: https://www.repatha.com/.
18. Burckbuchler, V., et al., *Rheological and syringeability properties of highly concentrated human polyclonal immunoglobulin solutions.* European Journal of Pharmaceutics and Biopharmaceutics, 2010. **76**(3): p. 351-356.
19. Allmendinger, A., et al., *Rheological characterization and injection forces of concentrated protein formulations: an alternative predictive model for non-Newtonian solutions.* Eur J Pharm Biopharm, 2014. **87**(2): p. 318-28.

20. Rathore, N., et al., *Characterization of protein rheology and delivery forces for combination products.* J Pharm Sci, 2012. **101**(12): p. 4472-80.
21. Krayukhina, E., A. Fukuhara, and S. Uchiyama, *Assessment of the Injection Performance of a Tapered Needle for Use in Prefilled Biopharmaceutical Products.* J Pharm Sci, 2020. **109**(1): p. 515-523.
22. Shieu, W. and Y.F. Maa, *Considerations and challenges when filling high-concentration monoclonal antibody formulations into prefilled syringes*, in *Development of Biopharmaceutical Drug-Device Products*, F. Jameel, J.W. Skoug, and R.R. Nesbitt, Editors. 2020. p. 591-612.
23. Furness, G., *Prefilled Syringes*. ONdrugDelivery. Vol. 95. 2019.
24. Furness, G., *Wearable Injectors*. ONdrugDelivery. Vol. 100. 2019.
25. Furness, G., *Prefilled Syringes - Injection Devices*. ONdrugDelivery. Vol. 101. 2019.
26. Furness, G., *Prefilled Syringes - Injection Devices*. ONdrugDelivery. Vol. 105. 2020.
27. Furness, G., *Delivering Injectables*. ONdrugDelivery. Vol. 107. 2020.
28. Izon Science Support Centre. *Video: Maintaining a stable baseline current*. Accessed 07 Feb. 2021]; Available from: Available at: https://support.izon.com/video-maintaining-a-stable-baseline.
29. Bowen, J.L. and C.J. Allender, *A Comparative Pulse Accuracy Study of Two Commercially Available Patch Insulin Infusion Pumps.* Eur Endocrinol, 2016. **12**(2): p. 79-84.
30. Jezek, J., et al., *Viscosity of concentrated therapeutic protein compositions.* Adv Drug Deliv Rev, 2011. **63**(13): p. 1107-17.
31. Galush, W.J., L.N. Le, and J.M. Moore, *Viscosity behavior of high-concentration protein mixtures.* J Pharm Sci, 2012. **101**(3): p. 1012-20.
32. Inoue, N., et al., *Arginine and lysine reduce the high viscosity of serum albumin solutions for pharmaceutical injection.* Journal of Bioscience and Bioengineering, 2014. **117**(5): p. 539-543.
33. Allahham, A., et al., *Flow and injection characteristics of pharmaceutical parenteral formulations using a micro-capillary rheometer.* Int J Pharm, 2004. **270**(1-2): p. 139-48.
34. Le Basle, Y., et al., *Physicochemical Stability of Monoclonal Antibodies: A Review.* J Pharm Sci, 2020. **109**(1): p. 169-190.
35. Her, C. and J.F. Carpenter, *Effects of Tubing Type, Formulation, and Postpumping Agitation on Nanoparticle and Microparticle Formation in Intravenous Immunoglobulin Solutions Processed With a Peristaltic Filling Pump.* J Pharm Sci, 2020. **109**(1): p. 739-749.
36. Strehl, R., et al., *Discrimination between silicone oil droplets and protein aggregates in biopharmaceuticals: a novel multiparametric image filter for sub-visible particles in microflow imaging analysis.* Pharm Res, 2012. **29**(2): p. 594-602.
37. Werner, B.P. and G. Winter, *Particle contamination of parenteralia and in-line filtration of proteinaceous drugs.* Int J Pharm, 2015. **496**(2): p. 250-67.
38. Werner, B.P., C. Schoneich, and G. Winter, *Silicone Oil-Free Polymer Syringes for the Storage of Therapeutic Proteins.* J Pharm Sci, 2019. **108**(3): p. 1148-1160.
39. Werner, B.P. and G. Winter, *Expanding Bedside Filtration-A Powerful Tool to Protect Patients From Protein Aggregates.* J Pharm Sci, 2018. **107**(11): p. 2775-2788.
40. Mahler, H.C., et al., *Adsorption behavior of a surfactant and a monoclonal antibody to sterilizing-grade filters.* J Pharm Sci, 2010. **99**(6): p. 2620-7.
41. Zaproudina, N., et al., *Reproducibility of infrared thermography measurements in healthy individuals.* Physiol Meas, 2008. **29**(4): p. 515-24.

Chapter 4

Novel cyclic olefin copolymer pouch (MiniBag) as primary packaging material for large volume subcutaneous injection of high concentrated biopharmaceuticals

This chapter, including supplementary data, is intended to be published.

Authors: Andreas Stelzl[1], Stefan Schneid[2], Gerhard Winter[1]

[1] Ludwig-Maximilians Universität München, Department of Pharmacy, Pharmaceutical Technology and Biopharmaceutics, Butenandtstraße 5-13, 81377 Munich, Germany

[2] Bayer AG, Pharmaceuticals, Formulation Development Parenterals, Friedrich-Ebert-Str. 475, 42096 Wuppertal, Germany

The presented experiments were conducted by Andreas Stelzl. Assistance was provided through the execution of the LC-MS analyses by the analytical department at Bayer, Wuppertal. Scientific guidance was provided by Dr. Stefan Schneid and Prof. Dr. Gerhard Winter.

Abstract

Subcutaneous (s.c.) injection of biopharmaceuticals has many benefits, including the possibility of self-administration of the drug by the patient. Innovative technologies and formulation approaches are under development to enable large volume subcutaneous injection of high concentrated protein formulations.

A flexible pouch (referred to as MiniBag), made from a cyclic olefin copolymer-polychlorotrifluoroethylene (COC/PCTFE) flexible film, was investigated in this study as a novel primary packaging material for a high concentration liquid antibody formulation. The MiniBag is bendable and remains flat even for versions holding more than 30 ml, which is a big advantage for patient convenience especially in combination with large volume injection devices.

In this study, a high concentrated mAb formulation was investigated during storage at 4°C, 25°C, and 40°C for 24 weeks in the MiniBag as well as in a glass and a cyclic olefin polymer (COP) syringe. Protein stability was evaluated based on particle formation and aggregation assessed by fluid imaging microscopy and SEC as well as chemical degradation by IEX chromatography. The relatively high gas permeability of polymer packaging materials, which might limit their use for oxidation-sensitive biopharmaceuticals, was considered, and both polymer packaging materials, MiniBag and COP syringe, were additionally stored in a N_2-filled outer aluminum pouch. Oxygen content in solution was monitored and linked to protein oxidation assessed by analytical protein A chromatography, peptide mapping as well as subunit mass analysis by LC-MS. Protein stability in the MiniBag was comparable to both glass syringe and COP syringe. Especially, lower particle levels were observed in both polymer packaging materials compared to the glass syringe, and less oxidation was detected in polymer packaging materials stored in N_2-filled secondary packaging. MiniBags present a promising alternative

for the storage of larger volumes of biopharmaceuticals and may facilitate the use of large volume subcutaneous injection in the future.

Keywords: primary packaging, cyclic olefin copolymer (COC), MiniBag, silicone oil free syringes, siliconized syringes, glass syringes, plastic syringes, high protein concentration, biopharmaceuticals, monoclonal antibody, large volume subcutaneous injection, protein oxidation, protein aggregation

1. Introduction

Subcutaneous (s.c.) administration of biopharmaceuticals is often used when frequent and chronic administration of the drug is necessary. Combination products such as prefilled syringes (PFS) or autoinjectors facilitate the API self-administration by the patient in home care [1, 2]. However, conventional s.c. injections are commonly limited to < 1.5 ml injection volume [1, 3], as larger volumes can cause issues like injection site leakage or injection-related adverse reactions including injection pain, itching, and erythema [1, 2, 4]. The limited injection volume also necessitates the development of high concentrated protein formulations, which are required in order to achieve therapeutic doses that can reach several hundred milligrams per patient for monoclonal antibodies (mAb), which is also influenced by the molecule-specific s.c. bioavailability [4]. This can lead to potentially high solution viscosities which influences manufacturability and administration. Additionally, reduced protein stability due to increased protein aggregation and an impact on bioavailability were reported [3, 5].

If the required high protein concentration is not achievable or the total dose required for a therapeutic dose does not remain below 1.5 ml injection volume, other approaches such as large volume injections, multiple injections of smaller volumes or the use of functional excipients like hyaluronidase need to be considered [1, 2, 4, 6]. To increase s.c. injection volumes, large volume injection devices were developed. By prolonging the injection time, volumes up to 20 ml can be delivered s.c. [7, 8].

Additionally, larger injection volumes allow increasing the dose for the patient, thereby enabling less frequent dosing. For example, the Repatha® Pushtronex® system offers patients a monthly dose of 420 mg evolocumab in 3.5 ml, whereas a conventional autoinjector (SureClick®) containing 140 mg/ml evolocumab requires a bi-weekly dosing scheme [9].

The development of large volume injection devices also drives the need of new large volume primary packaging materials as syringes, for example, are becoming very bulky at filling volumes >20 ml [2, 10]. It can be expected, that the carrying comfort for the patient will be compromised and could reduce patient compliance. A flexible pouch, referred to as MiniBag, has been developed by Weibel CDS AG (Waldstatt, Switzerland) as primary packaging system for storage of drug product solutions. It is laminated from a cyclic olefin copolymer-polychlorotrifluoroethylene (COC/PCTFE) flexible film, CETA160. The manufacturing process is compliant to cGMP standards, and the film itself is transparent, non-yellowing, high-barrier, US FDA-compliant and sterilizable by irradiation [11]. The form factor and size is a major advantage of the MiniBag System, as the bag remains flat even for versions holding > 30 ml [12, 13]. In addition, the flexible and bendable manner of the laminate could be more patient-convenient when larger filling volumes are targeted, since the container can bend according to the curvature of the application site (e.g. abdomen) [11]. Increased carrying comfort and therefore good patient compliance is expected when combining the MiniBag with large volume injection devices.

In contrast, glass syringes have a long history of use and the majority of PFS available on the market are made from glass [10, 14]. However, disadvantages associated with glass syringes are breakage risk, surface reactivity, glass delamination at higher pH and the need for siliconisation [10, 14-16]. While siliconisation of the glass barrel is required for the functionality of the syringe [17], silicone oil droplets can migrate into the drug product during filling or storage [18, 19], and the aggregation of proteins in the presence of silicone oil is regularly reported [20-25]. Baked-on or cross-linked siliconisation

techniques resulted in lower silicone oil levels and less silicone oil migration into the drug product, but are still not the standard configuration today [26, 27].

Polymer packaging materials made of cyclic olefin polymers (COP) or cyclic olefin copolymers (COC) can offer increased break resistance, decreased surface reactivity, and good durability over a broad pH range as advantages over glass materials [14, 16, 28]. Additionally, polymer syringes can be manufactured in silicone-oil free variants, which can provide an advantage for biopharmaceuticals sensitive to silicone oil [28]. Lower particle counts and similar chemical stability of a mAb and a cytokine in silicone oil free COP syringes were reported compared to glass syringes [28]. However, a main drawback of polymer packaging materials compared to their glass counterparts lays in the reduced barrier function for oxygen [14, 15, 29, 30]. The increased oxygen permeability can be detrimental to oxidation sensitive drugs upon storage [31, 32].

We assessed the chemical and physical stability of a high concentration liquid mAb formulation after storage in the novel MiniBag system for up to 24 weeks at three temperatures. In order to compare protein stability in the MiniBag system to commonly used packaging materials for s.c. administration, the stability of the mAb-formulation was additionally analyzed after storage in a glass and a cyclic olefin polymer (COP) syringe (compare Figure 17). In order to reduce protein oxidation as previously reported [28], the polymer primary packaging containers were further stored in N_2-filled aluminum pouches for comparison.

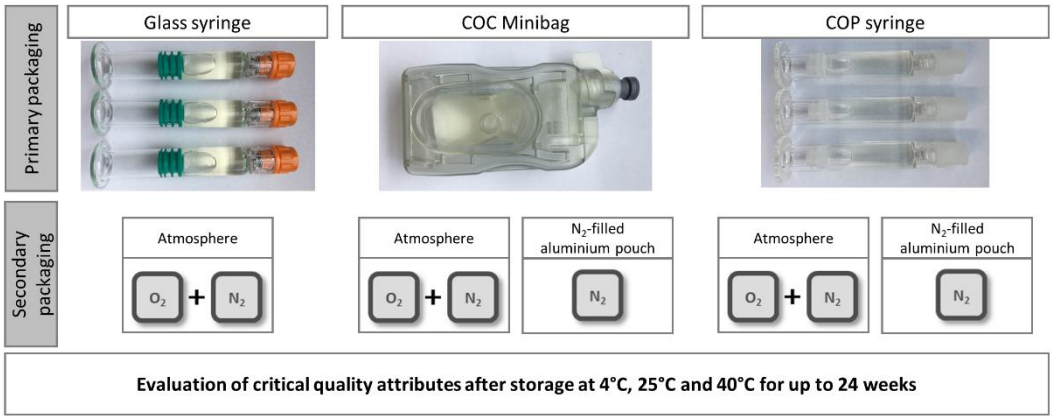

Figure 17: Overview of investigated primary and secondary packaging combinations

2. Materials and Methods

2.1 Materials

Glacial acetic acid, glycine, L-methionine, polysorbate 80, sodium chloride (NaCl), and sucrose were purchased from Merck KGaA (Darmstadt, Germany), and L-histidine and L-histidine monohydrochloride monohydrate from Alfa Aesar (Kandel, Germany). Monosodium phosphate dihydrate, potassium di-hydrogen phosphate and potassium chloride were obtained from AppliChem (Darmstadt, Germany), disodium phosphate dihydrate from Bernd Kraft (Duisburg, Germany). In-house highly purified water (HPW) (conductivity 0.055 µs/cm) was dispensed from an Arium®Pro purification system (Sartorius, Göttingen, Germany).

A COC MiniBag, obtained from Weibel CDS AG (Waldstatt, Switzerland), as well as a siliconized BD Hypak 2.25 ml luer-lock glass syringe with the respective tip-cap and chlorobutyl stopper (BD Medical – Pharmaceutical Systems, Franklin Lake, NJ, USA) and a silicone-oil free COP syringe (Daikyo Crystal Zenith® Polymer Ready-to-Use syringes, West Pharmaceutical Services, Inc., Lionville, PA) including the

respective tip-cap and stoppered with a Fluorotec® stopper (West) were used as primary packaging materials.

2.2 Protein bulk, filling and storage

A monoclonal antibody belonging to the IgG class 1 (mAb), was kindly provided by Bayer AG (Wuppertal, Germany). The bulk solution contained 140 mg/mL protein in 10 mM histidine buffer pH 5.5 with 130 mM glycine, 5% sucrose, 20 mM methionine, and 0.05% polysorbate 80. A solution with the identical composition of excipients without mAb was used as placebo throughout the study. Prior to filling, all solutions were filtered through a 0.22 µm polyethersulfone (PES) Sartolab® RF vacuum-filter (Sartorius, Goettingen, Germany). Filling for the long-term stability study was conducted under laminar air flow conditions. The solution was filled into siliconized 2.25 ml glass syringes (1.2 ml filling volume), silicone oil-free 1 ml cyclic olefin polymer (COP) syringes (1.2 ml filling volume), and silicone oil-free cyclic olefin copolymer (COC) MiniBags (2.4 ml filling volume). COP syringes were obtained in a ready to fill format (washed and pre-sterilized), MiniBags were pre-sterilized by the manufacturer, and glass syringes were pre-cleaned in-house by rinsing 5 times with HPW, followed by drying at 40°C. Both syringes were hand-stoppered with the respective stoppers using a fixture to set the air pocket to the same volume. Additionally, a secondary packaging step was conducted for some of the polymer packaging materials. For these COP syringe and MiniBag samples, the units for each time point were placed in an aluminum pouch (Drylok 3000; Advantek GmbH, Freiburg, Germany), and the pouch was flushed with gaseous nitrogen for 1 min before sealing the pouch. After sealing, the pouch was pierced and inflated with gaseous nitrogen (nitrogen 5.0 (≥ 99.999%), Linde GmbH, Pullach, Germany) twice before sealing-off the injection site and entrapping a volume of 1.1 ± 0.15 L of gaseous nitrogen within each pouch. All samples were stored for up to 24 weeks at 2-8°C, 25°C, and 40°C under exclusion of light without control of the relative humidity. At each time point (i.e. 0, 4, 12, and 24 weeks), MiniBags,

glass, and polymer syringes were opened and the content was transferred to cleaned 2R vials for analysis. Three MiniBags as well as six syringes per type were sampled at each time point. Samples of two syringes were pooled in one vial to reach sufficient volume for analysis resulting in three pooled samples per syringe type.

2.3 Subvisible particle (SVP) analysis

A FlowCam 8100 (Fluid Imaging Technologies, Inc., Scarborough, ME, USA) was used to analyze subvisible particles in the range of 1 – 80 µm. The system was equipped with a 10x magnification and a FOV80 flow-cell (80 µm × 700 µm). The sample volume was 150 µl and images were collected with a flow rate of 50 µl/min and an auto image frame rate of 9 frames/second. 3 µm distance to the nearest neighbor and thresholds of 10 and 13 for light and dark pixels, respectively, were used for particle identification after in-house method optimization. Particle size was reported as equivalent spherical diameter (ESD) using VisualSpreadsheet® 4.7.6 software for data collection and evaluation.

Morphological data recorded for each particle were analyzed. For particles larger than 5 µm, the aspect ratio, circularity, sigma intensity and transparency were combined into a shape-factor (compare equation 1) similar to Strehl et al., in order to discriminate between silicone oil and protein particles [33-38]. Specific subsets with only silicone oil particles or protein particles were used to determine silicone oil and protein particle shape factors. Particles were classified as silicone oil, if the individual shape factor for each particle was above a cut-off value defined by a linear fit (equation 2) through the midpoint between silicone oil and protein particle shape factor.

(1) $shape\ factor = \frac{aspect\ ratio * circularity * sigma\ intensity}{transparency}$

(2) $cut - off\ shape\ factor = diameter\ (ESD) * 37.1494 - 10.4154\ (R^2 = 0.61)$

2.4 Chromatographic methods

Mobile phases were prepared with highly purified water and sterile filtered through a 0.22 µm cellulose acetate membrane. All samples were 30-fold diluted in placebo (30 µl sample + 870 µl placebo) and centrifuged at 10,000 g for 10 min before analysis. Three samples per packaging system and storage condition were analyzed by duplicate injection resulting in a total 6 sub-runs.

2.4.1 Size exclusion chromatography (SEC)

A Dionex Ultimate 3000 system (Thermo Scientific, Dreieich, Germany) was used for size exclusion chromatography. 10 µg mAb were injected on a Waters Acquity UPLC® Protein BEH SEC column (200Å, 1.7 µm, 4.6 × 150 mm, Waters Corporation, Milford, MA, USA) and the elution of the protein was detected at 280 nm with a VWD-3400RS UV detector (Thermo Fisher). 50 mM sodium phosphate buffer (pH 6.5) containing 300 mM sodium chloride was used as mobile phase at a flowrate of 0.3 ml/min. The chromatograms were integrated with Chromeleon V7.2 (Thermo Fisher) and the relative areas of the monomer, high molecular weight aggregates (HMWA) and lower molecular weight species (LMWS) were calculated as percentage.

2.4.2 Ion exchange chromatography (IEX)

A Dionex Ultimate 3000 system (Thermo Fisher) was used for ion exchange chromatography. 50 µg mAb were injected on a ProPac WCX-10 Analytical Column (4x250 mm) with a ProPac WCX-10G Guard Column (4x50 mm) (Thermo Fisher), and the elution of the protein was detected at 280 nm with a VWD-3400RS UV detector (Thermo Fisher). The mobile phase was a combination of 20 mM sodium phosphate pH 6.5 (Solvent A), and Solvent A + 300 mM NaCl pH 6.5 (Solvent B). The flow rate was 1.0 ml/min in a linear gradient mode (time in min vs. percentage B = 0:0, 5:0, 35:30, 36:100, 46:100, 47:0, 57:0). The chromatograms were integrated with Chromeleon V7.2 (Thermo Fisher), and the relative areas of the acidic variants, main peak, and basic variants were calculated as percentage.

2.4.3 Protein A Chromatography (PAC)

A Waters 2695 separations module (Waters) was used for protein A chromatography. 250 µg mAb were injected on a Poros A column (4.6 x 30 mm; Applied Biosystems, Foster City, CA, USA), and the elution of the protein was detected at 280 nm with a 2487 DAD detector (Waters). The mobile phase was a combination of phosphate buffered saline, consisting of 10 mM Na_2HPO_4, 1.8 mM KH_2PO_4, 2.7 mM KCl, and 137 mM NaCl at pH 7.4 (Solvent A) and 100 mM AcOH with 150 mM NaCl at pH 2.8 (Solvent B). The flow rate was set to 2.0 ml/min for a run time of 51 min/injection and elution was performed in a linear gradient mode (time in min vs. percentage B = 0:0, 5:0, 29:36, 30:100, 40:100, 41:0, 51:0). The chromatograms were integrated with Chromeleon V6.8 (Thermo Fisher) and the relative area of the oxidized species, summing up all peaks and shoulders eluting prior to the main peak, was calculated in percentage according to Loew et al. [39].

2.5 Liquid chromatography–mass spectrometry (LC-MS)

2.5.1 Peptide mapping

mAb concentration was adjusted to 1 mg/ml with 0.1% RapiGest (Waters Corporation, Milford, MA, USA) to a total volume of 100 µl and incubated at 80°C for 15 min at 300 rpm. 5 µl 1,4-dithiothreitol (DTT) at a concentration of 100 mM were added and incubated for 15 min at 60°C and 300 rpm. Samples were alkylated with 5 µl 200 mM iodoacetamide while excluding light at room temperature for 1h. 2 µl trypsin (1 mg/ml) were added and samples were incubated at 37°C over-night before quenching the reaction by adjusting the pH to 2 with 10% formic acid. Then, the samples were diluted 1:5 with eluent A to a final concentration of around 1.1 pmol/µl.

For LC-MS analysis, an Aquity UPLC H-Class Bio (Waters) was coupled to a Xevo G2-XS mass spectrometer (Waters). 2 µl sample were loaded onto an ACQUITY UPLC Peptide CSH C18 column, 2.1 x 150 mm, 1.7 µm (Waters) at a column temperature of 60°C. Elution was performed in gradient mode with eluent A (0.1% formic acid in water) and eluent B (0.1% formic acid in acetonitrile). The following

conditions were used on the ESI source: source temperature 120°C, desolvation temperature 300°C, desolvation gas flow 800 l/min, cone gas flow 50 l/min, capillary voltage 1.7 kV and cone voltage 40 V. The samples were analyzed between 100 and 2000 m/z in ESI+ MSe mode. UV signals were recorded at 210 and 280 nm. Data were processed using the Expressionist® Refiner MS 13.0 software by Genedata (Basel, Switzerland).

2.5.2 Subunit mass analysis

50 µg mAb were adjusted to a volume of 25 µl with DPBS (Thermo Fisher) and 2.5 µl FabRICATOR (20 U/µl, Genovis Inc., Cambridge, Ma, USA) were added. The samples were vortexed and centrifuged before incubation for 30 min at 37 °C and 300 rpm. After incubation, 75 µl of a 6 M guanidinium-Cl solution and 7 µl of a 1M 1,4-dithiothreitol (DTT) solution were added. After vortexing and centrifugation, the samples were incubated at 37 °C and 300 rpm for 45 min.

For LC-MS analysis, an Aquity UPLC H-Class Bio (Waters) was coupled to a MaXis II mass spectrometer (Bruker Corporation, Billerica, Ma, USA). 20 µl sample were loaded onto an ACQUITY UPLC Protein BEH C4 column, 2.1 x 100 mm, 1.7 µm (Waters) at a column temperature of 75°C. Elution was performed in gradient mode with eluent A (0.1% formic acid in water) and eluent B (0.1% formic acid in 80% (v/v) n-propanol, 10% (v/v) acetonitrile and 10% (v/v) water). The following conditions were used on the ESI source: dry temperature 200 °C, dry gas flow 8.0 l/min, nebulizer gas flow 1.0 l/min, capillary voltage 4500 V and end plate offset 500 V. The samples were analyzed between 700 and 2750 m/z in ESI+ mode. UV signals were recorded at 280 nm. Data were processed using the Expressionist® Refiner MS 13.0 software by Genedata (Basel, Switzerland).

2.6 Oxygen content in solution

The concentration of soluble oxygen in the samples was analyzed using a Microx 4 fiber optic oxygen meter (PreSens Precision Sensing GmbH, Regensburg, Germany). The tip cap of the syringes was removed right before analysis, and the sensor inserted via the syringe bore into the protein formulation directly before the measurement was started. Since direct access to the protein formulation in the MiniBags was not possible with the oxygen sensor, the oxygen content in solution was detected immediately after transferring the protein formulation from the MiniBag to a 2R vial. Three packaging containers were analyzed at each time point and three recordings were made for each container. Further, oxygen content in the N_2-filled aluminum pouches was analyzed.

2.7 Injection force

Injection forces were determined using a texture analyzer (Texture Technologies Corp., Hamilton, MA, USA) at an injection speed of 0.1 ml/s using the glass and COP syringe, both fitted with a 27G 1 ½" needle (B. Braun Melsungen AG, Melsungen, Germany). The syringes were fixed and the stopper was pushed downwards until 1 ml sample was expelled, resulting in a distance of 17.78 mm and speed of 106.68 mm/min for the glass syringe, and of 25.83 mm with 155.00 mm/min for the COP syringe.

The maximum force between 0 and 1 mm of stroke distance was evaluated as break loose force (BLF) and the average plateau force required to push the stopper along the barrel of the syringe was evaluated as gliding force (GF) from 7.5 to 10 s after initialization of the recording.

2.8 Turbidity

2.8.1 Optical density

Optical density at 350 nm was determined with a Fluostar Omega (BMG Labtech GmbH, Ortenberg, Germany) in a 96-well quartz microplate filled with 200 µl sample per well.

2.8.2 Nephelometry

Turbidity was analyzed using a Nephla turbidimeter (Dr. Lange, Düsseldorf, Germany) by using static light scattering at 90° (λ = 860 nm). The turbidity was recorded in formazine nephelometric units (FNU). 1.5 ml of each sample was analyzed in triplicates.

2.9 Viscosity

The viscosity of the samples was measured using a mVROC viscometer (Rheosense Inc., San Ramon, CA, USA) equipped with a RA05-100-087 flow cell. Viscosity was determined for mAb samples filled in a 250 µl-Hamilton syringe without introducing air bubbles at 20°C and at a flow rate of 50 µl/min, resulting in a corresponding shear rate of $6.32*10^6$ 1/s.

2.10 pH

The pH was measured using a SevenEasy pH meter (Mettler Toledo, Columbus, OH, USA) equipped with an Inlab Micro pH electrode (Mettler).

2.11 Concentration

Protein concentration was verified with a Nanodrop One (Thermo Scientific) at an absorption wavelength of 280 nm using the predefined IgG profile and a baseline subtraction at 340 nm.

3. Results and Discussion

mAb formulation samples in MiniBags, glass syringes, and COP syringes were stored at regular atmosphere; based on the lower gas barrier properties of COP/COC [14, 15, 29, 30], MiniBags and COP syringes were additionally stored in nitrogen-filled aluminum pouches (referred to as MiniBag $+N_2$ and COP syringe $+N_2$). The physical and chemical stability of the mAb throughout storage for 24 weeks at 4°C, 25°C, and 40°C was evaluated by means of particle formation (visual inspection, turbidity, fluid

imaging), SEC, IEX, protein A chromatography, and LC-MS. Additionally, oxygen content in solution, pH, protein concentration, viscosity and injection force were determined.

3.1 Particle formation and aggregation behavior

No visual defects such as fluid leakage from the packaging materials, formation of visible particles, or increased turbidity were observed after filling (Figure 18 A). Throughout storage over 24 weeks, neither leakage, formation of visible particles, nor turbid solutions were observed in any container. A discoloration of samples containing mAb after storage at 40°C (Figure 18 D) was observed already after 12 weeks, which could be related to chemical instabilities of the protein or free amino acids present in the formulation [40-42]. The discoloration also caused an increase in optical density at 350 nm from 0.35 to 3.0 (supporting information, Figure 26S C). No discoloration (Figure 18 B and C) and consequently no or only a slight increase in optical density was observed in samples stored at 4°C and 25°C, respectively (supporting information, Figure 26S A and B). Analysis of turbidity via scattering intensity at 90° revealed no increase after storage at 4°C and 25°C in all samples, but a sharp increase was observed after storage at 40°C (supporting information, Figure 26S D). Solutions filled in the MiniBag and the glass syringe showed an increased to around 35 FNU and the highest turbidity was found in the MiniBag +N_2 with 100 FNU.

Figure 18: Visual inspection after filling (A) and after storage for 24 weeks at B.) 4°C, C.) 25°C, and D.) 40°C. Following sorting was used for each primary packaging material: Placebo (left) and mAb formulation (right).

Filling placebo into the primary packaging materials resulted in < 1000 Particles ≥ 1 µm per ml for the MiniBag and the COP syringe, whereas a higher particle level of 6500 Particles/ml ≥ 1 µm was found for the glass syringe (Figure 19 D). The particle levels in Placebo samples remained unchanged throughout storage over 24 weeks in all packaging materials, as exemplarily shown for placebo stored at 25°C. Subvisible particles ≥ 1 µm for the mAb solution (Figure 19 A-C) showed relevant differences between packaging materials already after filling. The particle level was at < 1000 Particles/ml in COP syringes, but higher levels of around 20500 Particles/ml and 28000 Particles/ml were found in the glass syringe and the MiniBag, respectively. The siliconisation of the glass syringe and the release of silicone oil droplets into solution may have caused the increase in particle level observed in the glass syringe after filling, due to protein aggregation induced by hydrophobic interactions with silicone oil droplets [18-25]. The high level of subvisible particles observed in the MiniBag after filling of the mAb

formulation was not related to a contamination of the MiniBags with SVPs during production, since the particle levels detected in placebo filled MiniBags were very low (< 1000 Particles/ml). Additionally, the sterilization process of the MiniBag could be excluded as a potential root cause by analyzing the initial particle levels after filling sterilized and non-sterilized MiniBags with the mAb formulation (data not shown). The root cause of the elevated particle level in MiniBags compared to COP syringes after filling is not yet fully understood and may be related to these specific primary packaging materials. However, also differences in surface characteristics between COC and COP materials could potentially provide an explanation and the authors encourage further investigations towards this direction.

After storage at 4°C for up to 24 weeks, the highest particle levels ≥ 1 µm were found for solutions in the glass syringe and the COP syringe filled with mAb formulation. No increase in particle levels were found for mAb formulations stored in the MiniBag, the MiniBag +N_2, and the COP syringe +N_2. After storage at 25°C, again the mAb formulation stored in the glass syringe showed the highest particle levels. No increase in particle level was observed in the MiniBag or the COP syringe after storage at 25°C. Strong formation of subvisible particles was found after 24 weeks storage at 40°C in the glass syringe and the MiniBag. The mAb formulation stored in the COP syringe still remained at a low concentration of SVPs.

Subvisible particle levels of particles ≥ 10 µm and ≥ 25 µm (supporting information, Figures 27S and 28S) followed similar trends as observed for particle levels ≥ 1 µm. Generally, particle levels remained within the FDA and Ph. Eur. requirements for injectable drugs also considering the specific filling volume of each container, despite the higher sensitivity of flow imaging in comparison to light obscuration for biopharmaceutical samples [18, 43-48]. An exception was found for particles ≥ 10 µm in the MiniBag, exceeding 7000 Particles/ml or 16800 Particles/container after 24 weeks at 40°C.

Overall, the highest subvisible particle levels were found after storage of the mAb formulation in the glass syringe. Migration of silicone oil into the drug product during filling or storage and the aggregation of proteins in the presence of silicone oil was already reported in literature [18-25]. The particles which were identified as silicone oil droplets in the Flowcam data were at a level around 2500 Particles/ml after filling of the glass syringes, accounting for approx. 75% of all particles ≥ 5 µm; no further migration of silicone oil into the solution was found during storage (Figure 20). Erroneous classification due to morphological similarities of some protein particles to silicone oil droplets resulted in a low percentage of silicone oil-like particles found in silicone oil-free MiniBags and COP syringes. Overall, as expected, particle levels of silicone oil-like particles in the MiniBag and the COP syringe was low compared to the silicone oil droplet concentration observed in the siliconized glass syringe.

Although the best performance regarding SVP levels was observed in silicone-oil free COP syringes, the MiniBag still showed significantly lower particle counts than a siliconized glass syringe which is still regularly used for many biopharmaceutical products [10, 19].

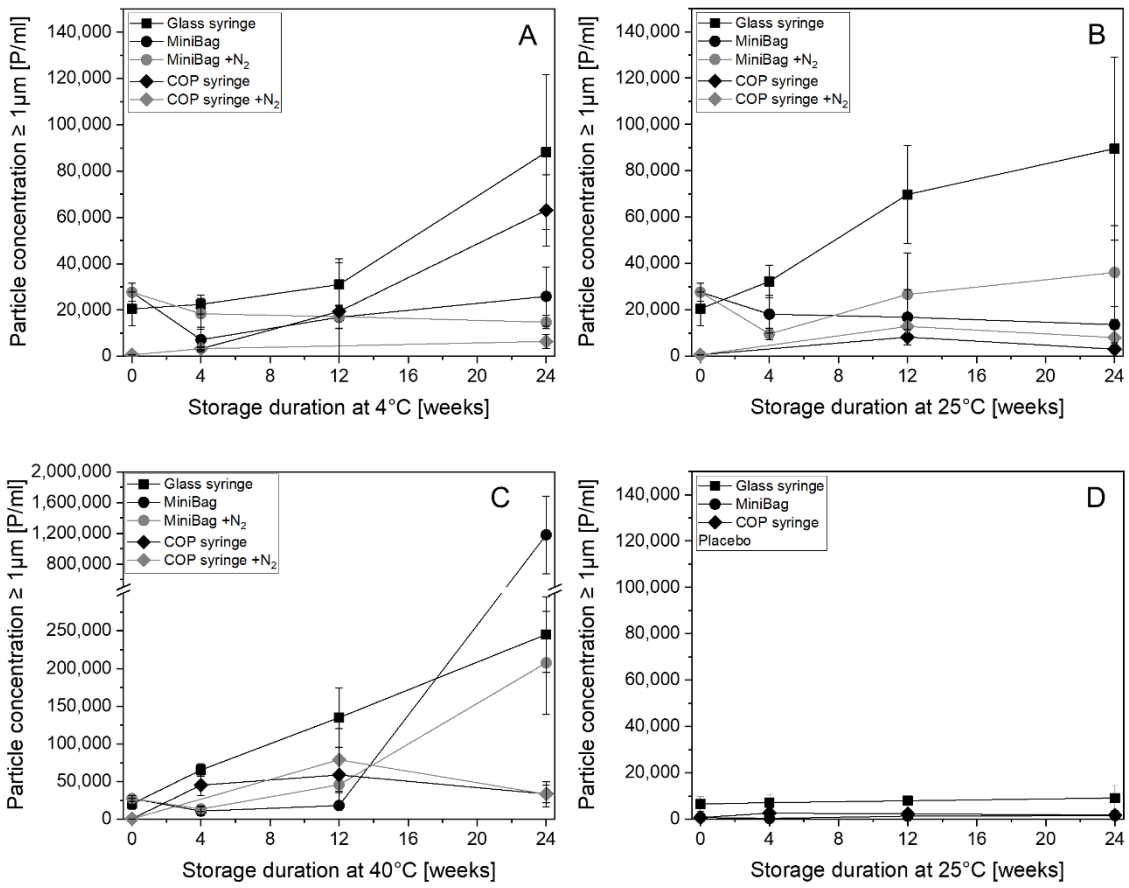

Figure 19: Particle levels ≥ 1 µm after storage for up to 24 weeks of mAb solutions at A.) 4 °C, B.) 25 °C, and C.) 40 °C, and placebo at D.) 25 °C.

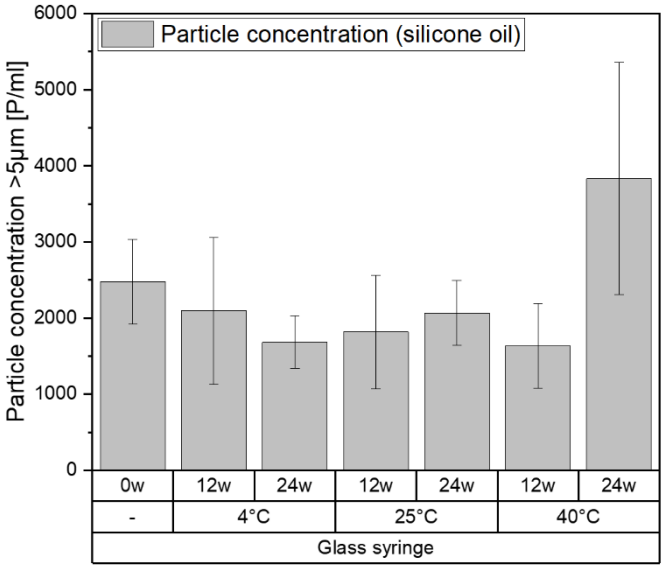

Figure 20: Particle level of silicone oil droplets ≥ 5 µm in the glass syringe after storage for up to 24 weeks at 4°C, 25°C, and 40°C.

The formation of soluble aggregates (Figure 21 A-C) or the fragmentation of the protein (Figure 21 D-F) was not observed in SEC throughout storage over 24 weeks at 4°C or 25°C in any packaging condition. After storage at 40°C for 24 weeks, LMWS content increased to 8% independent of the primary and secondary packaging. The content of dimers and small oligomers of up to ca. 450 kDa (summarized as HMWA) increased up to 22 – 25% among the different packaging materials. All packaging solutions performed comparably, and a packaging-specific negative impact was not observed in SEC analysis.

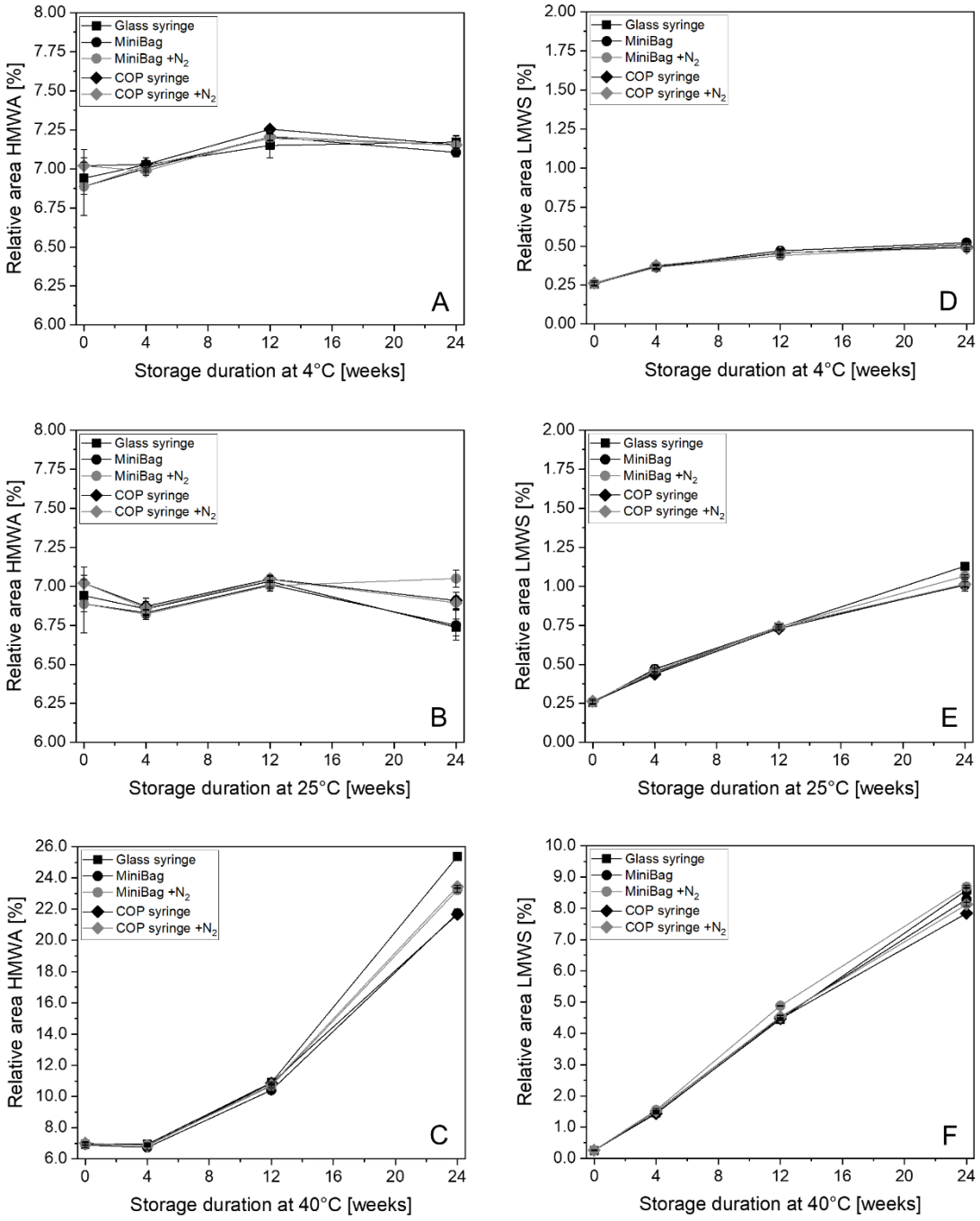

Figure 21: HMWA content after storage for 24 weeks at A.) 4°C, B.) 25°C, and C.) 40°C. LMWS content after storage for 24 weeks at D.) 4°C, E.) 25°C, and F.) 40°C.

3.2 Oxygen content and protein oxidation

The amount of soluble oxygen could be reduced drastically in polymer packaging containers using a N_2-filled aluminum pouch as secondary packaging material (Figure 22). The concentration of soluble oxygen could be reduced from 8.0 - 9.0 mg/l to 1.0 - 1.5 mg/l by application of N_2-filled pouches. At 4°C and 25°C, the oxygen content in the glass syringe was similar to the oxygen content in polymer packaging containers stored with atmosphere contact. However, oxygen content in the glass syringe was reduced to < 0.5 mg/l after storage at 40°C.

The remaining concentration of ≤ 1.5 mg/l oxygen for solution in polymer packaging after storage was achieved by placing them into nitrogen-filled pouches in a laboratory environment. It is expected that professional filling equipment and filling under inert atmosphere (e.g. N_2-gas) can lead to even lower oxygen levels in the bag. Additionally, the use of oxygen absorbers may provide easier handling, more reliable oxygen reduction, and lower oxygen levels [31].

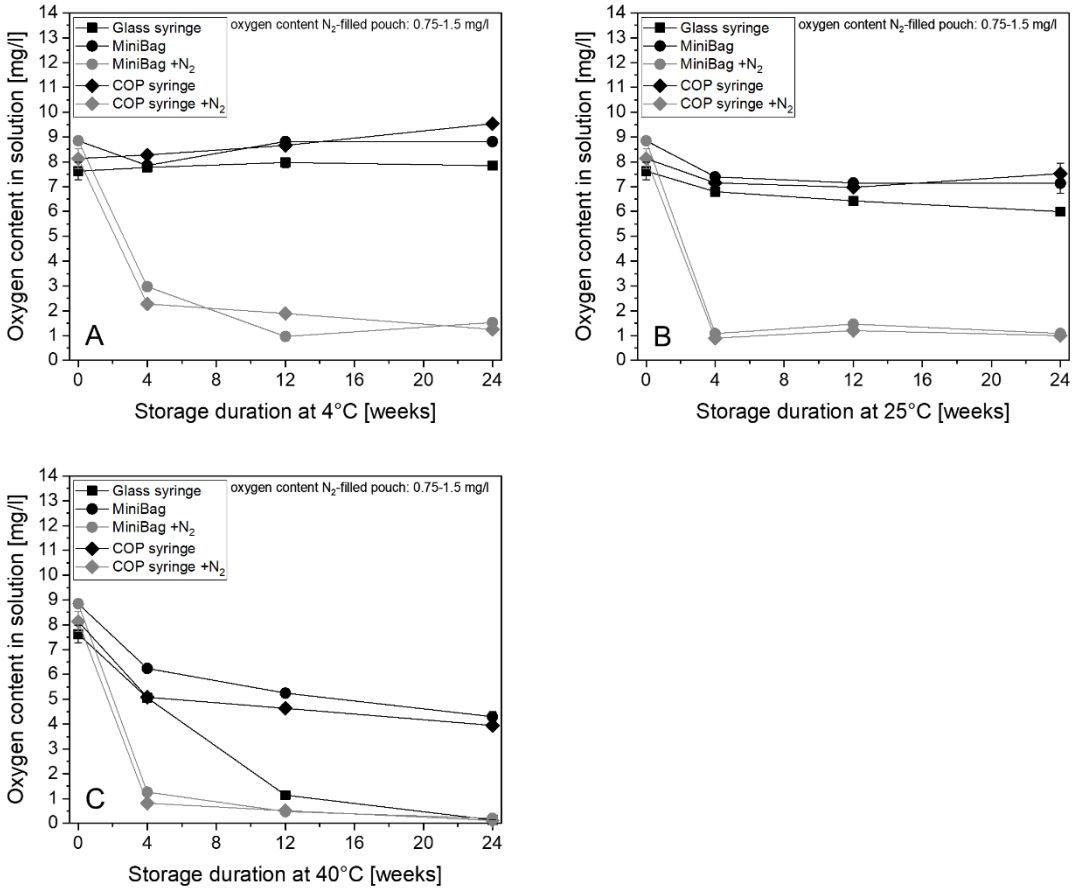

Figure 22: Oxygen content in solution after storage for 24 weeks at A.) 4°C, B.) 25°C, and C.) 40°C.

The formation of oxidized mAb was primarily investigated using analytical protein A chromatography [39]. Peptide mapping LC-MS was further used to identify oxidized methionines and calculate the amount of oxidized species after 24 weeks at 40°C. Additionally, the amount of oxidation was investigated using subunit mass analysis and detection by LC-MS after 24 weeks for all storage conditions.

Oxidation of the mAb was present in all samples and highly dependent on the storage temperature (Figure 23). As a consequence of the reduction of soluble oxygen, the rate of protein oxidation in polymer packaging containers in N_2-filled pouches was significantly lower than in polymer packaging materials exposed to atmosphere. Storage of the protein at 4°C resulted in the least increase in

oxidized species, with a change from 12.5% to around 16% independent of the packaging. Polymer packaging materials stored in a N_2-filled aluminum pouch at 25°C exhibited a lower increase in oxidized species compared to packaging materials stored under atmosphere. Although only a slight reduction was found for samples stored at 25°C, almost 7% difference was detected in 40°C samples between storage in N_2-filled pouch and atmosphere. In general, all species eluting prior to the main peak were reported as oxidized species in protein A chromatography and their content was found to reflect the extent of oxidation of all four Fc methionines in a mAb, correlating well with peptide mapping LC-MS [39]. The rate of oxidation of the mAb in both polymer packaging materials stored in N_2-pouch was comparable to the rate of oxidation within the glass syringe, providing a suitable solution to the disadvantage of higher gas permeability of polymer packaging materials [14, 15, 29, 30].

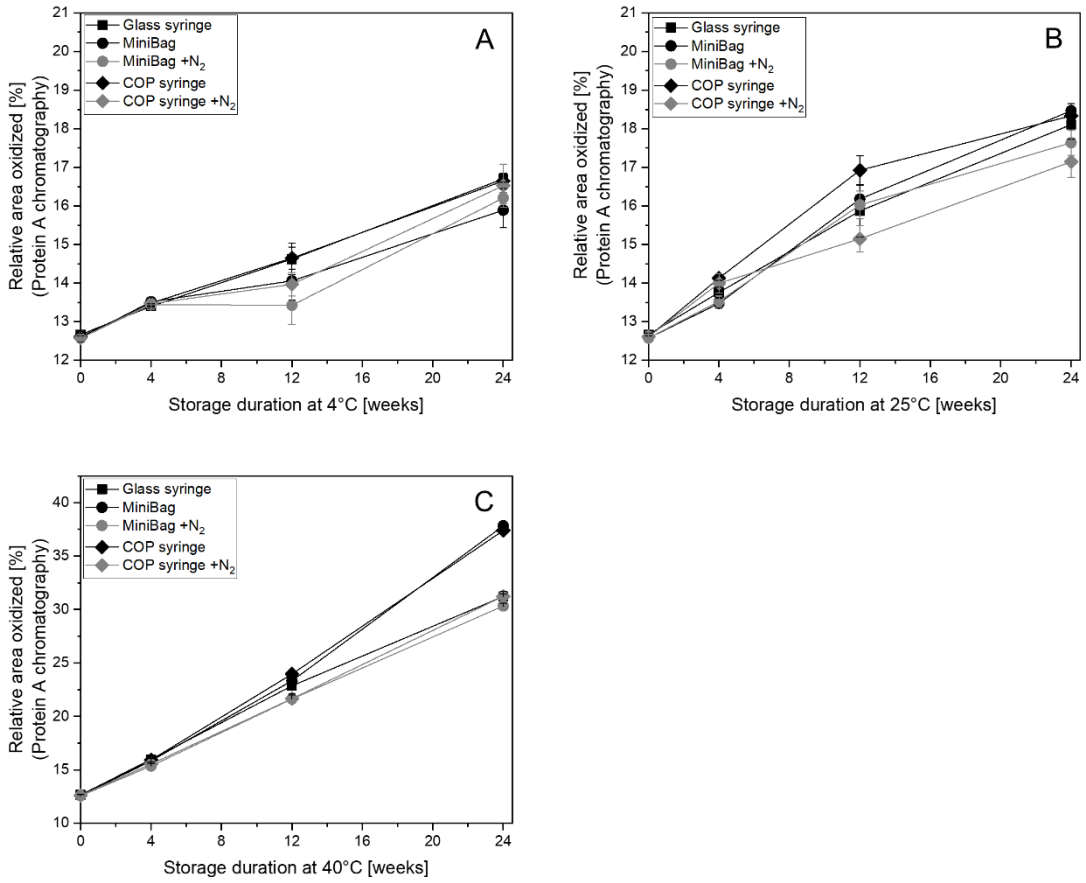

Figure 23: Amount of oxidized species determined by protein A chromatography after storage for 24 weeks at A.) 4°C, B.) 25°C, and C.) 40°C.

Peptide mapping LC-MS was used to identify and quantify methionine oxidation. The mAb sequence revealed 5 methionine residues in the heavy chain and 1 in the light chain. The oxidation of each methionine was investigated initially after filling, and after 24 weeks at 40°C for each packaging system (supporting information, Figure 29S). No oxidation was found for the methionine in the light chain and for 2 methionines in the heavy chain (M48 and M107). Methionine M93 showed only very minor oxidation with a change of < 3% throughout storage. M255 and M431 exhibited pronounced oxidation during storage and accounted for more than 80% of the protein oxidation. Both M255 and M431 were further detectable with PAC [39, 49, 50]. The cumulative amount of oxidized species for M255 and M431 (Figure 24A) indicated the least oxidation in the MiniBag +N_2 and the COP syringe +N_2, followed

by the glass syringe. The MiniBag and the COP syringe stored with contact to atmosphere showed the highest level of oxidized species of around 40%. Since peptide mapping indicated oxidation mainly in methionine residues which affects the binding affinity of protein A upon oxidation, the rank order of oxidation was comparable between PAC and peptide mapping LC-MS.

Additionally, subunit mass analysis (Figure 24B) was used to detect antibody oxidation [49, 50]. Again, the highest level of oxidation was observed in the MiniBag samples and the COP syringe stored at 40°C at the atmosphere. N_2-filled secondary packaging drastically reduced the degree of oxidation to a similar level compared to protein solutions filled into glass syringes. No oxidation was observed in subunit mass analysis after storage at 4°C or 25°C for 24 weeks.

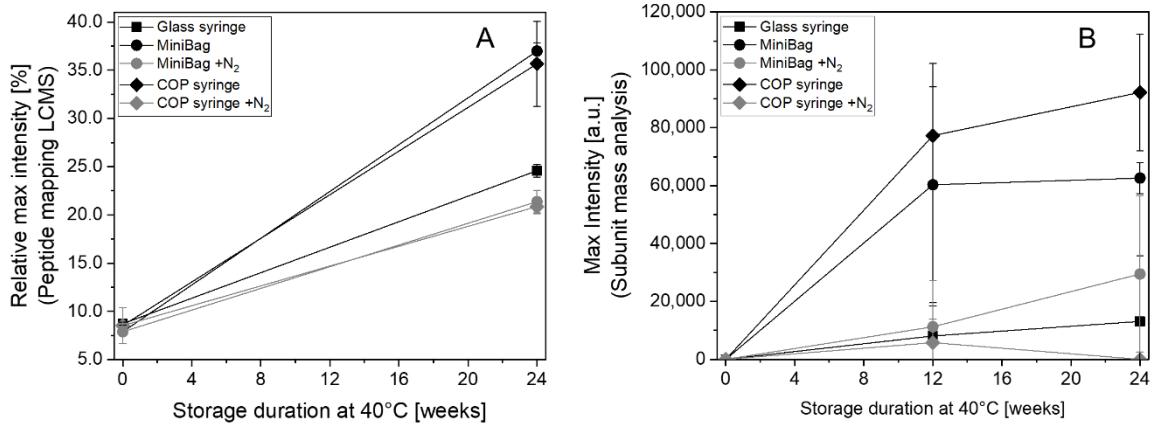

Figure 24: Amount of oxidized species determined by A.) peptide mapping LC-MS and B.) subunit mass analysis and detection by LC-MS after storage for 24 weeks at 40°C. For peptide mapping results, oxidation in M255 and M431 was summarized. Subunit mass analysis results are shown for the F_c-part.

Although oxidation in polymer packaging materials could be reduced through secondary packaging, it was not possible to prevent oxidation completely. Taking oxygen content and the total amount of antibody into consideration, a calculation of the theoretical degree of oxidation was possible. For example, 94 µmol oxygen (at e.g. 1 liter bag volume and 1.5 mg/l oxygen) were available within the

gas phase of a single pouch containing either 8 syringes (1.2 ml filling volume) or 4 MiniBags (2.4 ml filling volume) accounting for in total 5.4 µmol oxygen in solution (9.6 ml protein solution with 9.0 mg/l soluble oxygen after filling). Comparing the available amount of oxygen within a bag (99.4 µmol) to free methionine (9.6 ml at 20 mM methionine: 192 µmol free methionine) and the two methionines prone to oxidation per heavy chain (M255 and M431) in the antibody sequence (9.6 ml at 1 mg/ml mAb containing 2 heavy chains per mAb molecule: 35.8 µmol mAb methionine), a theoretical methionine oxidation of max. +43.6% can be expected. A further reduction of oxidation could be expected from a further reduction of available oxygen within the bag and in solution, either by automatic filling equipment with N_2-blanketing or the usage of oxygen absorbers in the pouch [31].

Additionally, the theoretical maximal degree of oxidation of solutions within a glass syringe was calculated, assuming no gas exchange between the inside and outside. At a filling volume of 1.2 ml and 9.0 mg/l soluble oxygen, 0.68 µmol oxygen were available within a single glass syringe. Comparing the amount of available oxygen per syringe to free methionine (1.2 ml at 20 mM methionine: 24 µmol free methionine) and the two methionines prone to oxidation per heavy chain (M255 and M431) in the antibody sequence (1.2 ml at 140 mg/ml mAb containing 2 heavy chains per mAb molecule: 4.5 µmol mAb methionine), a theoretical methionine oxidation of max. +2.4% should occur. However, an increase of +16% to +19% in oxidized species was observed in peptide mapping and PAC, respectively, which cannot be explained by the amount of oxygen in solution. Despite excellent barrier properties of the glass material, substantial ingress of oxygen through the tip-cap and stopper of the syringe must have happened, causing the observed oxidation [15, 29, 51]. However, oxygen ingress appears to be slower than in polymer packaging materials, as the content of soluble oxygen decreases during storage in the glass syringe due to consumption through oxidative reactions (Figure 22C).

3.3 Chemical degradation

Besides the main charge variant of the mAb, 22% acidic and 4.5% basic variants were found initially. Temperature-dependent decrease of the main peak area due to formation of acidic and basic isoforms was observed in IEX after storage at 4°C, 25°C and 40°C. Due to a loss in characteristic charge variants at 40°C, 24 weeks were not evaluated (Figure 25). No distinct differences were found between the packaging solutions at all storage conditions. Acidic variants were mainly formed at elevated storage temperatures, whereas basic isoforms were formed relatively independent of the storage temperature. The formation of basic variants combined with no or slight formation of acidic variants resulted in a slight increase of 0.2 pH units throughout storage over 24 weeks at 4°C and 25°C (supporting information, Figure 30S). The formation of both isoforms in samples stored at 40°C resulted in no pH shift throughout storage. This behavior was comparable in all packaging solutions and no distinct differences were observed in IEX analysis.

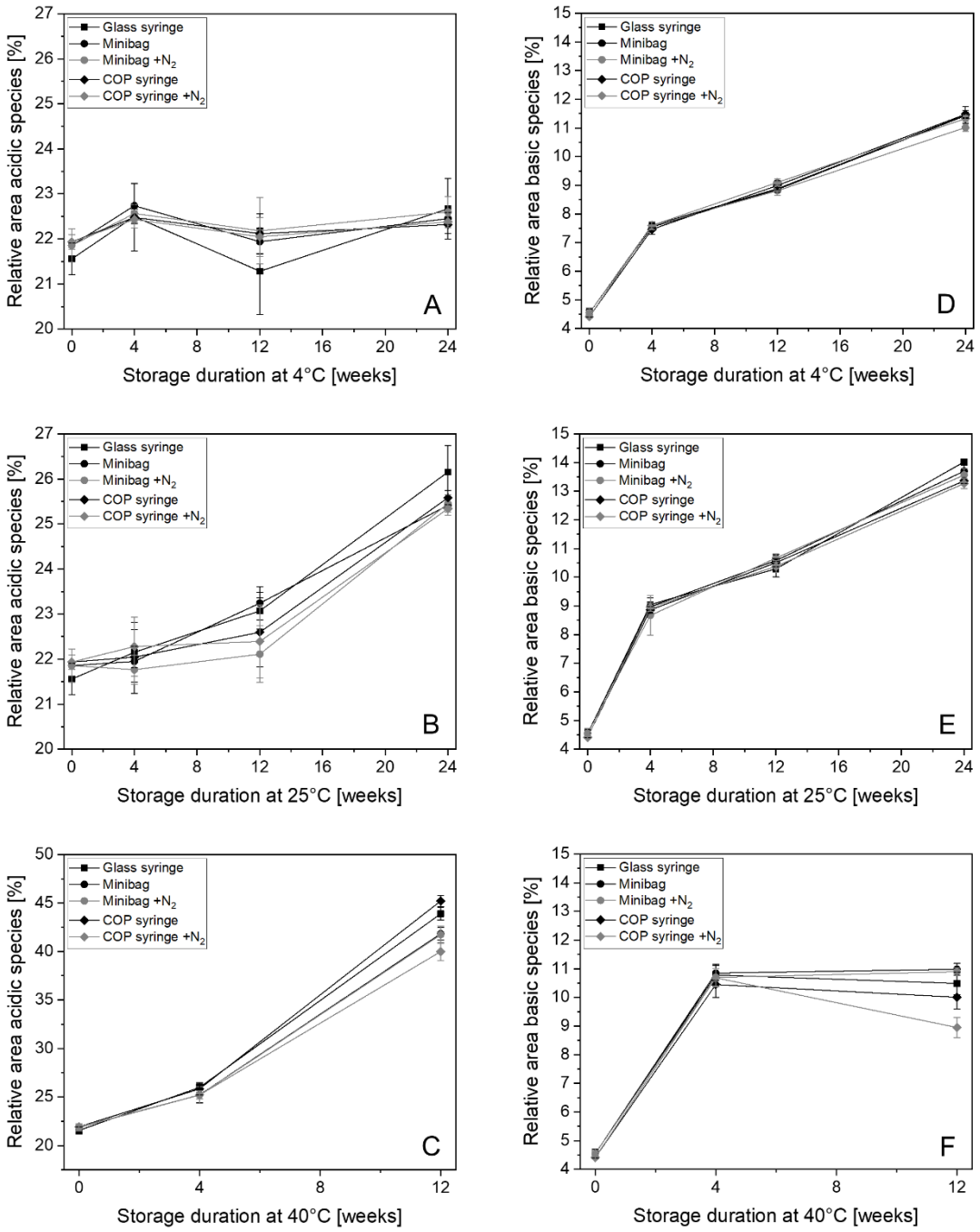

Figure 25: Relative area of acidic species after storage for 24 weeks at A.) 4°C, B.) 25°C, C.) 40°C and basic species after storage for 24 weeks at D.) 4°C, E.) 25°C, F.) 40°C.

3.4 Injection force and viscosity

The initial viscosity of the formulation after filling was compared to the viscosity after 24 weeks storage in the glass syringe, the MiniBag, and the COP syringe. Storage at 4°C and 25°C did not influence viscosity, but a slightly increase in viscosity upon storage at 40°C was observed (supporting information, Figure 31S A). The increase in viscosity was higher in polymer packaging materials than in the glass syringe, but a negative impact on injection force was not found (supporting information, Figure 31S B). Glide forces were higher in glass syringes (25 N) compared to polymer syringes (15 N), but remained constant upon storage. Break-loose forces laid between 7.5 and 12.5 N for both syringes. Both syringes, combined with a 27G ½" needle, could be considered as easy to inject throughout the whole study [52, 53]

4. Conclusion and outlook

A novel packaging material (MiniBag) comprising of a flexible bag, laminated from a COC polymer film, was investigated as primary packaging material for a high concentrated liquid mAb formulation. A variety of critical quality attributes were investigated, and results for solutions stored in the MiniBag at 4°C, 25°C, and 40°C over 24 weeks were compared to commonly used glass and COP syringes. To overcome the weak gas barrier properties of polymer packaging materials and the resulting oxidation of drug product, N_2-filled aluminum pouches were investigated as secondary packaging [14, 15, 28-31]. Protein stability after storage was found to be acceptable in all packaging materials after storage for up to 24 weeks at 4°C and 25°C, whereas substantial reduction in protein stability was observed after storage at 40°C. Differences in protein critical quality attributes between the different packaging systems were found only in subvisible particle formation and protein oxidation (Table 6).

After storage at 4°C and 25°C, the mAb stored in glass syringes showed a linear increase in particle levels over the storage duration, resulting in the highest particle levels overall. In contrast, the particle

level remained unchanged compared to the starting values in MiniBag and COP syringe. High levels of SVPs were found in both, glass syringes and MiniBags, after storage at 40°C. The content of soluble oxygen showed similar behavior at all storage temperatures and was highest in polymer packaging materials stored at atmosphere. It could be drastically reduced by N_2-filled aluminum pouches used as secondary packaging. The lower level of soluble oxygen in polymer packaging materials in N_2-pouches resulted in reduced protein oxidation. This effect was already observed after storage at 25°C, but was found to be more pronounced after storage at 40°C. The MiniBag and the COP syringe showed similar performance regarding oxygen content and levels of protein oxidation. A negative impact on protein stability with N_2-filled secondary packaging was not observed in this study.

Table 6: Critical quality attributes and relevant differences between packaging solutions

Critical quality attributes		Relevant differences between packaging systems
Monomer and aggregation	Visual inspection	-
	Turbidity	-
	FlowCam	X
	SEC	-
Oxidation	Oxygen content	X
	Protein A chromatography	X
	Peptide mapping	X
	Subunit mass analysis	X
Chemical degradation	IEX	-
Others	pH	-
	Viscosity	-
	Injection force	-*

"-": no differences, "X": relevant differences. * injection force not analyzed for MiniBag.

The MiniBag provided a stability profile comparable to other commonly used packaging options, with no differences in most investigated critical quality attributes. The MiniBag offered advantages in SVP levels compared to a glass syringe, and the potential drawback of higher protein oxidation due to weaker barrier properties could be solved with N_2-filled secondary packaging which reduced the oxidation level below the level in a glass syringe. Additionally, the MiniBag is intended to be used in

combination with a large volume subcutaneous injection device. In this setup, the flexible format of the MiniBag, in terms of filling volume, shape, and bendability will play an important role for patient compliance. In our study, we investigated a rather “worst case” for the MiniBag with a low filling volume and therefore high surface to volume ratio. Larger filling volumes will reduce the surface to volume ratio, which could indicate similar or better performance of the MiniBag in other studies. In summary, we suggest that the MiniBag could be considered as a packaging material for biopharmaceuticals or small molecules, when large volume subcutaneous injection of the API is intended. Furthermore, the use of secondary packaging in order to mitigate the high gas permeability of polymer packaging materials is strongly recommended.

5. Acknowledgements

The financial and material support of the project through Bayer AG is kindly acknowledged. Additionally, the authors want to thank Christoph Bruhn, Sandro Lamoratta, and Juliet Padden from the analytical department at Bayer, Wuppertal, for their contribution to the project through peptide mapping LC-MS and subunit mass analysis LC-MS.

6. Supplementary data

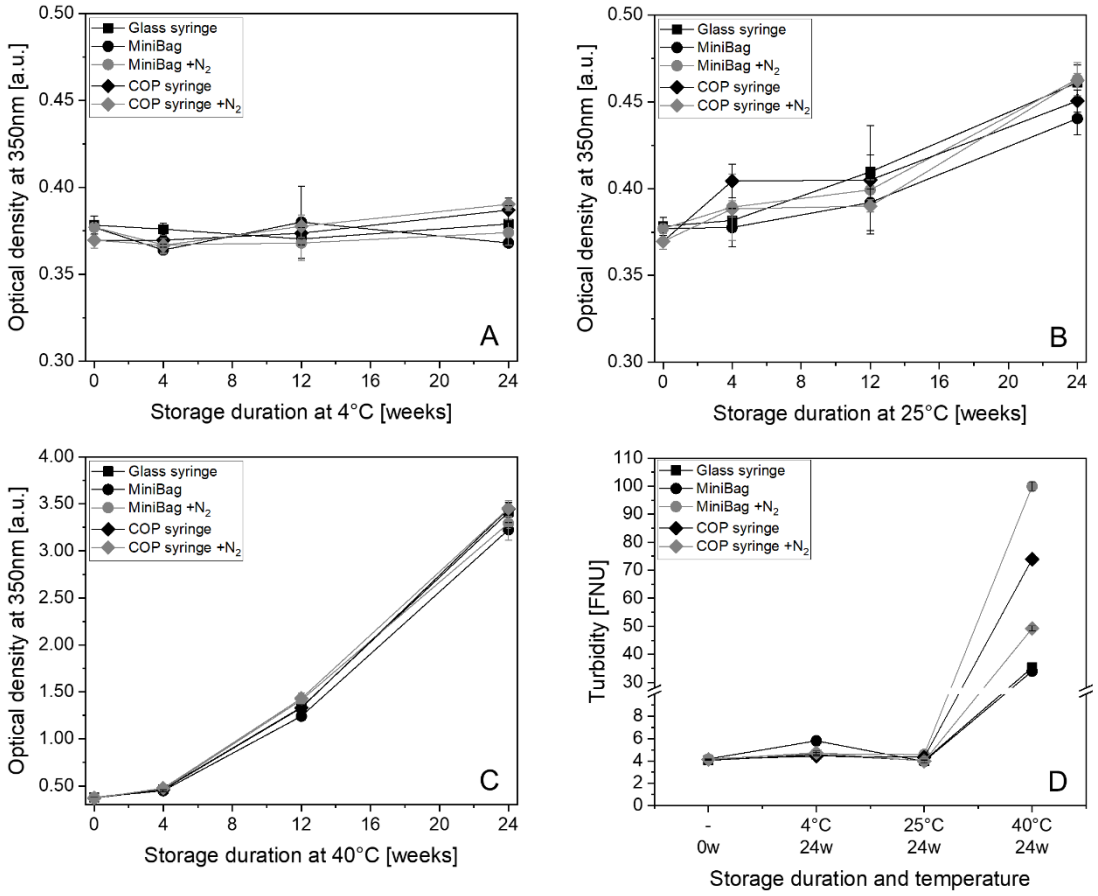

Figure 26S: Turbidity, determined as optical density at 350 nm, after storage for 24 weeks at A.) 4°C, B.) 25 °C, C.) 40°C and determined as scattering signal at 90° in FNU (D) after storage for 24 weeks at 4°C, 25 °C, or 40°C.

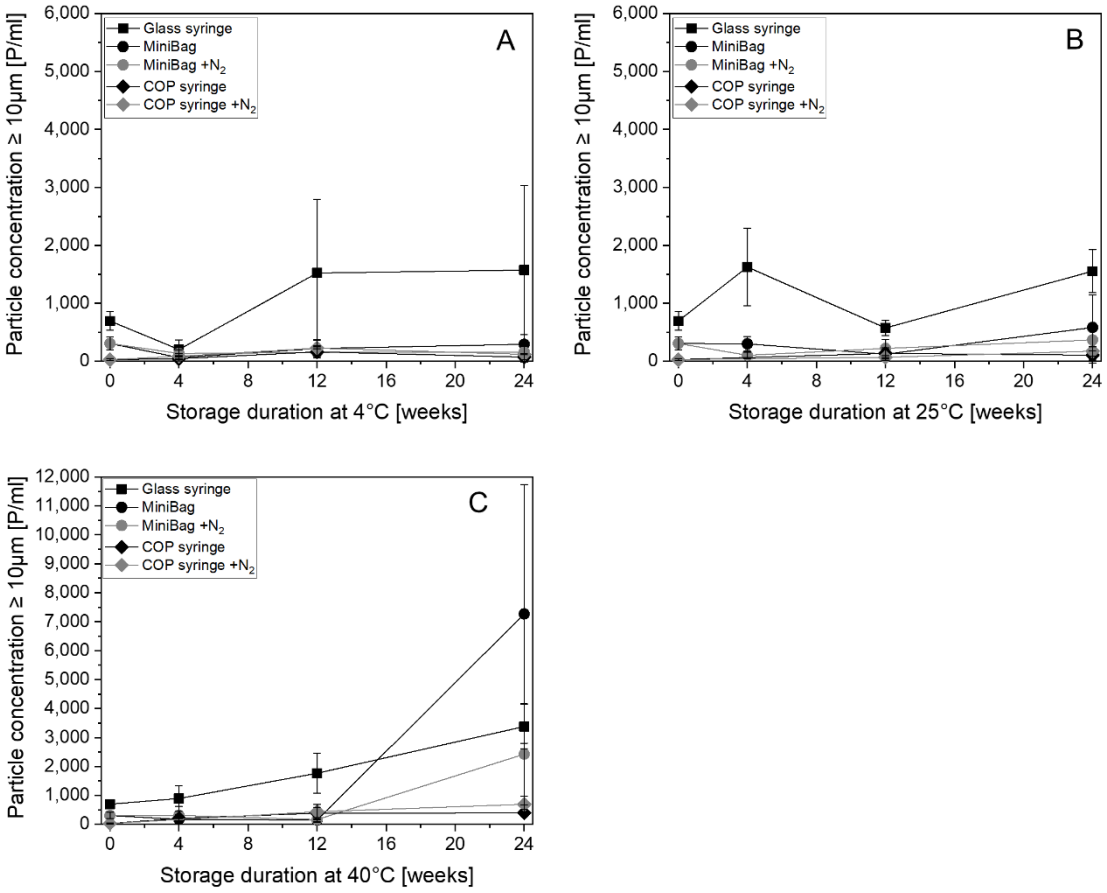

Figure 27S: Particle concentration ≥ 10 µm after storage for 24 weeks at A.) 4°C, B.) 25°C, C.) 40°C. Particle concentration per ml shown. Filling volume 1.2 ml for syringes and 2.4 ml for Minibag.

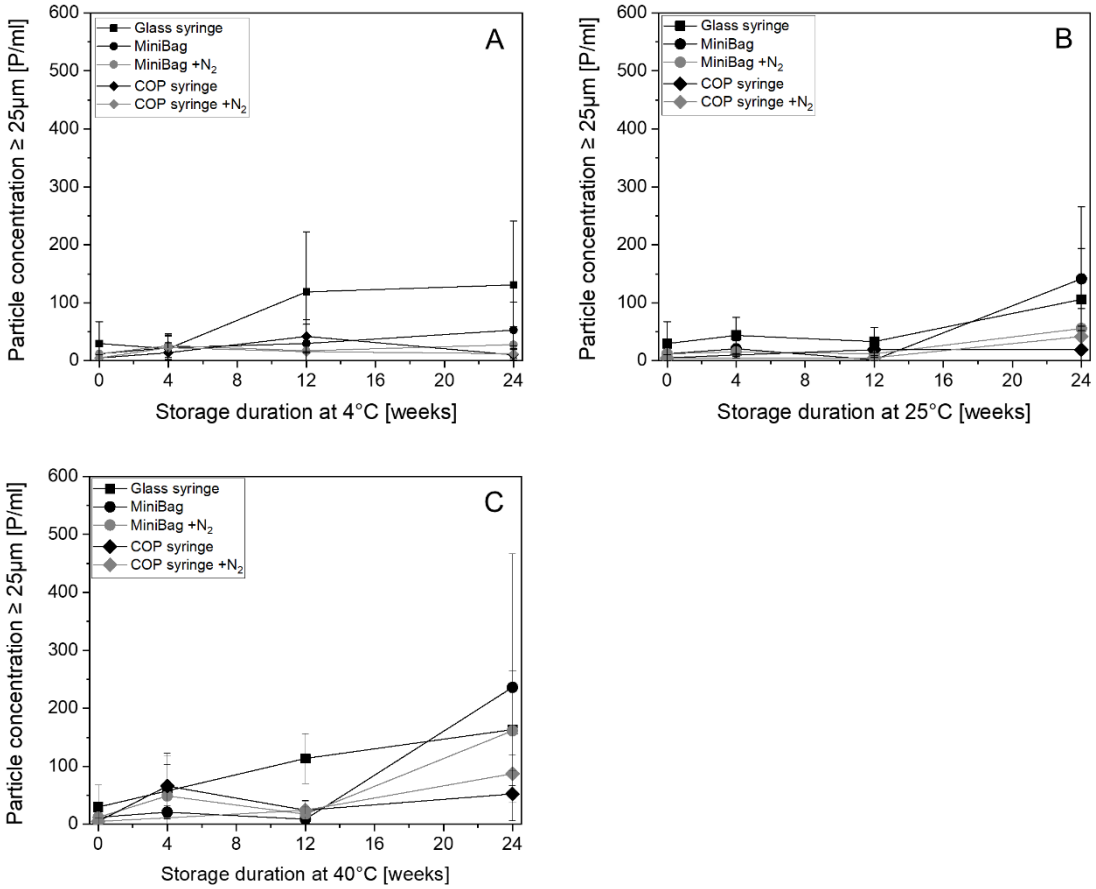

Figure 28S: Particle concentration ≥ 25 µm after storage for 24 weeks at A.) 4°C, B.) 25°C, C.) 40°C. Particle concentration per ml shown. Filling volume 1.2 ml for syringes and 2.4 ml for Minibag.

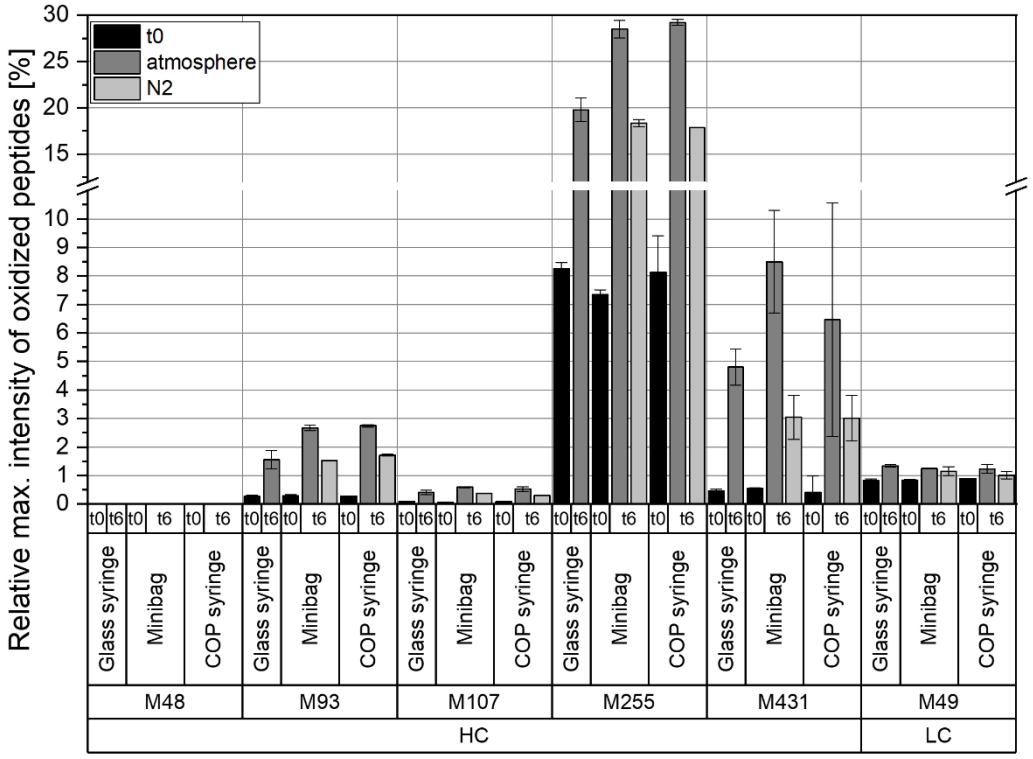

Figure 29S: Oxidation of methionine residues after 24 weeks at 40°C determined by peptide mapping LCMS.

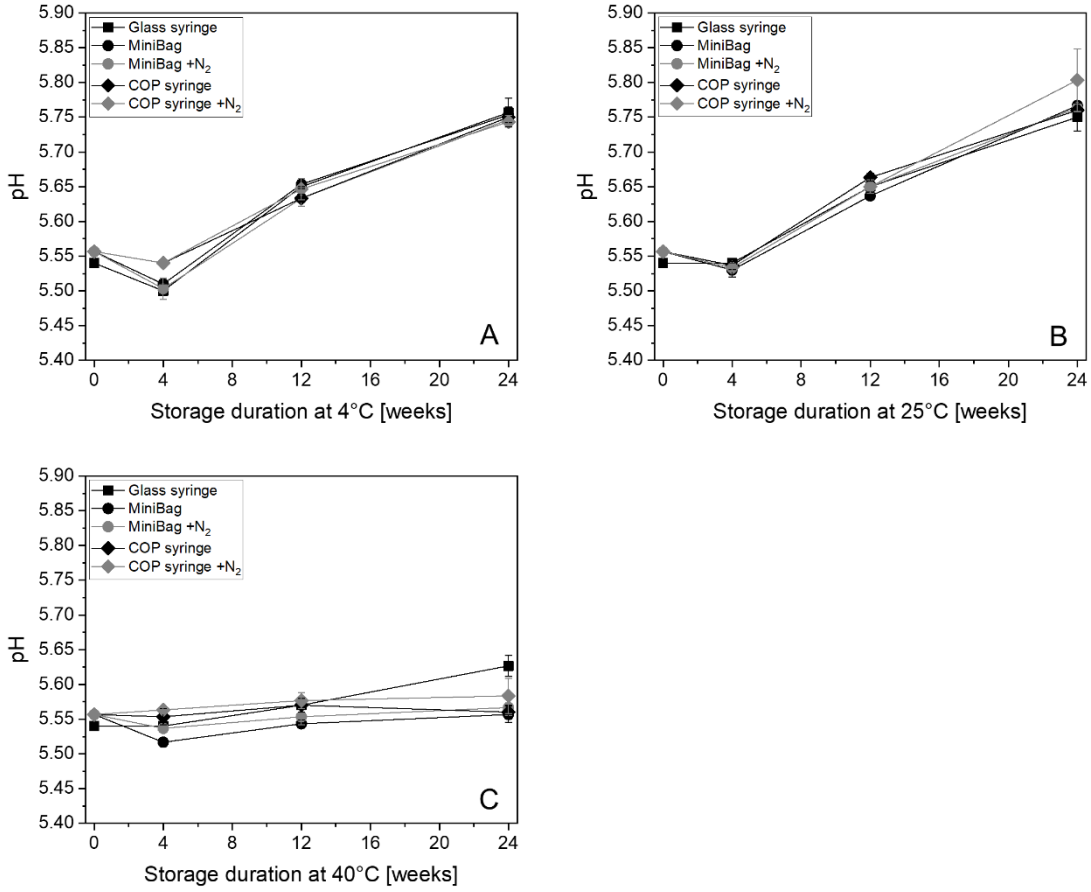

Figure 30S: pH after storage for 24 weeks at A.) 4°C, B.) 25 °C, C.) 40°C.

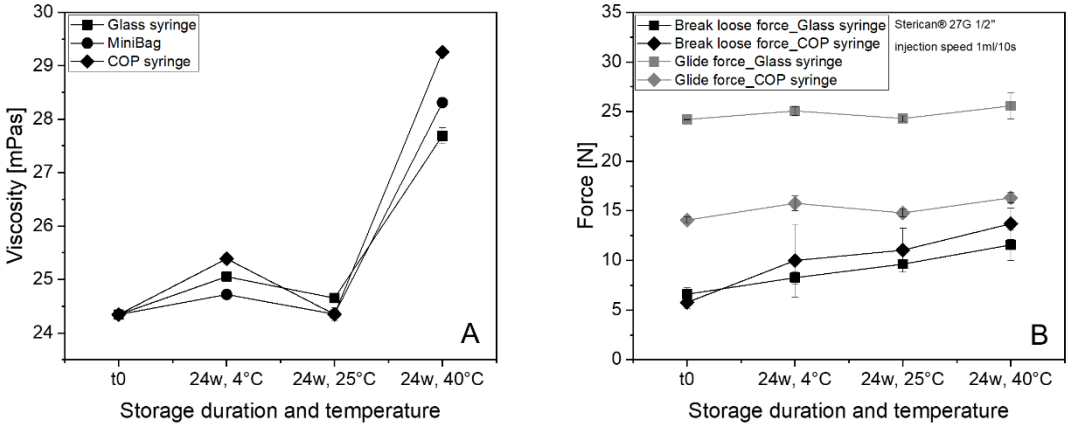

Figure 31S: A.) Viscosity and B.) break loose and gliding forces after storage for 24 weeks at 4°C, 25°C, and 40°C.

References

1. Mathaes, R., et al., *Subcutaneous Injection Volume of Biopharmaceuticals-Pushing the Boundaries.* J Pharm Sci, 2016. **105**(8): p. 2255-9.
2. Bittner, B., W. Richter, and J. Schmidt, *Subcutaneous Administration of Biotherapeutics: An Overview of Current Challenges and Opportunities.* BioDrugs, 2018. **32**(5): p. 425-440.
3. Shire, S.J., Z. Shahrokh, and J. Liu, *Challenges in the Development of High Protein Concentration Formulations.* Journal of Pharmaceutical Sciences, 2004. **93**(6).
4. Frost, G.I., *Recombinant human hyaluronidase (rHuPH20): an enabling platform for subcutaneous drug and fluid administration.* Expert Opin Drug Deliv, 2007. **4**(4): p. 427-40.
5. Narasimhan, C., H. Mach, and M. Shameem, *High-dose monoclonal antibodies via the subcutaneous route: challenges and technical solutions, an industry perspective.* Therapeutic Delivery, 2012. **3**(7): p. 889-900.
6. Bookbinder, L.H., et al., *A recombinant human enzyme for enhanced interstitial transport of therapeutics.* J Control Release, 2006. **114**(2): p. 230-41.
7. Shapiro, R., *Subcutaneous Immunoglobulin Therapy by Rapid Push is Preferred to Infusion by Pump: A Retrospective Analysis.* Journal of Clinical Immunology, 2010. **30**(2): p. 301-307.
8. Berger, M., *Principles of and advances in immunoglobulin replacement therapy for primary immunodeficiency.* Immunol Allergy Clin North Am, 2008. **28**(2).
9. Amgen Inc. *Prescribing information: Repatha®*. 2019; Available from: https://www.repatha.com/.
10. Sacha, G., J.A. Rogers, and R.L. Miller, *Pre-filled syringes: a review of the history, manufacturing and challenges.* Pharm Dev Technol, 2015. **20**(1): p. 1-11.
11. Manser, H.P., C. Egloff, and M.C. King, *Large-volume wearable drug delivery: a vision becomes reality.* ONdrugDelivery, 2019. **100**.
12. Manser, H.P. *MiniBag System*. [14.06.2020 10:30am]; Available from: https://weibelcds.com/products/minibag-system/.
13. Weibel, L.D. and H.P. Manser, *Drugdeliverysystems: Ready to use dor highest patient comfort.* ONdrugDelivery, 2015. **58**.
14. Krayukhina, E., et al., *Effects of syringe material and silicone oil lubrication on the stability of pharmaceutical proteins.* J Pharm Sci, 2015. **104**(2): p. 527-35.
15. Vilivalam, V.D. and F.L. DeGrazio, *Plastic packaging for parenteral drug delivery*, in *Pharmaceutical Dosage Forms: Parenteral Medications, Third Edition, Volume 1: Formulation and Packaging*, S. Nema and J.D. Ludwig, Editors. 2010.
16. Jezek, J., et al., *Biopharmaceutical formulations for pre-filled delivery devices.* Expert Opinion on Drug Delivery, 2013. **10**(6).
17. Yoshino, K., et al., *Functional evaluation and characterization of a newly developed silicone oil-free prefillable syringe system.* J Pharm Sci, 2014. **103**(5): p. 1520-8.
18. Demeule, B., et al., *Characterization of particles in protein solutions: reaching the limits of current technologies.* AAPS J, 2010. **12**(4): p. 708-15.
19. Badkar, A., et al., *Development of biotechnology products in pre-filled syringes: technical considerations and approaches.* AAPS PharmSciTech, 2011. **12**(2): p. 564-72.
20. Thirumangalathu, R., et al., *Silicone oil- and agitation-induced aggregation of a monoclonal antibody in aqueous solution.* J Pharm Sci, 2009. **98**(9): p. 3167-81.

21. Basu, P., et al., *IgG1 aggregation and particle formation induced by silicone-water interfaces on siliconized borosilicate glass beads: a model for siliconized primary containers.* J Pharm Sci, 2013. **102**(3): p. 852-65.
22. Gerhardt, A., et al., *Effect of the siliconization method on particle generation in a monoclonal antibody formulation in pre-filled syringes.* J Pharm Sci, 2015. **104**(5): p. 1601-9.
23. Uchino, T., et al., *Reconstitution of L-Asparaginase in Siliconized Syringes with Shaking and Headspace Air Induces Protein Aggregation.* Chemical and Pharmaceutical Bulletin, 2015. **63**(10): p. 770-779.
24. Majumdar, S., et al., *Evaluation of the effect of syringe surfaces on protein formulations.* J Pharm Sci, 2011. **100**(7): p. 2563-73.
25. Jones, L.S., A. Kaufmann, and C.R. Middaugh, *Silicone oil induced aggregation of proteins.* J Pharm Sci, 2005. **94**(4): p. 918-27.
26. Funke, S., et al., *Silicone Migration From Baked-on Silicone Layers. Particle Characterization in Placebo and Protein Solutions.* J Pharm Sci, 2016. **105**(12): p. 3520-3531.
27. Depaz, R.A., et al., *Cross-linked silicone coating: a novel prefilled syringe technology that reduces subvisible particles and maintains compatibility with biologics.* J Pharm Sci, 2014. **103**(5): p. 1384-93.
28. Werner, B.P., C. Schoneich, and G. Winter, *Silicone Oil-Free Polymer Syringes for the Storage of Therapeutic Proteins.* J Pharm Sci, 2019. **108**(3): p. 1148-1160.
29. Mathaes, R. and A. Streubel, *Parenteral Container Closure Systems*, in *Challenges in protein product development*, N.W. Warne and H.C. Mahler, Editors. 2018, Springer International Publishing.
30. Qadry, S.S., et al., *Model development for O2 and N2 permeation rates through CZ-resin vials.* International Journal of Pharmaceutics, 1999. **2**(188): p. 173-179.
31. Nakamura, K., et al., *A strategy for the prevention of protein oxidation by drug product in polymer-based syringes.* PDA J Pharm Sci Technol, 2015. **69**(1): p. 88-95.
32. Masato, A., F. Kiichi, and S. Uchiyama, *Suppression of Methionine Oxidation of a Pharmaceutical Antibody Stored in a Polymer-Based Syringe.* J Pharm Sci, 2016. **105**(2): p. 623-629.
33. Strehl, R., et al., *Discrimination between silicone oil droplets and protein aggregates in biopharmaceuticals: a novel multiparametric image filter for sub-visible particles in microflow imaging analysis.* Pharm Res, 2012. **29**(2): p. 594-602.
34. Sharma, D.K., P. Oma, and S. Krishnan, *Silicone Microdroplets in Protein Formulations - Detection and Enumeration.* Pharmaceutical Technology in Hospital Pharmacy, 2009. **33**(4): p. 74-79.
35. Weinbuch, D., et al., *Micro-flow imaging and resonant mass measurement (Archimedes)--complementary methods to quantitatively differentiate protein particles and silicone oil droplets.* J Pharm Sci, 2013. **102**(7): p. 2152-65.
36. Zolls, S., et al., *Flow imaging microscopy for protein particle analysis--a comparative evaluation of four different analytical instruments.* AAPS J, 2013. **15**(4): p. 1200-11.
37. Auge, K.B., et al., *Demonstrating the stability of albinterferon alfa-2b in the presence of silicone oil.* J Pharm Sci, 2011. **100**(12): p. 5100-14.
38. Sharma, D.K., et al., *Micro-flow imaging: flow microscopy applied to sub-visible particulate analysis in protein formulations.* AAPS J, 2010. **12**(3): p. 455-64.
39. Loew, C., et al., *Analytical protein a chromatography as a quantitative tool for the screening of methionine oxidation in monoclonal antibodies.* J Pharm Sci, 2012. **101**(11): p. 4248-57.

40. Li, Y., et al., *Characterization of the degradation products of a color-changed monoclonal antibody: tryptophan-derived chromophores.* Anal Chem, 2014. **86**(14): p. 6850-7.
41. Qi, P., et al., *Characterization of the photodegradation of a human IgG1 monoclonal antibody formulated as a high-concentration liquid dosage form.* J Pharm Sci, 2009. **98**(9): p. 3117-30.
42. Le Brun, V., *Physical properties of protein formulations*. 2009, LMU München: Fakultät für Chemie und Pharmazie.
43. European Directorate for the Quality of Medicines & HealthCare (EDQM), *Ph. Eur. 2.9.19 Partikelkontamination - Nicht sichtbare -Partikeln*. 2014.
44. United States Pharmacopeial Convention, *General chapter <788>. Particulate matter in injections*, United States Pharmacopeia, Editor. 2012.
45. United States Pharmacopeial Convention, *General chapter <787>. Subvisible particulate matter in therapeutic protein injections*, United States Pharmacopeia, Editor. 2014.
46. Kiyoshi, M., et al., *Collaborative Study for Analysis of Subvisible Particles Using Flow Imaging and Light Obscuration: Experiences in Japanese Biopharmaceutical Consortium.* J Pharm Sci, 2019. **108**(2): p. 832-841.
47. Sharma, D.K., et al., *Quantification and characterization of subvisible proteinaceous particles in opalescent mAb formulations using micro-flow imaging.* J Pharm Sci, 2010. **99**(6): p. 2628-42.
48. Werk, T., D.B. Volkin, and H.C. Mahler, *Effect of solution properties on the counting and sizing of subvisible particle standards as measured by light obscuration and digital imaging methods.* Eur J Pharm Sci, 2014. **53**: p. 95-108.
49. Gaza-Bulseco, G., et al., *Effect of methionine oxidation of a recombinant monoclonal antibody on the binding affinity to protein A and protein G.* J Chromatogr B Analyt Technol Biomed Life Sci, 2008. **870**(1): p. 55-62.
50. Chumsae, C., et al., *Comparison of methionine oxidation in thermal stability and chemically stressed samples of a fully human monoclonal antibody.* J Chromatogr B Analyt Technol Biomed Life Sci, 2007. **850**(1-2): p. 285-94.
51. Veale, J.R. and K.G. Victor, *Application Brief: Oxygen Permeation Rates Through Syringe Components*, Lighthouse Instruments, Editor. 2016.
52. Rungseevijitprapa, W. and R. Bodmeier, *Injectability of biodegradable in situ forming microparticle systems (ISM).* Eur J Pharm Sci, 2009. **36**(4-5): p. 524-31.
53. Sheikhzadeh, A., et al., *The effect of a new syringe design on the ability of rheumatoid arthritis patients to inject a biological medication.* Appl Ergon, 2012. **43**(2): p. 368-75.

Chapter 5

Application of tunable resistive pulse sensing for the quantification of submicron particles in pharmaceutical monoclonal antibody preparations

This chapter, including supplementary data, was published in the Journal of Pharmaceutical Sciences.

Authors: Andreas Stelzl[1], Stefan Schneid[2], Gerhard Winter[1]

[1] Ludwig-Maximilians Universität München, Department of Pharmacy, Pharmaceutical Technology and Biopharmaceutics, Butenandtstraße 5-13, 81377 Munich, Germany

[2] Bayer AG, Pharmaceuticals, Formulation Development Parenterals, Friedrich-Ebert-Str. 475, 42096 Wuppertal, Germany

The presented experiments were conducted by Andreas Stelzl. Scientific guidance was provided by Dr. Stefan Schneid and Prof. Dr. Gerhard Winter.

Abstract

Tunable resistive pulse sensing (TRPS, qNano Gold, IZON Ltd.) was investigated as a method to quantify submicron particles (SMPs) between 0.1 and 1 µm in solutions of biopharmaceuticals. To reduce sample dilution, a spiking-in approach was used to add the appropriate amount of electrolytes required for the measurement. For correct particle quantification, an electrolyte concentration of at least 50 mM sodium chloride was needed. Intra- and inter-nanopore variability were below 5% for size and below 10% for concentration measurements when analyzing polystyrene standard beads. Submicron particle counts in a stir stressed IgG1 monoclonal antibody formulation resulted in a non-symmetrical, almost bell-shaped size distribution with a maximum at 250 nm when using a NP300 nanopore (IZON Ltd.). It was shown that particle counts are heavily underestimated below 250 nm, and therefore it is recommended to quantify particle counts by TRPS in samples with heterogeneous particle size distributions (e.g., biopharmaceuticals) only starting from the maximum of the histogram towards the upper limit of detection.

1. Introduction

Today, submicron particle (SMP) characterization and quantification in biopharmaceuticals between 0.1 and 1 µm is often recommended or requested by regulatory agencies in addition to subvisible particle (SVP) monitoring [1]. Applicable techniques for determination of SMPs include resonant mass measurement (RMM) and nanoparticle tracking analysis (NTA) [2]. Recently, resistive pulse sensing (RPS) was introduced as new and orthogonal method for quantifying SMPs by two companies. Tunable resistive pulse sensing (TRPS, qNano Gold, IZON Ltd., Christchurch, New Zealand) uses a stretchable nanopore, whereas microfluidic resistive pulse sensing (MRPS, nCS1, Spectradyne LLC.) employs a microfluidic chip for particle analysis. The detection of particles by RPS relies on the Coulter counter principle, which determines the particles based on changes in conductivity when passing a capillary. Consequently, the detection depends on the ionic strength of the sample solution [3]. A dilution of the

sample in phosphate buffered saline (PBS) is regularly used to overcome the lacking conductivity in samples with low ionic strength [3-5]. Accurate determination of particle sizes with high resolution, even in multi-modal mixtures of three difference sizes of polystyrene beads, by using TRPS was reported allowing also qualitative comparisons of submicron particle populations [6]. Known applications of RPS include the analysis of extracellular vesicles, bacteria, viruses, nanoparticulate systems, and more [7].

In this study, a suitable sample preparation method and measurement protocol for submicron particle counting in biopharmaceuticals by using TRPS was developed. The main focus was to avoid strong dilution of the proteinaceous sample which might further reduce a potentially low particle concentration, by utilizing a spiking-approach for introduction of electrolytes to increase conductivity. Furthermore, a suitable data evaluation method is presented for proteinaceous samples typically containing protein aggregates with a heterogeneous size distribution [8].

2. Materials and Methods

2.1 Materials

L-Methionine, polysorbate 80, sodium chloride (NaCl), and sucrose were purchased from Merck KGaA (Darmstadt, Germany). Dibasic and monobasic sodium phosphate, tris base and tris hydrochloride, glycine and Dulbecco's phosphate buffered saline were obtained from Sigma-Aldrich (Steinheim, Germany). Histidine monohydrochloride monohydrate was purchased from Alfa Aesar (Kandel, Germany). A monoclonal antibody (Bayer AG, Leverkusen, Germany), belonging to the IgG class 1 (referred to as mAb), in 10 mM histidine buffer pH 5.5 with 130 mM glycine, 5% sucrose, 20 mM methionine, and 0.05% polysorbate 80 was used as model protein. The identical formulation not containing the mAb was used as placebo throughout the study. Coating solution and calibration beads

were purchased from IZON Ltd. (Christchurch, New Zealand). In-house highly purified water (HPW) (conductivity 0.055 µs/cm) was dispensed from an Arium®Pro purification system (Sartorius, Göttingen, Germany). All diluents used in the study were freshly filtered using a 0.02-µm Anotop 25 syringe filter (Whatman, Maidstone, UK). A 0.22 µm polyethersulfone (PES) syringe filter (VWR International GmbH, Darmstadt, Germany) was used for sterile filtration of mAb samples. A 5 µm Acrodisc® syringe filter with Supor® membrane (Pall Corporation, Port Washington, NY, USA) was used to remove large protein aggregates prior to TRPS analysis.

2.2 Conductivity Measurements

Electric conductivities of samples were measured in triplicate at 20°C by using an Inolab Cond Level 2 P conductivity meter equipped with a TetraCon 325 electrode (WTW, Weilheim, Germany) calibrated with a 100 µS/cm standard.

2.3 Preparation of polystyrene bead standards

Polystyrene (PS) standard beads with diameters of 110 nm (CPC100, $1.10*10^{13}$ particles/ml), 203 nm (CPC200, $2.17*10^{12}$ particles/ml), and 350 nm (CPC 400, Lot 1: $9.5*10^{11}$ particles/ml and Lot 2: $9.0*10^{11}$ particles/ml) were purchased from IZON Ltd. (Christchurch, New Zealand). Calibration beads CPC100 and CPC200 were diluted 1000-fold and CPC400 were diluted 10000-fold in two steps in filtered (0.02 µm) placebo solution and spiked with NaCl stock solution to a NaCl concentration of 50 mM in the sample immediately prior to analysis. To compare intra- and inter-nanopore variability of the investigated spiking-approach, the calibration beads CPC100 and CPC200 were diluted 1000-fold and CPC400 were diluted 10000-fold in two steps in filtered (0.02 µm) PBS immediately prior to analysis.

2.4 Preparation of proteinaceous particles

A monoclonal antibody was used as model protein to generate proteinaceous particles at a concentration of 5 mg/mL. The solution was filtered by using a 0.22-µm PES syringe filter and an aliquot of 30 ml was subsequently stressed by stirring at 300 rpm for 15 min at room temperature. Prior to analysis, stir-stressed samples were filtered through a 5-µm PES membrane filter in order to remove large aggregates which could lead to blocking of the nanopore. The samples were further aliquoted (190 µl), and each aliquot was spiked with 10 µl of a 1 M 0.02-µm filtered NaCl stock solution to reach a NaCl concentration of 50 mM in the sample. Each aliquot was analyzed for SMPs immediately after NaCl addition using a NP300 nanopore.

2.5 TRPS method on IZON qNano Gold

SMPs were quantified by tunable resistive pulse sensing (TRPS) on a qNano Gold system (IZON Ltd., Christchurch, New Zealand). With the TRPS instrument, particle concentration is measured in a particle-by-particle analysis and results obtained from sample measurements can be calibrated with a single-point calibration at the same measurement conditions (stretch, voltage, and pressure) using polystyrene standard beads of known size and concentration [9]. Frequency and amplitude of particles in the sample run can thereby be calibrated, which allows the calculation of particle concentration [9] and size [10] of the sample.

A nanopore NP300 with an analysis range of 150 - 900 nm was fitted to the qNano Gold system and a radial stretch of 47 mm was applied. A volume of 70 µl and of 35 µl of filtered (0.22 µm) coating solution was added to the lower and upper fluid cell, respectively. A pressure of +20 mbar for 30 minutes and -20 mbar for 15 minutes was applied using IZON's variable pressure unit. The coating solution was removed and both fluid cells were cleaned by rinsing with highly purified water (HPW) and blowing dry with filtered (0.22 µm) pressurized air without removing the nanopore from the

qNano Gold system. A volume of 70 µl of electrolyte, in this case placebo solution spiked with a 1 M 0.02-µm filtered NaCl stock solution to reach a NaCl concentration of 50 mM, was added to the lower fluid cell. For the measurements, a volume of 35 µl of sample was added to the upper fluid cell and measurements were conducted in "monomodal" mode (single pressure setting, +10 mbar). Voltage was adjusted to reach a current of approximately 100 nA, as recommended by the manufacturer. Cleanliness of the system was checked by recording of the particle count in electrolyte (<10 particles in 10 minutes required). A particle read of at least 500 particles or a maximum recording time of 10 minutes were chosen as measurement limits for calibration beads or proteinaceous samples. The measurement was stopped when either of the limits was reached. The recording was paused when blockages occurred and the nanopore was unblocked according to the manufacturer's guidance [11] before resuming the recording.

3. Results and Discussion

3.1 Electrolyte concentration for TRPS analysis

Different concentrations of electrolyte (20 – 100 mM NaCl) in HPW were used to determine the minimal electrolyte concentration required for stable measurement conditions on nanopores of different sizes (NP300 (150-900 nm), NP600 (275-1570 nm), NP1000 (490-2900 nm)). In order to keep the current constant at around 100 nA (Figure 32A) the voltage was increased exponentially with decreasing electrolyte concentration. At low electrolyte concentrations the baseline signal became noisy and particles were no longer detectable. Larger nanopores required in general a lower electrolyte concentration than smaller nanopores. A concentration of at least 50 mM NaCl was needed using a NP300 (Figure 32A) to reach a current of around 100 nA with a voltage below 1.0 V, as recommended by the manufacturer's user manual. TRPS therefore requires a conductivity to reach stable measurement conditions similar to microfluidic resistive pulse sensing (MRPS) [12].

Formulation buffers contribute to the sample's conductivity, and the extent was investigated by conductivity measurements and the correlation to a sodium chloride calibration curve. It was found that commonly used buffer systems in protein formulation (phosphate, tris, and histidine at 20mM buffer salt concentration) contribute an equivalent of 5-10 mM NaCl (histidine) or 15-25 mM NaCl (phosphate, tris) to the overall electrolyte concentration (Figure 32B). The mAb formulation, which was used for our further studies, comprised a histidine/glycine buffer with an electrolyte concentration equivalent to 7.5 mM NaCl. The low conductivity of the formulation led to the conclusion to spike a concentration of 50 mM of sodium chloride from a 1 M NaCl stock solution into the sample to facilitate measurements on a NP300. Spiking with 10 µl of a 1 M NaCl solution to a 190 µl sample (e.g. placebo or mAb) accounted for a dilution of 5.2% in comparison to dilution factors of 100- or 1000-fold in commonly used protocols [3-5].

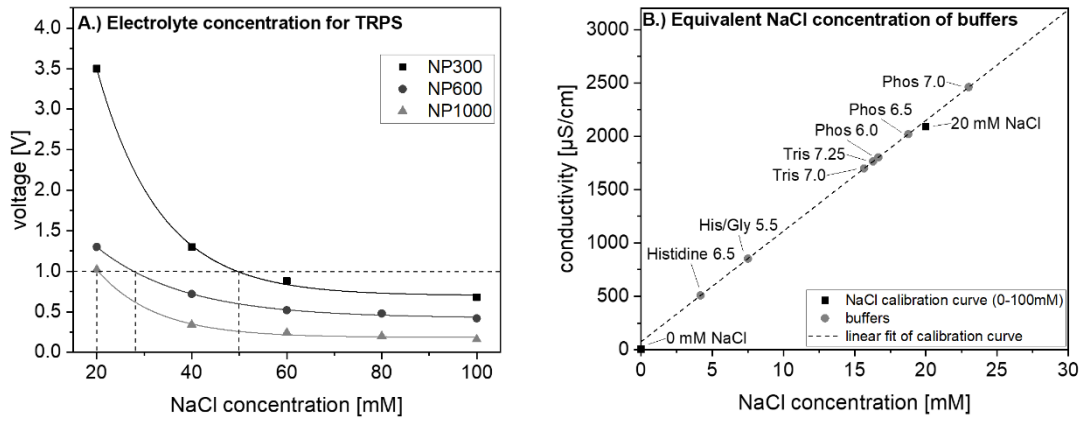

Figure 32: Determination of electrolyte concentration for TRPS measurements. A) Applied voltage to reach 100 nA current on different nanopores in dependence of the sodium chloride concentration. B) Conductivity and equivalent NaCl concentration of different formulation buffers.

A sodium chloride concentration of at least 50 mM is required to stay below a voltage of 1 V on a NP300 nanopore. Formulation buffers, at a concentration of 20 mM, contribute to the conductivity at an equivalent sodium chloride concentration between 3-25 mM NaCl.

3.2 Intra- and inter-nanopore variability with spiking-in approach

Counting and sizing precision was verified for the new sample preparation method by using polystyrene reference beads (CPC400) dispersed in placebo + 50 mM NaCl or in PBS. Particle concentration and size were measured in triplicate on three different NP300s at 47 mM stretch and a current of around 100 nA. Determination of particle concentration (Figure 33) was accurate with 100.1 ± 5.6% and 100.6 ± 3.9% relative concentration using the spiking approach or dilution in PBS, respectively. Size was determined with an accuracy of 98.1 ± 1.3% and 99.2 ± 2.1% in placebo + NaCl and PBS, respectively. Intra-nanopore and inter-nanopore variability for size were in the range of ±5% and for concentration in the range of ±10% of the expected values for the spiking approach (Figure 33A) and for dilution in PBS (Figure 33B).

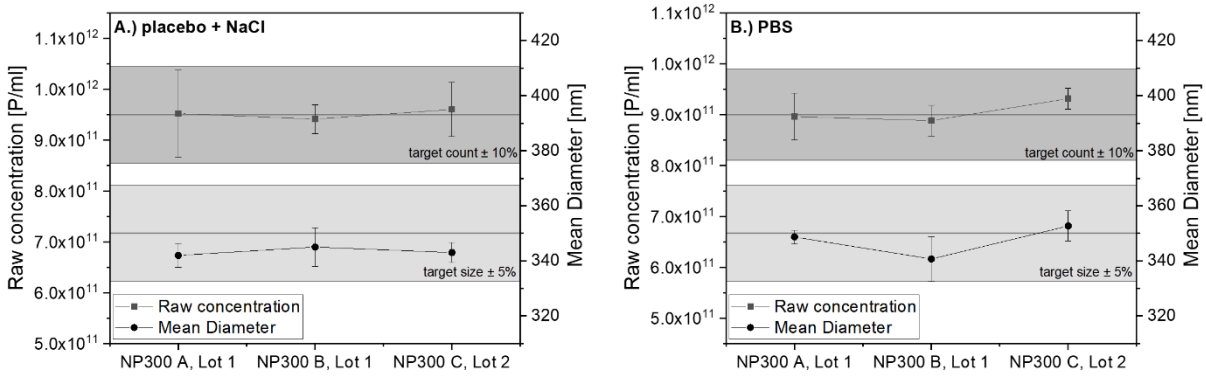

Figure 33: Intra- and Inter-nanopore variability measured in A.) placebo + NaCl, B.) PBS.

Mean ± standard deviation (n=3) shown for size and concentration of a polystyrene standard beads (350 nm; placebo + NaCl 9.5*10^{11} Particles/ml; PBS: 9.0*10^{11} Particles/ml) determined with three different nanopores. Target count ± 10% marked as dark grey area. Target size ± 5% marked as light grey area. Dilution of polystyrene beads in placebo spiked with NaCl resulted in similar intra- and inter-nanopore variability compared to dilution in PBS.

3.3 Data evaluation for submicron particle concentration in protein samples

Prior to submicron particle analysis using TRPS, large protein aggregates were removed through a 5 µm filtration, as they were identified as a main cause of blockages of the nanopore and therefore instable measurement conditions (Supplementary Figure 35S). Particle concentration < 1 µm was not impacted by this filtration step, indicated by identical particle rates of SMPs in the range 200-900 nm in samples with and without 5 µm filtration when no blockages occurred. On the contrary, particles were prevented from passing the nanopore when regular blockages occurred. Without filtration, the probability of blockages was very likely, with blockages occurring every few seconds. After 5 µm filtration, measurement durations of several minutes were possible without blockages. In addition, particle concentrations ≥ 1 µm are typically determined using other well established techniques such as light obscuration and flow imaging [13].

Submicron particle concentration as obtained on a NP300 nanopore for a stir-stressed sample after 5 µm filtration (Figure 34A) indicate a non-symmetrical, almost bell-shaped distribution with a maximum around 250 nm. A decrease in particle concentration below 250 nm is considered not plausible since, based on a 10 nm mAb monomer, aggregates are formed over a wide size range from small to large sizes rather than forming a distinct particle population [14-16]. We hypothesize that particle concentration is underestimated at the lower size limit of the nanopore since the particles get too small in relation to the orifice, resulting in a weak signal. Consequently, many smaller particles remain unrecognized by the detection algorithm resulting in an underestimation of the particle concentration. A quantification of submicron particles is therefore suggested in the range from 250 nm onwards.

This hypothesis was confirmed by determining the particle concentration of count standards with different sizes below (CPC100), around (CPC200) and above (CPC400) the proposed measurement

range for the used instrument setup (Table 7). Particles with a size below the measurement range were not detected, whereas particles with a size above the measurement range were counted in their nominal concentration. Particle concentration was underestimated by 40% for particles with a size around the lower limit of the measurement range of the given instrument setup. Therefore, we propose to evaluate particle concentration in samples containing a heterogeneous particle size distribution (e.g., stressed protein samples) by accumulating particle counts starting at the maximum of the histogram and towards larger sizes. Consequently, underestimation of the particle concentration for particles smaller than the maximum is avoided (Figure 34B).

A significant increase in SMPs was observed even after a short duration of exposure to stirring stress by using the described way of data evaluation. Particle concentration increased from $1.4 \pm 0.26*10^6$ to $3.3 \pm 0.35*10^6$ particles/ml larger than 250nm through stirring for 15 min at 300 rpm. TRPS was thereby shown to be a suitable technique to reliably detect and quantify SMPs in proteinaceous samples.

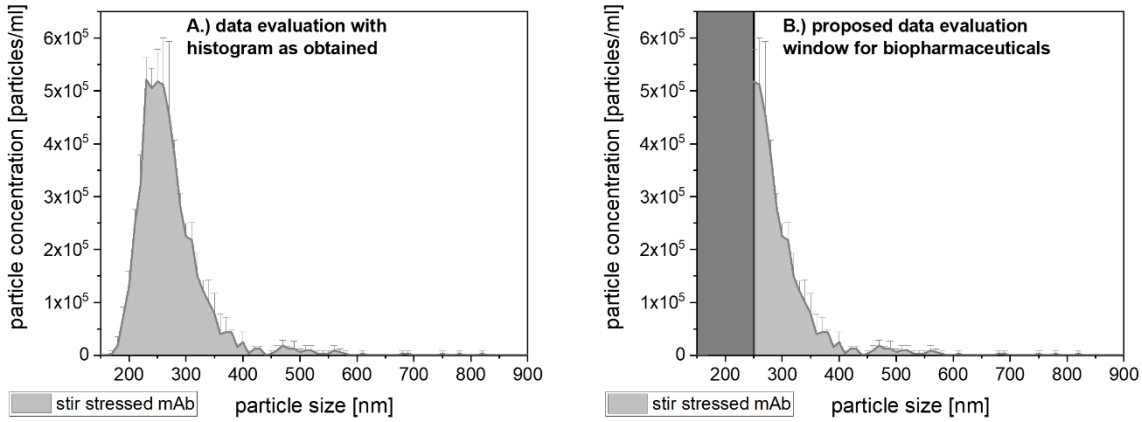

Figure 34: A) Particle size distribution histogram as obtained on a NP300 nanopore at 47 mm stretch for stir-stressed mAb. B) Proposed way of data evaluation for a sample with heterogeneous particle size distribution (e.g. aggregated IgG). The dark grey area is omitted from analysis due to underestimation of the particle concentration. Particle concentration is recommended to be reported from maximum of the histogram onwards.

Table 7: Determination of measurement range on an NP300 nanopore at 47 mm stretch using polystyrene beads of different sizes. Actual concentration is shown as mean ± standard deviation (n=3) and relative concentration was calculated using the nominal particle concentration of the polystyrene standard. No size cutoff was applied for data analysis.

Substantial underestimation of the particle concentration observed for CPC200 beads, which are close to the proposed lower quantification limit, whereas nominal concentration was determined for larger polystyrene beads (CPC400).

Polystyrene beads	Nominal size of the standard beads	Nominal Concentration	Actual concentration measured	Relative concentration
	[nm]	[particles/ml]	[particles/ml]	[%]
CPC100	110	$1.10*10^{13}$	$4.12*10^{10} \pm 5.19*10^{10}$	0.4 ± 0.5
CPC200	203	$2.17*10^{12}$	$1.27*10^{12} \pm 1.33*10^{11}$	58.7 ± 6.1
CPC400	350	$9.50*10^{11}$	$9.13*10^{11} \pm 3.64*10^{10}$	96.1 ± 3.8

4. *Conclusion and Outlook*

The conductivity of commonly used buffering agents at a concentration of 20 mM was found to be not sufficient for submicron particle analysis using TRPS. The addition of electrolytes via dilution in PBS to overcome the lack in conductivity is an approach regularly reported in literature [3-5]. To avoid substantial dilution of the proteinaceous sample, which may further reduce potentially low particle concentrations, a spiking-approach to introduce electrolytes to increase conductivity was investigated in this study. Changing the sample preparation protocol from dilution in PBS to spiking-in the appropriate concentration of electrolytes from a concentrated stock solution of NaCl to low ionic-strength samples offered the benefit of minor sample dilution without affecting the data quality obtained in submicron particle counting and sizing by TRPS. The ionic strength of a 50 mM NaCl solution was sufficient for TRPS measurements with a nanopore size of NP300 or larger, thereby covering the particle size range from 0.15 to 2 µm. Intra- and inter-nanopore variability was good with <5% deviation for sizing accuracy and <10% deviation for counting accuracy on three different nanopores, which can be considered remarkably low for counting in the nanometer size range [17]. The spiking-in approach resulted in an accuracy of 98.1 ± 1.3% for size and 100.1 ± 5.6% for concentration determination, compared to the target size and concentration of polystyrene standard beads. The spiking-in approach offers the advantage of a minor dilution factor of 5.2% when spiking with NaCl stock solution to a NaCl concentration of 50 mM in the sample without compromising data accuracy compared to a dilution in PBS (e.g. 1000-fold) [3].

TRPS was successfully applied to proteinaceous samples, for which an increase in submicron particle counts was detected after a short duration of stirring stress. Data analysis for proteinaceous samples is proposed to be conducted by integrating the obtained histograms from the maximum towards the upper limit of the measurement range. An underestimation of the particle count at particle sizes lower than the peak maximum was proven, adversely affecting the data quality, if the particle concentration

across the whole size range is reported. A similar approach as suggested in this study for the data evaluation of TRPS results was performed during data analysis of MRPS (nCS1, Spectradyne LLC.) measurements of proteinaceous samples [12, 18]. Particles below the detection threshold were similarly excluded from the reported particle concentration resulting in similar particle size distributions compared to TRPS (when using the proposed cutoff) [12, 18]. Therefore, both resistive pulse sensing technologies are capable of quantifying the submicron particle concentration in proteinaceous samples and report particle concentration of heterogeneous samples (e.g. stressed protein samples) in a comparable way.

This study presents TRPS as a promising technology for submicron particle analysis in biopharmaceuticals. Further studies will investigate the comparability of TRPS to other submicron particle counting techniques used for SMP analysis in biopharmaceutical formulations and investigate the impact of the sample handling procedure on sub-micron particle populations.

5. Supplementary data

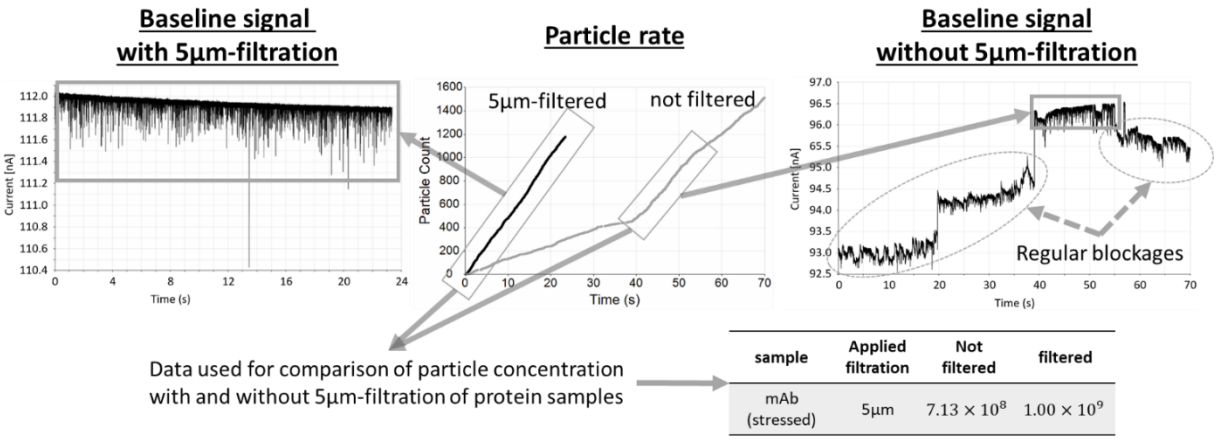

Figure 35S: Particle rate and concentration in protein samples after 2 days heat stress at 50 °C, with and without 5µm filtration. Particle rate and baseline were not obstructed by blockages in samples after 5µm-filtration. Regular blockages were observed in samples without 5µm-filtration prior to measurement. Particle concentration was found to be comparable in filtered and unfiltered samples, in case particle rate was not hampered by blockages.

References

1. U.S. Department of health and human services FDA (Center for Drug Evaluation and Research and Center for Biologics Evaluation and Research), *Guidance for Industry: Immunogenicity Assessment for Therapeutic Protein Products*. 2014.
2. Hawe, A., et al., *Subvisible and Visible Particle Analysis in Biopharmaceutical Research and Development*, in *Biophysical Characterization of Proteins in Developing Biopharmaceuticals*. 2015. p. 261-286.
3. Anderson, W., et al., *Observations of Tunable Resistive Pulse Sensing for Exosome Analysis: Improving System Sensitivity and Stability.* Langmuir, 2015. **31**(23): p. 6577-87.
4. Maas, S.L., J. De Vrij, and M.L. Broekman, *Quantification and size-profiling of extracellular vesicles using tunable resistive pulse sensing.* J Vis Exp, 2014(92): p. e51623.
5. Vogel, R., et al., *A standardized method to determine the concentration of extracellular vesicles using tunable resistive pulse sensing.* J Extracell Vesicles, 2016. **5**: p. 31242.
6. Anderson, W., et al., *A comparative study of submicron particle sizing platforms: accuracy, precision and resolution analysis of polydisperse particle size distributions.* J Colloid Interface Sci, 2013. **405**: p. 322-30.
7. Weatherall, E. and G.R. Willmott, *Applications of tunable resistive pulse sensing.* Analyst, 2015. **140**(10): p. 3318-34.
8. Scherer, T.M., et al., *Issues and challenges of subvisible and submicron particulate analysis in protein solutions.* AAPS J, 2012. **14**(2): p. 236-43.
9. Roberts, G.S., et al., *Tunable pores for measuring concentrations of synthetic and biological nanoparticle dispersions.* Biosens Bioelectron, 2012. **31**(1): p. 17-25.
10. Vogel, R., et al., *Quantitative sizing of nano/microparticles with a tunable elastomeric pore sensor.* Anal Chem, 2011. **83**(9): p. 3499-506.
11. Izon Science Support Centre. *Video: Maintaining a stable baseline current*. Accessed 07 Feb. 2021]; Available from: Available at: https://support.izon.com/video-maintaining-a-stable-baseline.
12. Grabarek, A.D., et al., *Critical Evaluation of Microfluidic Resistive Pulse Sensing for Quantification and Sizing of Nanometer- and Micrometer-Sized Particles in Biopharmaceutical Products.* Journal of Pharmaceutical Sciences, 2019. **108**(1): p. 563-573.
13. Zolls, S., et al., *Particles in therapeutic protein formulations, Part 1: overview of analytical methods.* J Pharm Sci, 2012. **101**(3): p. 914-35.
14. Roberts, C.J., *Therapeutic protein aggregation: mechanisms, design, and control.* Trends Biotechnol, 2014. **32**(7): p. 372-80.
15. Yoneda, S., et al., *Quantitative Laser Diffraction for Quantification of Protein Aggregates: Comparison With Resonant Mass Measurement, Nanoparticle Tracking Analysis, Flow Imaging, and Light Obscuration.* J Pharm Sci, 2019. **108**(1): p. 755-762.
16. Zidar, M., D. Kuzman, and M. Ravnik, *Characterisation of protein aggregation with the Smoluchowski coagulation approach for use in biopharmaceuticals.* Soft Matter, 2018. **14**(29): p. 6001-6012.
17. Hubert, M., et al., *A Multicompany Assessment of Submicron Particle Levels by NTA and RMM in a Wide Range of Late-phase Clinical and Commercial Biotechnology-Derived Protein Products.* J Pharm Sci, 2019. **109**(1): p. 830-844.

18. Barnett, G.V., et al., *Submicron Protein Particle Characterization using Resistive Pulse Sensing and Conventional Light Scattering Based Approaches.* Pharmaceutical Research, 2018. **35**(3): p. 58.

Chapter 6

Electrolyte induced formation of submicron particles in heat stressed monoclonal antibody and implications for analytical strategies

This chapter, including supplementary data, was submitted for publication in the Journal of Pharmaceutical Sciences.

Authors:
Andreas Stelzl[1], Adam Grabarek[2], Stefan Schneid[3], Wim Jiskoot[2,4,†], Tim Menzen[2], Gerhard Winter[1]

[1] Ludwig-Maximilians Universität München, Department of Pharmacy, Pharmaceutical Technology and Biopharmaceutics, Butenandtstraße 5-13, 81377 Munich, Germany

[2] Coriolis Pharma Research GmbH, Fraunhoferstr. 18 b, 82152 Martinsried, Germany

[3] Bayer AG, Pharmaceuticals, Formulation Development Parenterals, Friedrich-Ebert-Str. 475, 42096 Wuppertal, Germany

[4] Division of BioTherapeutics, Leiden Academic Centre for Drug Research (LACDR), Leiden University, PO Box 9502, 2300 RA Leiden, The Netherland

The presented experiments were conducted by Andreas Stelzl. Assistance was provided through the support by Adam Grabarek. Scientific guidance was provided by Dr. Stefan Schneid, Dr. Tim Menzen, Prof. Dr. Wim Jiskoot and Prof. Dr. Gerhard Winter.

† In memoriam of Prof. Dr. Wim Jiskoot.

Abstract

Within this study, the performance and limitations of tunable resistive pulse sensing (TRPS) was evaluated to characterize submicron particles in unstressed and heat stressed monoclonal antibody (mAb) solutions. These were compared with microfluidic resistive pulse sensing (MRPS), resonant mass measurement (RMM), and nanoparticle tracking analysis (NTA). For TRPS and MRPS measurements, adjustment of ionic strength was required but seen critical for protein formulations. Influences of sodium chloride concentration and pH on colloidal stability with respect to submicron particle levels were investigated.

Heat stress caused a sharp increase in particle levels between 250-900 nm, observable in all four techniques. Due to reduced colloidal stability, indicated by increased attractive forces and reduced aggregation onset temperatures in the presence of sodium chloride, protein aggregation was observed in heat stressed mAb only after the addition of sodium chloride. Achieving adequate ionic strength by replacing sodium chloride with other electrolytes similarly resulted in reduced colloidal stability and protein aggregation. It is recommended that protein samples prone for aggregation in the presence of high ionic strength should not be analyzed by RPS measurements after the addition of electrolytes. However, protein samples containing already required ionic strength can be analyzed by any of the four techniques.

1. Introduction

Biopharmaceuticals, such as monoclonal antibodies, can undergo several routes of degradation due to the complexity of the molecules [1, 2]. Among other degradation pathways, the formation of protein aggregates can be detrimental for product quality [3]. Submicron aggregates, despite being often overlooked, are an important category of aggregates due to their potential role in protein immunogenicity [4, 5]. However, submicron particle analysis in biopharmaceutical products in the size

range of 0.1 – 1 µm is increasingly expected by regulatory agencies [6]. Resonant mass measurement (RMM) and nanoparticle tracking analysis (NTA) are two commonly used methods to quantify the particle level in the submicron size range, but both come with certain drawbacks [7]. NTA is able to detect particles between 50 – 1000 nm based on the scattering of light and is therefore biased towards larger particles if heterogeneous particle populations are measured [7]. Depending on the used sensor, RMM is able to detect particles between 100 – 4000 nm based on their mass, which is then converted it into particle size based on the density of the particle and the density of the fluid [7]. Due to differences in particle detection and subsequent differences in particle characterization, the comparison of results obtained by RMM or NTA can be difficult. For example, a difference of 1-2 orders of magnitude in particle concentration was observed for the same sample when analyzed with both techniques [8]. Additionally, a low reproducibility in particle sizing and quantification compared to established micrometer-sized particle analysis techniques is reported [8].

Owing to improvements in micro- and nano-fabrication [9, 10], resistive pulse sensing (RPS) was introduced as new technique for submicron particle analysis. Hereby, the detection of particles in solutions relies on the Coulter counter principle (electrical sensing zone), which detects particles based on changes in the electric field between two electrodes upon particle passage through a sensing orifice [11], thereby overcoming technical limitations of RMM and NTA as discussed above. Studies have shown great accuracy of RPS in characterizing concentration and size of polystyrene bead mixtures or exosomal vesicles, giving RPS a potential advantage over other techniques [12, 13].

With tunable resistive pulse sensing (TRPS, IZON Ltd., Christchurch, New Zealand) and microfluidic resistive pulse sensing (MRPS, Spectradyne LLC., Torrance, CA, USA) two RPS-based instruments are currently available for submicron particle characterization. TRPS uses a stretchable nanopore and MRPS a microfluidic channel to create a nano-constriction, which separates both electrodes and can

therefore be used as sensing zone. Despite their structural differences, both techniques rely on sufficient ionic strength present in the sample solution [11, 14] in order to establish a stable electric current between both electrodes. Thus, particles are detected as drop in electrical resistance by crossing the nano-constriction between both electrodes. For samples with low conductivity, it is recommended to add electrolytes during sample preparation by i.e., dilution in phosphate buffered saline (PBS) [14-16] or by spiking-in electrolytes from a stock solution [17].

Applicability of RPS for different biopharmaceutical samples including protein formulations was previously presented [17, 18]. In the present study, we investigated the comparability of TRPS to other submicron particle measurement techniques, namely RMM, NTA and MRPS, for the analysis of biopharmaceuticals. Therefore, particle concentrations in the size ranges between 250 - 900 nm and 600 – 900 nm present in an unstressed and heat stressed monoclonal antibody (mAb) formulation were evaluated by using the four instruments and the results were compared. Additionally, the effect of adding electrolytes to (un-)stressed protein formulations prior to particle analysis on the formation of sub-micron proteinaceous particles was critically investigated. A guide to choose a suitable submicron particle characterization technique for biopharmaceuticals based on the conductivity of the samples concludes the paper.

2. Materials and Methods

2.1 Materials

Calcium chloride, glacial acetic acid, L-arginine hydrochloride, L-lysine monohydrochloride, L-methionine, polysorbate 80, sodium acetate, sodium chloride (NaCl), sodium sulfate, and sucrose were purchased from Merck KGaA (Darmstadt, Germany). L-histidine, L-histidine monohydrochloride monohydrate and sodium succinate hexahydrate were purchased from Alfa Aesar (Kandel, Germany). Magnesium chloride hexahydrate, monosodium phosphate dihydrate, and potassium chloride were obtained from Applichem (Darmstadt, Germany). Citric acid was obtained from USBiological Life Sciences (Hamburg, Germany), disodium phosphate dihydrate from Bernd Kraft (Duisburg, Germany), and sodium citrate from Caesar&Lorentz GmbH (Hilden, Germany). In-house highly purified water (conductivity 0.055 µs/cm) was dispensed from an Arium®Pro purification system (Sartorius, Göttingen, Germany). All diluents used in the study were freshly filtered through a 0.02-µm Anotop 25 syringe filter (Anopore membrane, Whatman, Maidstone, UK).

A mAb (Bayer AG, Leverkusen, Germany), belonging to the IgG1 subclass in 10 mM histidine buffer at pH 5.5 with 130 mM glycine, 5% sucrose, 20 mM methionine, and 0.05% polysorbate 80 was used as model protein. The identical formulation not containing the mAb was used as placebo throughout the study. Different formulations of mAb at pH 4.5 and pH 6.5 were prepared via dialysis at room temperature by using a Spectra/Por® 8000 MWCO dialysis tubing (Spectrum laboratories Inc., Rancho Dominguez, USA). A 100-fold excess of the respective histidine/glycine based formulation was used and media exchanges were performed 2 h and 4 h after the start of the dialysis. Dialysis was performed for a total duration of 24 h.

Coating solution and calibration beads (350 nm, polystyrene) for TRPS measurements were purchased from IZON Ltd. (Oxford, UK) and calibration beads for MRPS (496 nm, polystyrene) and RMM (994 nm, polystyrene) were obtained from Fisher Scientific (Ulm, Germany).

2.2 Preparation of proteinaceous particles

All mAb solutions were filtered through a 0.22-µm polyethersulfone (PES) syringe filter prior to use. To generate heat stressed samples, the mAb solution was incubated at 50 °C for 72 h (Eppendorf Thermomix, Hamburg, Germany). Prior to analysis, heat stressed and unstressed samples were diluted to 5 mg/mL mAb concentration by using 0.02-µm filtered placebo solution. The diluted samples were subsequently filtered through a 5-µm PES membrane filter in order to remove large aggregates, if any, which may cause blockages during submicron particle analysis. Furthermore, the samples were aliquoted for particle analysis and individually spiked with 1 M sodium chloride (0.02-µm filtered) stock solution to a target concentration of 50 mM sodium chloride (e.g., 190 µL sample + 10 µL electrolyte) prior to analysis. Analysis on all four submicron particle characterization techniques as well as micrometer-sized particle analysis were performed within a single working day, but particle analysis was performed not later than 2 min after the addition of sodium chloride to each individual aliquot.

2.3 Evaluation of electrolytes to increase conductivity in low-ionic-strength samples for RPS

Stock solutions of eight different electrolytes, $CaCl_2$, KCl, $MgCl_2$, NaCl, Na_2SO_4, histidine buffer pH 6.0, citrate buffer pH 6.0, and phosphate buffer pH 6.0 were prepared as spiking solutions. Concentrations were chosen to reach a conductivity of 4.5 mS/cm after 20-fold dilution and the respective values are given in Table 8. Ten microliter electrolyte stock solution or placebo were added to 190 µL 0.22-µm filtered (PES-membrane) mAb at 5 mg/mL. Because of solubility limits of histidine, required at a relatively high concentration due to low conductivity of histidine solutions, the histidine stock solution was prepared at 450 mM and 20 µL were spiked into 40 µL 5 mg/mL mAb, accounting for a 3-fold

dilution of histidine solution. Aggregation onset temperatures were analyzed by using a Prometheus NT.48.

Additionally, submicron particles were characterized by using RMM and NTA after spiking 200 µL placebo, 150 mM sodium chloride, or 450 mM histidine to 400 µL unstressed or heat stressed mAb to investigate the aggregation behavior of the heat stressed mAb in the presence of a high histidine concentration instead of sodium chloride.

Table 8: Conductivity and solute concentration at 4.5mS/cm for various excipients.

Substance class	***Electrolyte***	***Measured conductivity at 50 mM***	***Calculated concentration at 4.5 mS/cm***
		[mS/cm]	***[mM]***
Inorganic salt	***$CaCl_2$***	2.1	109.2
	KCl	6.2	36.1
	$MgCl_2$	2.2	104.2
	NaCl	4.5	50.0
	Na_2SO_4	8.5	26.6
Buffer component	***Citrate buffer, pH 6.0***	8.6	26.2
	Histidine buffer, pH 6.0	1.5	150.0
	Phosphate buffer, pH 6.0	2.4	93.4

2.4 Tunable resistive pulse sensing (TRPS)

Submicron particles were analyzed by tunable resistive pulse sensing (TRPS) on a qNano Gold system (IZON, Oxford, UK). A nanopore NP300 with an analysis range of 150 - 900 nm was fitted to the qNano Gold system and submicron particle counts were recorded and evaluated as described as previously published [17]. Three technical replicates per sample were measured.

2.5 Microfluidic resistive pulse sensing (MRPS)

A nCS1 system equipped with disposable TS-900 (125 – 900 nm) polydimethylsiloxane cartridges (Spectradyne, Torrance, CA, USA) was used for MRPS measurements. Phosphate buffered saline at pH

7.4 containing 1% polysorbate 20 was used as running buffer to generate an appropriate electrical current. For each sample, the loading volume was 3 µL and at least 500 particles were recorded per measurement. Three technical replicates per sample were analyzed. Size calibration with polystyrene beads (496 nm) was performed for each cartridge after a sample measurement to ensure appropriate sizing. False-positive signals were excluded in data analysis (Data Analysis software V2.4.0.202, Spectradyne) by applying filters based on transit time, signal-to-noise ratio, peak symmetry, and/or diameter, following the manufacturer's recommendation.

2.6 Resonant mass measurement (RMM)

An Archimedes system equipped with a Hi-Q Micro sensor (Malvern Instrument, Malvern, UK) was used for RMM. The system was calibrated with polystyrene beads (994 nm) prior to each set of measurements. Between each sample measurement, 2 sneeze operations were performed, and the system was flushed with highly purified water to ensure system cleanliness. The lower limit of detection (LOD) was determined automatically by ParticleLab software version 2.01. Density was set to 1.05 g/cm³ for polystyrene beads and to 1.34 g/cm³ for protein particles. Only negatively buoyant particles and measurements with at least 50 particle counts were used for data evaluation. Three sub-runs were performed per measurement. Three technical replicates were measured of each sample, yielding nine replicates in total.

2.7 Nanoparticle tracking analysis (NTA)

A NanoSight (Model LM20, Malvern Instrument, Malvern, UK) was used to obtain NTA data at a wavelength of 405 nm (blue laser). Purging volume of the sample chamber was 0.3 mL. By using a video capture, three sub-runs of 60 s each were performed per measurement immediately after injection at room temperature. Three technical replicates were measured of each sample, yielding nine replicates

in total. The camera levels were set to optimal values and 200 valid tracks were defined as lower limit for valid measurements. NanoSight software version 3.2 was used for data evaluation.

2.8 Dynamic light scattering (DLS)

Aggregation onset temperature ($T_{agg,onset}$) and diffusion interaction parameter (k_D) measurements were performed by using a DynaPro plate reader III (Wyatt, Santa Barbara, CA, USA) with a sample volume of 20 µL in 384-well plates (Corning Inc., Corning, NY, USA). Prior to analysis, samples were centrifuged at 2000 g for 2 min and sealed with 5 µL silicone oil to prevent evaporation and centrifuged again for 2 min at 2000 g.

k_D was determined in duplicate with 3-10 mg/mL mAb and different sodium chloride concentrations ranging from 0-150 mM. The diffusion coefficient was obtained from 20 acquisitions at 5 s/acquisition with the attenuation level set to Auto at 25 °C. k_D was evaluated by using Dynamic V7.8.2 software.

$T_{agg,onset}$ of the mAb was determined in formulations containing 5 mg/mL mAb (0.22-µm PES membrane filtered) at pH 4.5, 5.5, or 6.5 after adding 0, 50, and 150 mM sodium chloride. Samples were equilibrated at 25 °C and temperature was increased linearly to 85 °C at a rate of 0.1 °C/min. DLS was measured and each data point was recorded with 3 acquisitions of 3 s per acquisition with the attenuation level set to Auto. $T_{agg,onset}$ was determined in Dynamics V7.8.2 software.

2.9 Temperature of aggregation

A Prometheus® NT.48 (NanoTemper Technologies, Munich, Germany) was used to study thermal unfolding and aggregation of mAb formulations. Standard glass capillaries (NanoTemper) were filled with the respective formulation and placed in the Prometheus NT.48 in duplicates. Temperature was ramped from 20 – 95 °C at 1 °C/min. Protein aggregation was detected by measuring the back-reflection intensity of a light beam passing twice through the capillary [19]. The aggregation onset

temperature, $T_{agg,onset}$, was calculated with PR.ThermControl V2.1 software (NanoTemper) from the increase in scattering signal detected with the back-reflection optics.

2.10 Micrometer-sized particle (SVP) analysis

mAb samples were analyzed for the presence of micrometer-sized particles (sized within the range of 1 – 80 µm) with a FlowCam 8100 (Fluid Imaging Technologies, Inc., Scarborough, ME, USA). The system was equipped with a 10x magnification and a FOV80 flow-cell (80 µm × 700 µm). A sample volume of 150 µL was used for the analysis and the images were collected with a flow rate of 0.15 mL/min with an auto image frame rate of 28 frames/second. A distance of 3 µm to the nearest neighbor and thresholds of 10 and 13 for light and dark pixels, respectively, were used for particle detection. Particle size was reported as equivalent spherical diameter (ESD) by using VisualSpreadsheet® 4.7.6 software for data collection and evaluation.

2.11 Size exclusion chromatography (SEC)

A Dionex Ultimate 3000 system (Thermo Scientific, Dreieich, Germany) was used for SEC. Ten microgram of mAb were injected on a Waters Acquity UPLC® Protein BEH SEC column, 200Å, 1.7 µm, 4.6 × 150 mm column (Waters Corporation, Milford, MA, USA) and the elution of the protein was detected at 280 nm with a VWD-3400RS UV detector (Thermo Fisher, Dreieich, Germany). The running buffer consisted of 50 mM sodium phosphate (pH 6.5) with 300 mM sodium chloride at a flowrate of 0.3 mL/min. The chromatograms were integrated with Chromeleon V7.2 (Thermo Fisher) and the relative area of the high-molecular-weight species (i.e., small soluble aggregates) was calculated in percentage.

2.12 Viscosity

The viscosity of the prepared samples was measured by a mVROC viscometer (Rheosense Inc., San Ramon, CA, USA) using a RA05-100-087 flow cell with a 50 µm flow channel at 20 °C. Prepared samples

were filled into a 250-µL Hamilton syringe, without introducing any air bubbles. All measurements were performed at a flow rate of 250 mL/min and a corresponding shear rate of 3160 s^{-1}. Control software V2.6 was used for data recording.

2.13 Protein concentration

Protein concentration was determined on a NanoDrop One (Thermo Scientific) by measuring the absorbance at 280 nm with a baseline subtraction at 340 nm. Protein concentrations were calculated using a mass extinction coefficient of 13.7 at 280 nm for a 1% w/v IgG solution.

2.14 Conductivity measurements

Electric conductivity of samples was measured in triplicate at 20 °C by using an Inolab Cond Level 2 P conductivity meter equipped with a TetraCon 325 electrode (WTW, Weilheim, Germany) calibrated with a 100 µS/cm standard.

3. Results and discussion

3.1 Comparison of submicron particle characterization techniques

Submicron particle concentrations in placebo, unstressed and heat stressed protein (5 mg/mL mAb) samples were determined by using four different submicron particle characterization techniques. Particle size distributions were compared as obtained and particle concentrations were compared in the ranges between 250 - 900 nm and 600 - 900 nm.

3.1.1 Particle size distribution

The average particle size distributions of three replicates measured for unstressed and heat stressed mAb with any of the four particle characterization methods are shown in Figure 36. A bin size of 10 nm was applied to the obtained data for all four methods, however, the scale of the y-axis was varied in order to compare the observed particle size distributions due to differences in the observed particle

concentration between the four analytical methods as discussed in section 3.1.2. Quantitative descriptors of the particle size distributions of unstressed and heat stressed mAb as such as mean diameter, mode of the peak and D10/D50/D90 values, corresponding to the diameters below which 10%, 50% and 90% of the particles are measured, are provided in Table 9 [20, 21]. TRPS and MRPS measurements revealed a narrow particle size distribution with the vast majority of particles detected below 400 nm. RMM revealed substantial particle concentrations for particles above 600 nm, which were hardly detected with both RPS techniques. However, the high LOD values determined with heat stressed mAb samples resulted in no detected particles below 500 nm. Placebo and unstressed samples resulted in much lower LOD values in RMM measurements compared to heat stressed mAb formulations, however no particles below 250 nm were detected. NTA showed the broadest size distribution ranging from 150 nm to 900 nm with a large fraction of particles being larger than 400 nm.

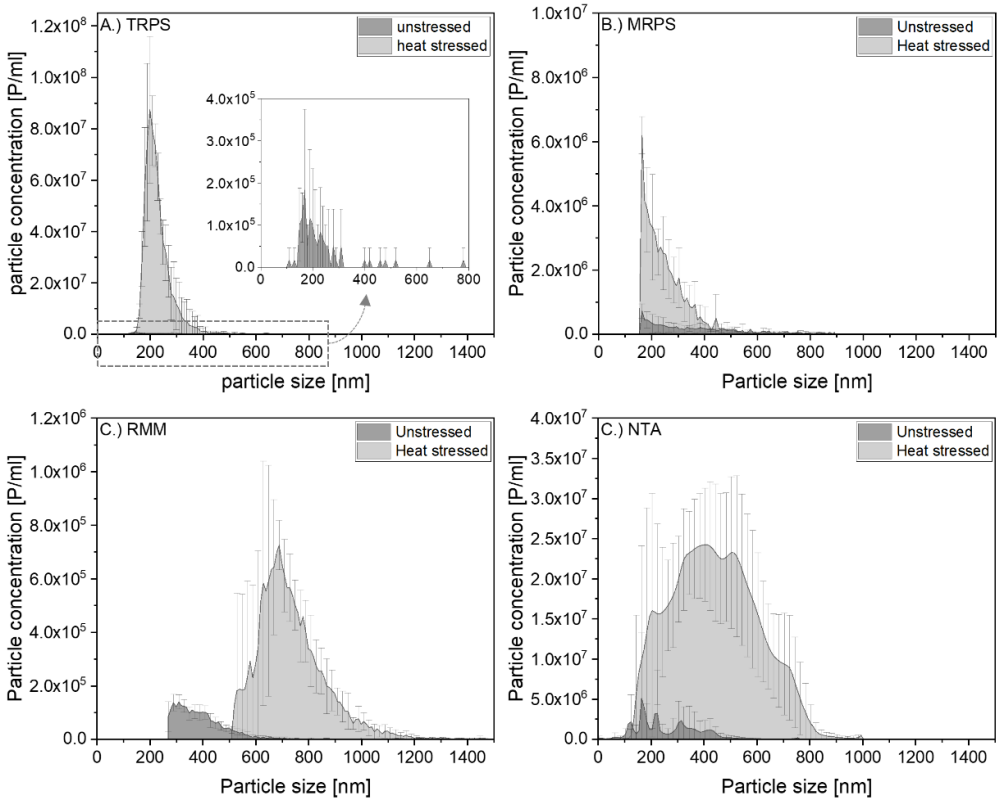

Figure 36: Particle size distribution of unstressed and heat stressed mAb formulation determined by A.) TRPS, B.) MRPS, C.) RMM, and D.) NTA. Error bars represent mean ± standard deviation (10 nm bin size) of three technical replicates. Samples were analyzed at 5 mg/mL protein concentration, except for RMM analysis of heat stressed mAb (2.5 mg/mL). All samples were spiked with 50 mM sodium chloride prior to particle analysis.

Table 9: Quantitative descriptors of the particle size distributions of unstressed and heat stressed mAb formulation

		Mean diameter [nm]	Mode [nm]	D10* [nm]	D50* [nm]	D90* [nm]
Unstressed	TRPS	232	170	150	195	305
	MRPS	358	165	170	305	625
	RMM	369	290	280	350	470
	NTA	258	165	125	225	410
Heat stressed	TRPS	226	200	175	210	280
	MRPS	250	165	165	225	355
	RMM	733	690	590	710	890
	NTA	441	405	225	430	655

*** D10/D50/D90 correspond to the diameters below which 10%, 50% and 90% of the particles are measured**

3.1.2 Particle concentration in the size ranges 250-900 nm and 600-900 nm

The comparison of particle concentrations for placebo, unstressed and heat stressed mAb formulations obtained by the four different techniques is shown in Figure 37 and Figure 43S (supplementary data). In contrast to Hubert et al. [8], particle concentrations were compared in the limited size ranges from 250 nm to 900 nm and 600 nm to 900 nm, to eliminate biases due to different size ranges inherent to the four methods.

All submicron particle characterization techniques detected an increase in particle concentration after three days of heat stress at 50 °C compared to an unstressed protein control (Figure 37 and Figure 43S, supplementary data). A narrow standard deviation of the analyzed replicates indicated a high precision in concentration determination for all four methods. However, absolute particle concentrations differed between the four measurement techniques. Between 250 – 900 nm, MRPS and TRPS detected particle concentrations of $6.5x10^7$ and $2.0x10^8$ particles/mL in heat stressed mAb samples, respectively, whereas no increase in particle concentration was observed in the size range from 600 – 900 nm. In the 250 – 900 nm size range, particle concentration in heat stressed mAb samples was highest in NTA with $9.6x10^8$ particles/mL and lowest in RMM with $2x10^7$ particles/mL. Both methods also detected a significant increase in particle levels in the size range above 600 nm. Overall, particle levels in heat stressed mAb samples detected by NTA were found to be 7.5- to 30-fold higher than particle levels obtained by RMM in the size ranges from 600 nm to 900 nm and 250 nm to 900 nm, respectively. An increase in particle concentration after heat stress in the 250 – 900 nm size range was observed with a minimum of 3-fold in RMM and up to 35-fold in NTA compared to the unstressed mAb samples. In the size range from 600-900 nm, the difference in particle concentration between unstressed and heat stressed mAb was up to three orders of magnitude.

In general, placebo formulations showed the lowest particle concentrations with up to two orders of magnitude lower concentrations measured than in unstressed protein samples. However, especially for clean samples, particle concentrations and particle size distributions relied on less than 50 detected particles for TRPS and RMM. In placebo samples, for example, less than 10 particles were typically detected within a measurement time of 10 min (TRPS) or in a measurement volume of 150 nL (RMM). After heat stress, all results derived from any of the four instruments relied on at least 500 particles per measurement for evaluation of the particle size distribution and the particle concentration.

The substantial differences in the submicron particle levels in stressed formulations detected by the four techniques was not only influenced by a high LOD value in RMM, as described in the previous section, but also by differences in particle detection between the methods [7]. For example, differences in particle concentration between RMM and NTA have been reported previously for various protein formulations with higher particle concentrations being detected in NTA, whereas RMM and MRPS showed only minor differences in particle concentration in stressed BSA samples [8, 18, 22, 23]. Comparability of the particle concentrations obtained by either of the four methods is restricted by the underlying physical parameters that are used to detect particles in solution. Additionally, an adjustment of the ionic strength was required for TRPS and MRPS measurements, but is seen critical for protein formulations. Influences of sodium chloride concentration and pH on colloidal stability with respect to submicron particle formation was therefore investigated.

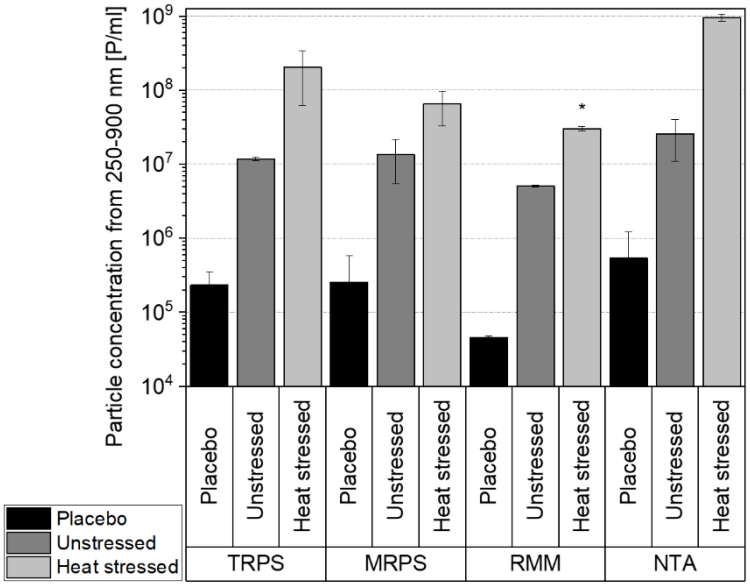

Figure 37: Comparison of particle concentrations in the size range from 250-900 nm measured by four submicron particle characterization techniques for placebo, unstressed and heat stressed mAb formulations. Error bars represent mean ± standard deviation of three technical replicates. * Particle concentration was analyzed at 5 mg/mL protein concentration, except for RMM analysis of heat stressed mAb (2-fold diluted sample was analyzed and particle concentration was corrected for dilution afterwards). All samples were spiked with 50 mM sodium chloride prior to particle analysis.

3.1.3 Dimers, oligomers and micrometer-sized particles

Particle concentrations in a size range above 1 µm were measured with flow imaging microscopy (Figure 44S A, supplementary data). Total particle concentrations in placebo and unstressed mAb samples were below 400 particles/mL above 1 µm. A slight increase to 1200 particles/mL was detected after heat stress.

The content of dimers and oligomers (Figure 44S B, supplementary data) as well as viscosity (1.4 ± 0.1 mPas) and protein concentration remained unchanged after heat stress.

3.2 Sodium chloride-induced aggregation through spiking to heat stressed mAb

The addition of electrolytes can be necessary to provide sufficient ionic strength for both RPS methods to achieve reliable results [17, 18]. To investigate the effect of adding electrolytes, RMM and NTA were used to analyze the submicron particle concentration in samples with and without electrolyte addition (Figure 38). Increasing ionic strength in unstressed mAb samples resulted in no change in submicron particle concentration in NTA measurements and only in a minor increase in particle concentration in RMM measurements. The addition of sodium chloride to heat stressed samples led to immediate particle formation, resulting in a 25-fold increase in particle concentration in RMM measurements for the entire size range measured. In NTA, the particle concentration in heat stressed mAb without sodium chloride spiking was already close to the upper limit of the measurement range of 10^{10} particles/mL [24], but an increase was still observed upon addition of sodium chloride prior to particle analysis.

In order to understand the aggregation phenomenon in heat stressed mAb solutions after adding sodium chloride, protein interactions and thermal stability of the mAb was investigated. At pH 5.5, the mAb is positively charged (isoelectric point (IEP): 8.2) and thus net repulsive electrostatic forces inhibit attractive interactions and thus stabilize the molecules from forming aggregates. Shielding positive charges by ions has been found as a cause of protein aggregation [25]. We found that the k_D was only slightly negative with -7.5 mL/g at pH 5.5 (without sodium chloride), indicating weak attractive forces between antibody molecules (Figure 39) [26]. However, k_D rapidly dropped to more negative values upon addition of small amounts of sodium chloride. At 50 mM sodium chloride, the concentration needed for RPS measurements, k_D was reduced to -29 mL/g. The decrease in k_D in the presence of sodium chloride indicates an increase in net attractive protein interactions, probably because of a

decrease in repulsive electrostatic interactions. The increase in attractive protein interactions is a likely cause for aggregation of the heat stressed mAb as discussed in the previous sections.

To further assess aggregation behavior of the mAb, $T_{agg,onset}$ was determined for antibody formulations at different pH values (pH 4.5, 5.5, and 6.5) and at different sodium chloride levels (0, 50, and 150 mM sodium chloride) by temperature-ramped DLS and Prometheus measurements. An increase in pH towards the IEP of the protein reduces the net-charge of the protein whereas decreasing pH results in higher net-charge [27]. Increased net-charge was reported to show the highest degree of repulsion and the addition of sodium chloride was furthermore found to decrease repulsive forces (via charge shielding) for various antibodies [27]. We therefore hypothesize that at lower pH (i.e., higher net charge and therewith stronger repulsive forces between protein molecules), protein aggregation should occur at higher temperatures or at higher sodium chloride concentrations compared to mAb solutions at higher pH.

Without sodium chloride, aggregation was found only in pH 6.5 samples (Figure 40A), whereas aggregate formation was not observed at pH 4.5 and 5.5. Increasing the ionic strength by adding 50 mM sodium chloride led to aggregation in pH 5.5 and 6.5 samples (Figure 40B) with a $T_{agg,onset}$ reduced from > 95 °C and 76.5 °C to 76.3 °C and 72.6 °C, respectively. At pH 4.5 only a weak scattering signal was detected at 50 mM sodium chloride, suggesting that less aggregation occurred compared to the formulations at higher pH value. At a concentration of 150 mM sodium chloride (Figure 40C), the charge shielding effects of sodium chloride supposedly overpowered electrostatic repulsion between mAb molecules, resulting in aggregation in all samples to a comparable extent. Similar trends were found in $T_{agg,onset}$ determined by using DLS (supplementary data, Figure 45S).

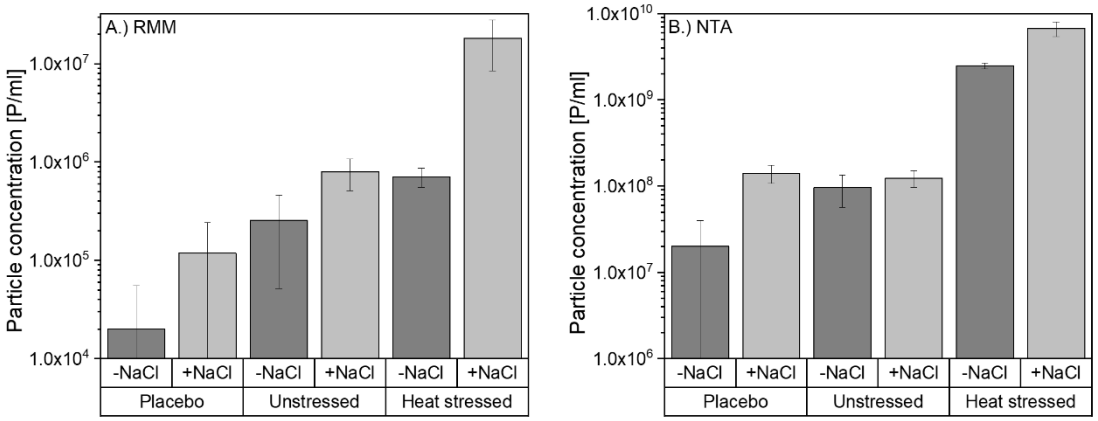

Figure 38: Submicron particle concentration with and without sodium chloride spiking, as determined by A.) RMM and B.) NTA. Mean ± standard deviation of triplicate measurements for the entire size range measured.

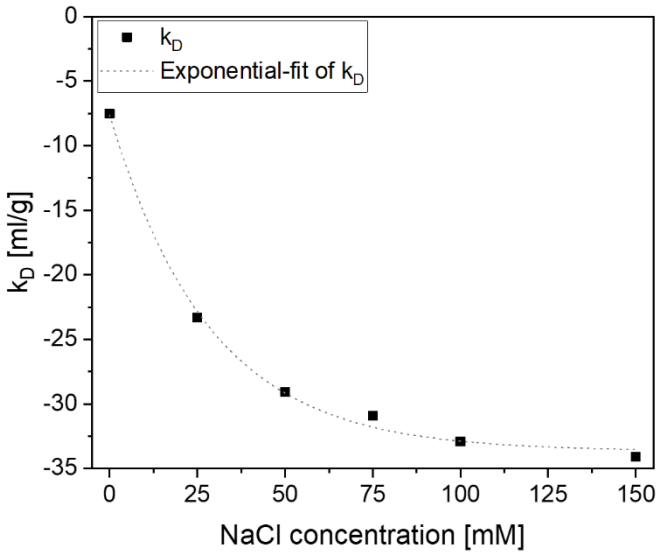

Figure 39: Dependence of k_D as a function of sodium chloride concentration in the mAb formulation at pH 5.5.

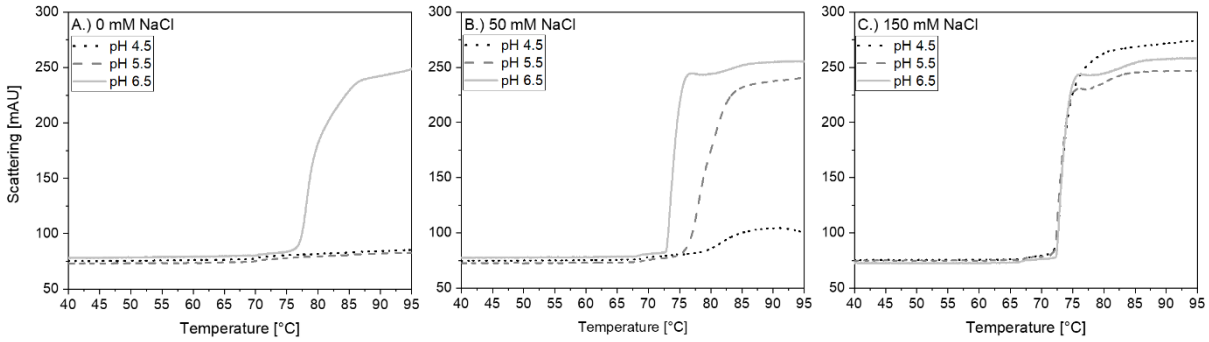

Figure 40: Scattering signal in Prometheus measurements at different formulation pH's and sodium chloride concentrations: A.) 0 mM sodium chloride, B.) 50 mM sodium chloride, C.) 150 mM sodium chloride.

3.3 Evaluation of other electrolytes as alternative to sodium chloride

Addition of alternative electrolytes, which provide sufficient conductivity to allow submicron particle analysis by using RPS without inducing so strong mAb aggregation, was evaluated. Tested electrolytes include inorganic salts and buffer components (Table 1).

All tested electrolytes showed a similar scattering signal compared to sodium chloride with aggregation onset temperatures ranging from 69.9 °C to 74.4 °C (Figure 41). None of the tested electrolytes revealed a significantly different result compared to sodium chloride.

The spiking of histidine, replacing sodium chloride as spiking solution, was investigated since histidine was already present in the formulation at a lower concentration. RMM and NTA measurements were conducted after spiking placebo, 150 mM sodium chloride, or 450 mM histidine into unstressed or heat stressed mAb formulation. Thereby, the conductivity was either unchanged when placebo was added to the sample or the conductivity was increased to a level suitable for both RPS techniques with an addition of 150 mM histidine or 50 mM sodium chloride to the sample after spiking with either of the electrolytes. Both, RMM and NTA, showed an increase in submicron particle concentration in heat

stressed mAb samples in the presence of additional histidine (Figure 42). The behavior was similar to sodium chloride spiking: Particle formation was not observed when the conductivity was not changed by spiking in placebo solution, and particle formation was not observed in unstressed mAb upon addition of placebo, sodium chloride or histidine.

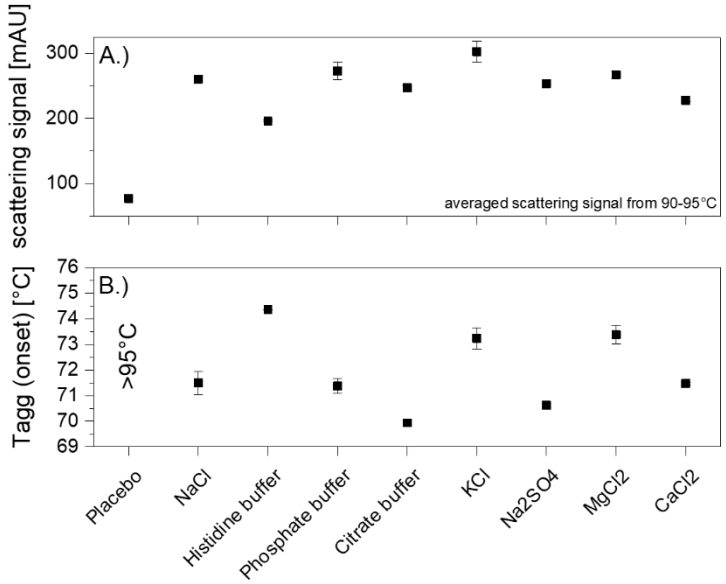

Figure 41: Aggregation of the mAb at pH 5.5 with different electrolytes at a conductivity of 4.5 mS/cm or placebo as control in Prometheus measurements. A.) Averaged light scattering signal in the temperature range from 90 °C to 95 °C, B.) Aggregation onset temperature.

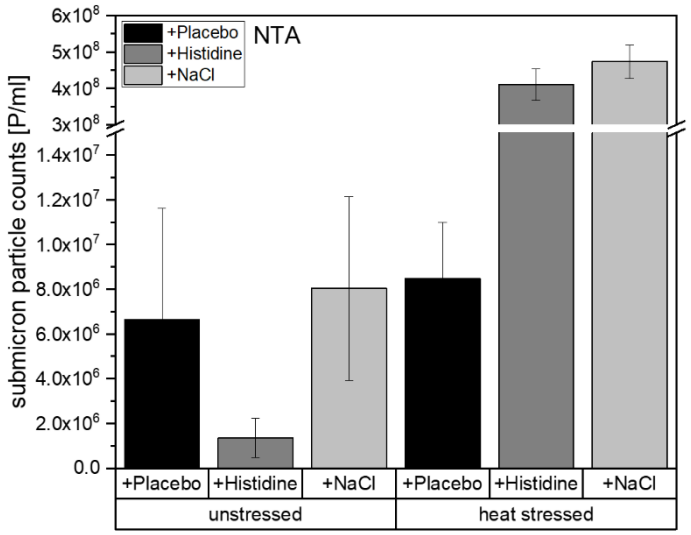

Figure 42: Submicron particle concentrations from NTA with placebo, histidine, or sodium chloride spiking to unstressed or heat stressed mAb. Mean ± standard deviation of triplicate measurements.

4. Conclusion and selection guide for submicron particle characterization methods

Four submicron particle characterization techniques were compared with regards to their capabilities of quantifying and characterizing submicron particles in proteinaceous samples. Based on previously published work [17, 18], an electrical conductivity exceeding 3 mS/cm or 4.5 mS/cm is required for MRPS or TRPS measurements, respectively, and by spiking-in electrolytes from a stock solution, suitable measurement conditions could be achieved for samples of low ionic strength. A sharp increase in SMPs after three days of heat stress at 50°C compared to unstressed mAb samples was observed by each submicron particle characterization technique and replicates yielded in a narrow standard deviation indicating a high precision in concentration determination for all four methods. Predominantly smaller particles below 400 nm were detected by both RPS techniques, whereas a larger fraction of particles above 500 nm were detected in RMM and NTA. A pronounced increase in

submicron particle levels up to $2x10^7$ to $1x10^9$ particles per milliliter in the size range from 250 – 900 nm was observed after heat stress, depending on the characterization technique. However, only a minor increase micrometer-sized particles and unchanged dimer and oligomer content were observed. SMP quantification during formulation development is therefore an important parameter to assess aggregation behavior of protein formulations without eventually waiting until aggregates have grown larger.

However, as a conductivity level of larger than 4.5 mS/cm is required for both RPS techniques, electrolyte addition was needed to meet this requirement. The addition of sodium chloride caused protein aggregation in heat stressed mAb samples due to reduced colloidal stability indicated by increased protein-protein interactions and decreased aggregation onset temperatures. The formation of submicron particles in heat stressed mAb samples was observed in RMM and NTA analysis after ionic strength adjustment compared to samples without addition of sodium chloride. The use of other inorganic salt or buffer components, such as histidine, for increasing ionic strength resulted in similar $T_{agg, onset}$ temperatures and submicron particle formation after spiking to heat stressed mAb samples. Therefore, the addition of electrolytes in order to increase conductivity of the sample for RPS measurement is not recommended.

Since RPS methods require a certain conductivity for particle detection, we recommend to first determine the conductivity of the sample and in case this complies with the mandatory requirements for RPS analysis, any of the four methods is suitable for submicron particle analysis [17, 18]. If the requirements are not met, only RMM and NTA can be recommended for the quantification of submicron particles since the measurement principle is independent of the ionic strength, giving those two methods an advantage over RPS methods.

5. *Supplementary data*

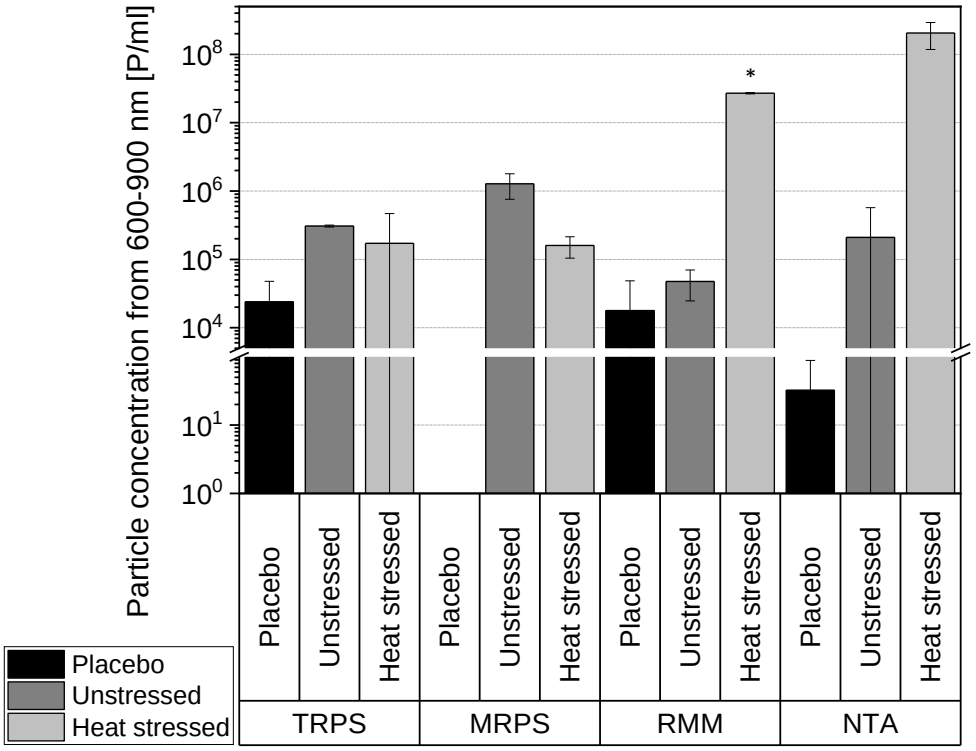

Figure 43S: Comparison of particle concentrations in the size range from 600-900 nm measured by four different submicron particle characterization techniques for placebo, unstressed and heat stressed mAb formulations. Error bars represent mean ± standard deviation of three technical replicates. * Particle concentration was analyzed at 5 mg/mL protein concentration, except for RMM analysis of heat stressed mAb (2-fold diluted sample was analyzed and particle concentration was corrected for dilution afterwards). All samples were spiked with 50 mM sodium chloride prior to particle analysis.

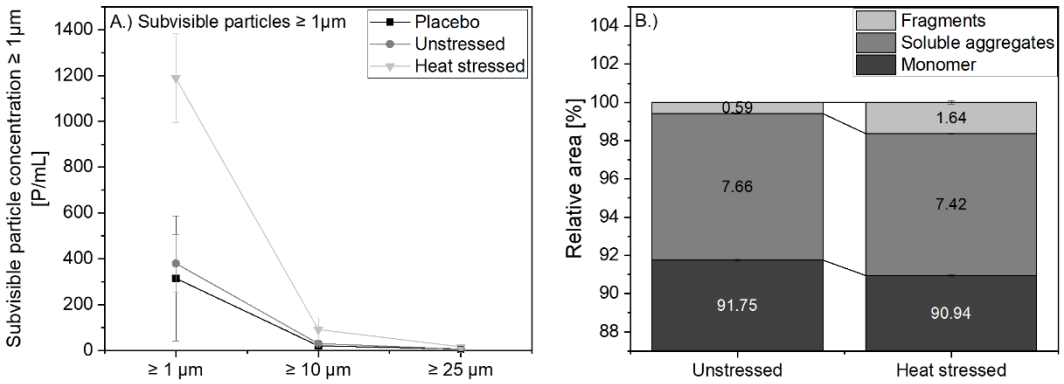

Figure 44S: A.) Subvisible particle concentrations obtained by FlowCam analysis, B.) Relative area of monomers, soluble aggregates, and fragments obtained by size exclusion chromatography. Placebo and unstressed samples were measured at t0, heat stressed samples after 3 days at 50°C.

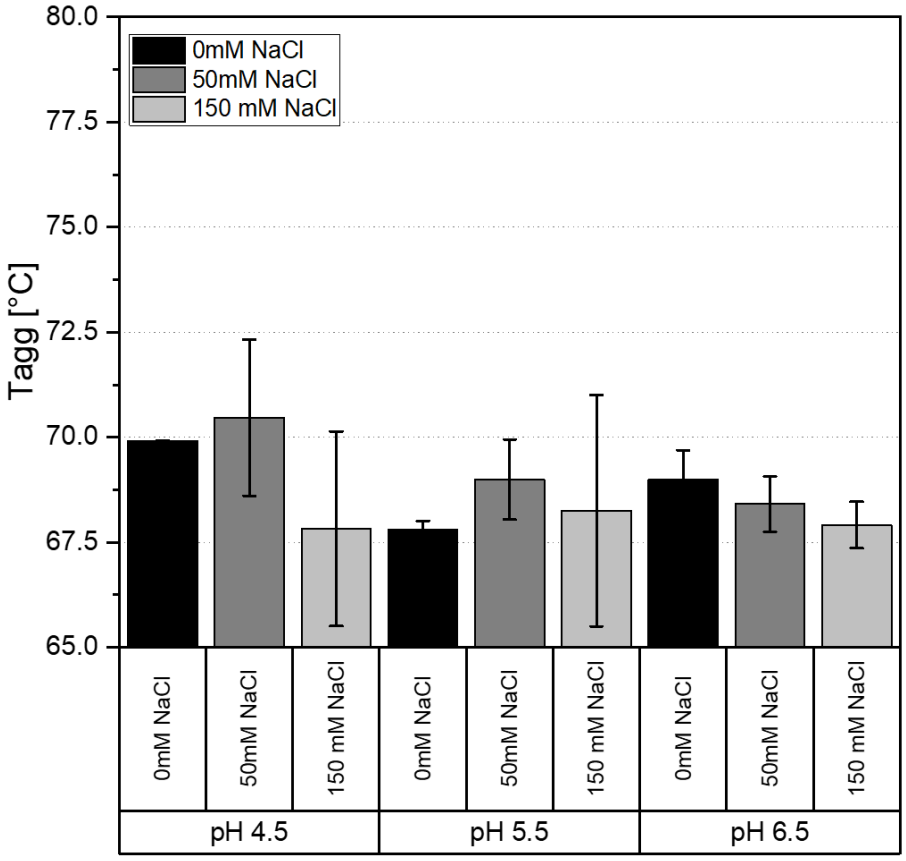

Figure 45S: $T_{agg,\ onset}$ of *the mAb* at different formulation pH's and sodium chloride concentrations, as determined by using dynamic light scattering.

References

1. Le Basle, Y., et al., *Physicochemical Stability of Monoclonal Antibodies: A Review.* J Pharm Sci, 2020. **109**(1): p. 169-190.
2. Mahler, H.C., et al., *Protein aggregation: pathways, induction factors and analysis.* J Pharm Sci, 2009. **98**(9): p. 2909-34.
3. Roberts, C.J., *Protein aggregation and its impact on product quality.* Curr Opin Biotechnol, 2014. **30**: p. 211-7.
4. Kijanka, G., et al., *Submicron Size Particles of a Murine Monoclonal Antibody Are More Immunogenic Than Soluble Oligomers or Micron Size Particles Upon Subcutaneous Administration in Mice.* J Pharm Sci, 2018. **107**(11): p. 2847-2859.
5. Moussa, E.M., et al., *Immunogenicity of Therapeutic Protein Aggregates.* Journal of Pharmaceutical Sciences, 2016. **105**(2): p. 417-430.
6. U.S. Department of health and human services FDA (Center for Drug Evaluation and Research and Center for Biologics Evaluation and Research), *Guidance for Industry: Immunogenicity Assessment for Therapeutic Protein Products*. 2014.
7. Hawe, A., et al., *Subvisible and Visible Particle Analysis in Biopharmaceutical Research and Development*, in *Biophysical Characterization of Proteins in Developing Biopharmaceuticals*. 2015. p. 261-286.
8. Hubert, M., et al., *A Multicompany Assessment of Submicron Particle Levels by NTA and RMM in a Wide Range of Late-phase Clinical and Commercial Biotechnology-Derived Protein Products.* J Pharm Sci, 2019. **109**(1): p. 830-844.
9. Song, Y., J. Zhang, and D. Li, *Microfluidic and Nanofluidic Resistive Pulse Sensing: A Review.* Micromachines (Basel), 2017. **8**(7).
10. Kozak, D., et al., *Advances in Resistive Pulse Sensors: Devices bridging the void between molecular and microscopic detection.* Nano Today, 2011. **6**(5): p. 531-545.
11. Rhyner, M.N., *The Coulter principle for analysis of subvisible particles in protein formulations.* AAPS J, 2011. **13**(1): p. 54-8.
12. Anderson, W., et al., *A comparative study of submicron particle sizing platforms: accuracy, precision and resolution analysis of polydisperse particle size distributions.* J Colloid Interface Sci, 2013. **405**: p. 322-30.
13. van der Pol, E., et al., *Particle size distribution of exosomes and microvesicles determined by transmission electron microscopy, flow cytometry, nanoparticle tracking analysis, and resistive pulse sensing.* J Thromb Haemost, 2014. **12**(7): p. 1182-92.
14. Anderson, W., et al., *Observations of Tunable Resistive Pulse Sensing for Exosome Analysis: Improving System Sensitivity and Stability.* Langmuir, 2015. **31**(23): p. 6577-87.
15. Vogel, R., et al., *A standardized method to determine the concentration of extracellular vesicles using tunable resistive pulse sensing.* J Extracell Vesicles, 2016. **5**: p. 31242.
16. Maas, S.L., et al., *Possibilities and limitations of current technologies for quantification of biological extracellular vesicles and synthetic mimics.* J Control Release, 2015. **200**: p. 87-96.
17. Stelzl, A., S. Schneid, and G. Winter, *Application of Tunable Resistive Pulse Sensing for the Quantification of Submicron Particles in Pharmaceutical Monoclonal Antibody Preparations.* J Pharm Sci, 2021.

18. Grabarek, A.D., et al., *Critical Evaluation of Microfluidic Resistive Pulse Sensing for Quantification and Sizing of Nanometer- and Micrometer-Sized Particles in Biopharmaceutical Products.* Journal of Pharmaceutical Sciences, 2019. **108**(1): p. 563-573.
19. Söltl F., et al., *Analysis of formulation-dependent colloidal and conformational stability of monoclonal antibodies.* 2016.
20. Allen, T., *Particle Size Measurement, Volume 1: Powder Sampling and Particle Size Determination*. 2003, Elsevier B.V.
21. Matteucci, M.E., et al., *Drug Nanoparticles by Antisolvent Precipitation: Mixing Energy versus Surfactant Stabilization.* Langmuir, 2006. **22**.
22. Barnard, J.G., K. Babcock, and J.F. Carpenter, *Characterization and quantitation of aggregates and particles in interferon-beta products: potential links between product quality attributes and immunogenicity.* J Pharm Sci, 2013. **102**(3): p. 915-28.
23. Yoneda, S., et al., *Quantitative Laser Diffraction for Quantification of Protein Aggregates: Comparison With Resonant Mass Measurement, Nanoparticle Tracking Analysis, Flow Imaging, and Light Obscuration.* J Pharm Sci, 2019. **108**(1): p. 755-762.
24. Hawe, A., et al., *Submicrometer, micrometer and visible particle analysis in biopharmaceutical research and development*, in *Biophysical Characterization of Proteins in Developing Biopharmaceuticals*. 2020. p. 285-310.
25. Arosio, P., et al., *On the role of salt type and concentration on the stability behavior of a monoclonal antibody solution.* Biophys Chem, 2012. **168-169**: p. 19-27.
26. Shi, S., et al., *Method qualification and application of diffusion interaction parameter and virial coefficient.* Int J Biol Macromol, 2013. **62**: p. 487-93.
27. Lehermayr, C., et al., *Assessment of net charge and protein-protein interactions of different monoclonal antibodies.* J Pharm Sci, 2011. **100**(7): p. 2551-62.

Chapter 7

Final summary

The present thesis focused mainly on three aspects in the context of subcutaneous delivery of high concentrated biopharmaceuticals, which have not been explored yet in detail: i) determining the performance of large volume injection devices **(Chapter 3)** with regards to the application of high concentrated biopharmaceuticals and their impact on the stability of the delivered product, ii) investigating protein stability in a novel, flexible COC-pouch (MiniBag) and comparing it to the stability in a commonly used glass and COP syringe to address the need for new large volume primary packaging materials **(Chapter 4)** and iii) developing a suitable sample preparation and data analysis method for a new submicron particle analysis technique **(Chapter 5)** and comparing the results to other available techniques **(Chapter 6)**.

In **Chapter 3** two injection devices, both using a valve-free dual piston suction pump design, were evaluated. The small pump was found to be capable of delivering high concentrated mAb solutions up to 150 mg/ml, or 30 mPas dynamic viscosity, while remaining at high relative doses of > 80 %. For this purpose, a low flow rate of less than 100 µl/min was required, resulting in a duration of 30-60 min for the application of a 3 ml dose of the respective mAb solution. At a higher flow rate of 200 µl/min the limit of the small pump was found to be at around 10-15 mPas or around 100 mg/ml mAb concentration. The large pump on the other hand was capable of delivering up to 200 mg/ml mAb solutions, which possessed a dynamic viscosity of 100 mPas, with flow rates of up to 3 ml/min while maintaining high relative doses of > 80 %. The application of a 3 ml dose is therefore achieved within 1 min of injection duration. The main factor influencing injection device performance was found to be the increased solution viscosity at high protein concentration. An improvement of the relative dose

was observed, when the set flow rate of the injection device or the protein concentration was reduced. Besides this, an increase in set flow rate was found to result in a decrease in delivery duration for a 3 ml dose on the small pump only up to a certain level, due to the concomitant decrease in relative dose at high pump rotation speeds, when this level was exceeded. The observed limitations were mainly caused by an insufficient filling of the pump chamber during the filling cycle and may be unique to suction pump designs. An alteration of the inlet design, by exchanging the inlet cannula of the small device with cannulas of larger diameter or shorter length, subsequently led to an increase in relative dose. Other factors influencing viscosity such as injection temperature and shear behavior were found to affect the observed relative dose as well. Shear thinning behavior of the high concentrated mAb solution at high shear rates as well as the reduced solution viscosity at higher temperatures of up to 32 °C resulted in higher relative doses.

Protein stability after pumping a mAb solution with both injection devices was investigated and no impact on charge variants or the level of HMWS or LMWS was observed. However, subvisible particle formation was induced through the pumping action of both pumps, but in this study the small pump exhibited a more pronounced formation of aggregates. Particle formation was not only limited to the pumping action itself, but also drastically influenced by the primary packaging material. To overcome this, a thoughtful selection of the primary packaging material (e.g. silicone-oil free variants or collapsible bags) or the implementation of an in-line filtration step is suggested. A sufficient reduction in subvisible and submicron particles through in-line filtration with a 0.22 µm was proven and the impact of an in-line filter on the performance of the large injection device was investigated. Due to the implementation on the inlet of the suction pump, a reduced injection device performance was observed at high protein concentration of > 100 mg/ml, but an implementation on the outlet of the pump is expected to result in better performance.

In **Chapter 4**, a novel packaging material (MiniBag) comprising of a flexible bag, laminated from a COC polymer film, was investigated as packaging material for a high concentrated liquid mAb formulation. A variety of critical quality attributes was investigated and results of the MiniBag after storage at 4°C, 25°C, and 40°C for up to 24 weeks were compared to commonly used glass and COP syringes. In addition to storage of all packaging materials at atmosphere, polymer packaging materials were stored in N_2-filled aluminum pouches in order to reduce protein oxidation. Of the investigated critical quality attributes, differences between packaging options were found in subvisible particle concentration, content of soluble oxygen and subsequently degree of protein oxidation. Compared to a glass syringe, both polymer packaging materials, MiniBag and COP syringe, offered advantages through lower subvisible particle levels over time. However, a high degree of protein oxidation was observed for both polymer packaging materials stored at atmosphere. N_2-filled secondary packaging was found to reduce the content of soluble oxygen within the MiniBag and COP syringe. Consequently the degree of protein oxidation in both polymer packaging materials could be reduced to a level below the degree of oxidation in a glass syringe. Improved protein stability compared to storage in a glass syringe supports the future use of the MiniBag as a primary packaging material for high concentrated biopharmaceuticals and offers the option of a new large volume primary packaging material for the development of large volume injection devices.

In **Chapter 5 and Chapter 6**, tunable resistive pulse sensing was investigated as submicron particle analysis technique to characterize and quantify submicron particles between 0.1 – 1.0 µm in proteinaceous samples. Since the conductivity of commonly used buffering agents at a concentration of 20 mM was found to be not sufficient for submicron particle analysis using TRPS and a large sample dilution in electrolyte solutions should be avoided, a spiking-approach to introduce electrolytes to increase conductivity was investigated in **Chapter 5**. The addition of 50 mM sodium chloride through spiking from a 1 M sodium chloride stock solution accounted for only 5.2% dilution of the sample

without affecting the data quality obtained from submicron particle counting and sizing of polystyrene standards. By spiking of sodium chloride to proteinaceous samples after applying a short duration of stir stress, TRPS was successfully used to quantify a significant increase in submicron particle levels, and a virtually bell-shaped particle size distribution with a maximum at around 250 nm was obtained for a NP300 nanopore. TRPS was proven to underestimate the particle concentration of heterogeneous samples (e.g. stressed protein samples) at sizes below the maximum of the histogram which adversely affects the data quality, if the particle concentration across the whole size range is reported. Data analysis is therefore suggested to be performed from the maximum of the histogram towards the upper limit of the measurement range, if a heterogeneous particle size distribution can be expected. TRPS was subsequently compared to three other submicron particle characterization techniques in **Chapter 6**. Sample preparation contained the addition of 50 mM sodium chloride to all samples immediately prior to analysis, in order to ensure comparability of the results. All four investigated submicron particle characterization techniques were capable of detecting a sharp increase in SMPs after three days of heat stress at 50°C. TRPS and MRPS mainly detected small particles below 400 nm, whereas RMM and NTA also detected particles in the range above 500 nm. When comparing the obtained particle concentrations in a size range from 250 – 900 nm, both RPS techniques showed similar particle levels, whereas RMM showed the lowest and NTA the highest particle levels. The increase in ionic strength, as required for RPS analysis, through spiking of sodium chloride was found to result in lower k_D values and decreased aggregation onset temperatures, indicating increased protein-protein interactions. An exchange of sodium chloride to other inorganic salt or buffer components resulted in similar aggregation onset temperatures. Furthermore, the addition of sodium chloride or histidine immediately prior to submicron particle analysis was found to cause protein aggregation and the formation of submicron particles in heat stressed mAb samples as determined by RMM and NTA analysis in the presence and absence of spiked sodium chloride or histidine. Since RPS

methods require a conductivity of 3-4.5 mS/cm for particle detection, a selection guide was developed to support the decision process for a suitable submicron particle characterization technique. All four submicron particle characterization techniques can be used, if the conductivity of the sample is sufficient to support RPS analysis. As the addition of electrolytes to heat stressed mAb caused protein aggregation, only RMM and NTA can be recommended for the quantification of submicron particles in samples of low ionic strength, since the measurement principle is independent of the ionic strength.

In summary, this thesis provided numerous new findings regarding the large volume subcutaneous delivery of high concentrated mAb formulations. We investigated and improved the performance of large volume injection devices and determined the impact of delivering a high concentrated mAb solution with the injection device on protein stability. Additionally, we were able to suggest an in-line filtration step in order to sufficiently reduce subvisible as well as submicron particle concentration in the delivered solution while maintaining sufficient performance of the injection device. A novel primary packaging material (MiniBag), comprising a flexible bag laminated from a COC polymer film, was investigated as option for the storage of larger volumes of a high concentrated biopharmaceutical product. Protein stability is not negatively affected in this novel packaging material compared to commonly used glass or polymer syringes. The initial drawback of higher gas permeation of polymer packaging materials was used to reduce protein oxidation through N_2-filled secondary packaging and thereby enhance protein stability. A suitable method to analyze submicron particles in proteinaceous samples by using TRPS was presented and compared to other submicron particle analysis techniques. A selection guide was developed to support the decision process for a suitable submicron particle analysis technique based on the characteristics of the sample.